Summer 8-19-2022

Archaeological Bivalves as El Niño-Southern Oscillation (Enso) Proxies

Frankie St. Amand
University of Maine, frankie.stamand@maine.edu

ARCHAEOLOGICAL BIVALVES AS EL NIÑO-SOUTHERN OSCILLATION (ENSO) PROXIES

By

Frankie St. Amand

B.A. Geography/Anthropology, University of Southern Maine, 2015

M.S. Quaternary Studies, University of Maine, 2019

A DISSERTATION

Submitted in Partial Fulfillment of the

Requirements for the Degree of

Doctor of Philosophy

(in Interdisciplinary Studies)

The Graduate School

The University of Maine

August 2022

Advisory Committee:

Daniel H. Sandweiss, Anthropology Department, Climate Change Institute, School of Earth and Climate Sciences, Advisor

Alice R. Kelley, School of Earth and Climate Sciences, Climate Change Institute, Advisor

Kirk A. Maasch, School of Earth and Climate Sciences and Climate Change Institute

Karl Kreutz, School of Earth and Climate Sciences, Climate Change Institute

Alan Wanamaker, Department of Geological and Atmospheric Sciences at Iowa State University and Cooperating Faculty Member, Climate Change Institute

ARCHAEOLOGICAL BIVALVES AS EL NIÑO-SOUTHERN OSCILLATION (ENSO) PROXIES

By Frankie St. Amand

Dissertation Co-Advisors: Dr. Daniel H. Sandweiss and Dr. Alice R. Kelley

An Abstract of the Dissertation Presented
in Partial Fulfillment of the Requirements for the
Degree of Doctor of Philosophy
(in Interdisciplinary Studies)
August 2022

El Niño-Southern Oscillation (ENSO) is a climate phenomenon with periodic events that impact humans in the study area along the North Coast of Peru. In this region, Eastern Pacific and Coastal El Niño events are associated with anomalously high sea surface temperature (SST), reduced upwelling, and heavy precipitation (Grados et al., 2018; Sandweiss et al., 2020). Major changes in ENSO occurred during the Mid- to Late-Holocene, ca. 5.8 and 2.9 ka, resulting in rapid increases in event frequency to modern conditions. To better identify human adaption to changing climate during the Holocene, we must improve our understanding of ENSO. Though limited climate records exist along coastal Peru, marine bivalves present unique opportunities for studying ENSO (Sandweiss et al., 2020). Common in coastal archaeological middens, they are among the most promising ENSO proxies in this region (Sandweiss and Kelley, 2012; Sandweiss et al., 2020).

This research explores two understudied bivalves, *Tivela hians* and *Anadara tuberculosa* and determines their growth lines are discrete and can be sampled. Carbonate material from lunar periods in their outer shell is sampled and analyzed to investigate oxygen and carbon stable isotopes. Fractionation rates of oxygen isotopes in shell carbonate is temperature and salinity dependent and well understood (Branscombe, Schulting, Lee-Thorp, and Leng, 2021; Dettman, Reische, and Lohmann, 1999; Carré et al., 2013; Grossman and Ku, 1986). Resulting $\delta^{18}O_{aragonite}$ records are evaluated using a standard SST equation and $\delta^{18}O_{aragonite}$-derived SSTs are compared to SST and salinity measurements from harvest locations.

T. hians $\delta^{18}O$ accurately represents measured SST in 75% of the study collection. Salinity variations do not correlate with unexplained variance in one of the four specimens, which may be attributed to sampling error. $\delta^{18}O$ in *A. tuberculosa* growth rings appears to be influenced by seasonal salinity gradients which form in the near-equatorial Gulf of Guayaquil, complicating the temperature-dependent relationship of oxygen isotope fractionation in carbonate shell material. More information about regional salinity is required to account for the impact of salinity on $\delta^{18}O$ precipitation in *A. tuberculosa*, as well as to determine if visually identified growth disruptions represent slowed or stopped growth during temperature stress.

DEDICATION

This research was conducted at the University of Maine at Orono, which is built on land stolen from the Penobscot Nation. This dissertation is dedicated to Linda Holtslander, professional badass and friend.

ACKNOWLEDGEMENTS

This research project would not have been possible without the formative recommendations and guidance from my co-advisor Dan Sandweiss. I am also indebted to support and assistance from Alice Kelley, co-chair of my committee and co-advisor during my graduate studies at UMaine. I am deeply appreciative of Kirk Maasch, Alan Wanamaker, and Karl Kreutz, who also participated on my committee and asked difficult questions and offered feedback and advice. Matthieu Carré opened his laboratory at Universidad Peruana Cayetano Heredia and shared *A. tuberculosa* samples and guidance during my fieldwork in Peru. I am grateful to him and his students for their support.

TABLE OF CONTENTS

LIST OF FIGURES

LIST OF TABLES

CHAPTER 1

RECONSTRUCTING EL NIÑO SOUTHERN OSCILLATION (ENSO) DURING THE HOLOCENE

In Peru, common high resolution and long-term continuous climate records such as tree rings and lake cores are scarce to nonexistent along the arid coast (Sandweiss and Kelley, 2012). Most marine cores lack accumulations of Mid-Holocene sediments and corals don't grow in the normally cold water of the coastal equatorial Pacific Ocean (Carré et al., 2005; Rein et al., 2005; Sandweiss et al., 2007; Sandweiss et al., 2020). Without these sources of paleoenvironmental information, it is difficult to understand past changes in ENSO that have dominated coastal human occupations and subsistence patterns for millennia.

This dissertation addresses the need for a more complete suite of paleoenvironmental proxies on the North Coast of Peru during two key periods of abrupt change in the frequency and intensity of El Niño events in the Mid- and Late-Holocene. The work described here extends the usefulness of bivalves recovered from archaeological sites to reconstruct marine conditions. Short-lived marine bivalves present a unique opportunity for studying past changes in ENSO. Marine bivalves have inhabited the entirety of the Peruvian coast for the duration of the Holocene. Humans have exploited this marine resource for as long as they are known to have been present, and shells found in archaeological middens along the coast have proved to be among the most promising sources of information about ENSO in Peru (Andrus, 2011; Warner, DeLong, Chicoine, Thirumalai, and Andrus, 2022; Sandweiss et al., 2007; Sandweiss and Kelley, 2012).

Two of the chapters in this dissertation assess the potential of two under-researched bivalves as records of ENSO events. For species such as *T. hians* and *A. tuberculosa*, which are found in Holocene-age archaeological sites and are thus a potential source of paleoenvironmental information, the relationship between their growth and their marine environment must be established. Chapter 2 addresses the need for calibrating $\delta^{18}O_{aragonite}$ SST from modern bivalves by assessing the validity and

reliability of satellite-derived SST records and their potential use as SST data in areas lacking in-situ measurements. To examine correlations between bivalve $\delta^{18}O_{aragonite}$ SST and measured SST, it is necessary to assess the validity of bivalve SST records. Chapter 5 compares high resolution satellite derived SST to in-situ measurements in order to assess the validity of these records. Comparisons indicate that in some areas, satellite images accurately capture both average SST and seasonal variability. In other areas, more research is needed to identify unexplained variation between the datasets, possibly due to cloud coverage, rainfall, or aeolian dust.

In Chapter 3, the author discusses the use of second order growth lines in the Peruvian marine bivalve *Tivela hians.* These lines guide microsampling for $\delta^{18}O$ and $\delta^{13}C$ and subsequent paleoenvironmental analyses. Identified in four *T. hians* valves examined in this research, these growth lines helped guide sampling of monthly sections of outer shell. A standard SST equation describing the relationship between $\delta^{18}O$ and SST was adjusted and $\delta^{18}O$-derived SST records were compared to measured SST from near the harvest locations. Because these four bivalves were not alive during an ENSO event, their geochemistry reflects ENSO neutral conditions. Overall, *T. hians* appears to capture average SST and seasonal variability during one to two annual cycles. This species is a promising candidate for the reconstruction of SST variability associated with ENSO, but more research is needed to confirm that *T. hians* is not too temperature-sensitive to survive and record changes in $\delta^{18}O$ associated with El Niño warming events.

Chapter 4 discusses the author's analyses of *Anadara tuberculosa* specimens from the far northern coast of Peru that were contributed by Matthieu Carré and his students. These samples were examined with the goal of determining the use of this species as an indicator of El Niño warming events by examining growth breaks in the shells apparent in visual analysis and indicated in their isotopic records. All four specimens examined were alive during the 2017 Coastal El Niño event, and two were alive during the 2015-2016 El Niño. $\delta^{18}O_{aragonite}$ values from *A. tuberculosa* growth rings were compared

to SST to quantify the relationship between stable oxygen isotopes and ambient SST. In addition to river discharge and precipitation data, $\delta^{13}C$ was assessed in relation to $\delta^{18}O$ to identify freshwater influx and abrupt negative changes in salinity that might impact fractionation of stable oxygen isotopes in carbonate material.

The remainder of this chapter provides a brief introduction to El Niño and the current state of knowledge about El Niño during the approximately 15 millennia that humans have inhabited the north coast of Peru.

El Niño Southern Oscillation (ENSO)

ENSO is a coupled atmospheric and oceanic system with global impacts at sub-decadal timescales relevant to humans. This aperiodic climate phenomenon primarily impacts the central and east Equatorial Pacific Ocean bordering the west coast of South America. ENSO fluctuates between neutral events and cooling and warming events, known as La Niña and El Niño. The neutral phase of ENSO represents 'normal' conditions in the equatorial South Pacific. La Niña and El Niño are characterized by abnormally low or high SST, changes in oceanic currents and upwelling, changes in atmospheric pressure and wind patterns, and changes in precipitation.

Neutral, El Niño, and La Niña conditions

During neutral ENSO conditions, the northward flowing Perú Ocean Current transports cold and fresh water toward the Gulf of Guayaquil near the border of Ecuador before deflecting further seaward (Gandy Maria Rosales Quintana et al., 2021; Grados et al., 2018). While this and other current systems are discussed further in Chapter 2, it is important to note that the conjunction of the northward Peru Ocean Current and prevailing trade winds crossing the Pacific from South America westward support strong upwelling of colder, nutrient dense water directly along the coast.

La Niña events reinforce neutral conditions by means of strengthened trade winds and upwelling, causing SST anomalies 1–2 °C lower than average along the coast of Peru (Grados et al.,

2018). El Niño, on the other hand, has several known manifestations, which occur every 2-7 years on average (Hu et al. 2019; Sandweiss et al. 2020; Sulca et al. 2018). The most well-known is the Eastern Pacific event, characterized by diminished trade winds across the south Equatorial Pacific resulting in high SST anomalies up to 3–4 °C along coastal Peru (Grados et al., 2018; Sandweiss et al., 2020). Heavy precipitation and terrestrial flooding produce landslides and erosion, impacting coastal terrestrial ecosystems. Coastal events are like Eastern Pacific events in that they are associated with heavy rainfall and coastal erosion but are much shorter compared to the timespan of other El Niño events. They are also unique among warming events in that their impact is not experienced south of 12°S (Sandweiss et al., 2020). This latitude is a major climate boundary; to the south, the impacts of Eastern Pacific El Niño events are attenuated poleward (Sandweiss et al., 2020).

In contrast, Central Pacific (Modoki) events feature abnormally high SST in the Central Pacific with relatively minor impact on SST along coastal Peru (Ashtok et al., 2007; Grados et al., 2018). Central Pacific events do influence Peruvian highland precipitation, resulting in decreased precipitation in the highlands and diminished riverine flow to the coast (Sandweiss, A, 2019; Sandweiss et al., 2020).

ENSO during the Holocene

Although ENSO's coupled ocean-atmosphere dynamics have remained similar throughout historical records, the frequency and intensity of events has varied throughout the Holocene. During the early Holocene, ca. 11.6 ka, ENSO events were uncommon, and their frequency decreased or even stopped entirely during the Mid-Holocene (ca. 9-6 ka). Major and abrupt transitions in the behavior of ENSO occurred ca. 5.8 and 2.9 ka. These are evidenced by the recurrence of ENSO in geoarchaeological records north of 12°S and subsequently by the rapid increase in event frequency from once or twice a century to modern day conditions (Sandweiss et al., 2020).

Archaeological evidence of ENSO

Some of the earliest known human occupations in South America date to the Early Holocene and Late Pleistocene transition. From that time to present, coastal Peruvian populations have responded to both the disruptions and opportunities presented by El Niño events (St. Amand et al., *in press*). Changes in terrestrial water availability as well as flooding and landslides associated with Eastern Pacific and Coastal events challenge subsistence practices in coastal Peru. Increasingly, research is focusing on human adaptations to abrupt changes in climate along the North Coast of Peru (see Caramanica et al. 2018 and 2020; Caramanica and Koons 2016; Dillehay et al. 2017; Goodbred et al. 2020; Nesbitt, 2016; Prieto 2015; Reitz, Sandweiss, and Cannarozzi, 2019; Sandweiss and Kelley 2012; Sandweiss and Maasch, 2022; Sandweiss and Quilter 2012; Sandweiss et al. 2007).

To better understand cultural shifts, including changes in subsidence technologies, settlement patterns, and trade, it is necessary to refine our understanding of ENSO's variability, spatial extent, and frequency throughout the Holocene. Challenges exist in establishing complex relationships of cause and effect between cultural shifts and changes in ENSO behavior throughout the Holocene. Foremost among these is a dearth of climate records along Peru's 2,500 km long arid coastline, where commonly used high resolution, long-term continuous proxies such as tree rings and lake cores are often nonexistent (Sandweiss et al., 2020).

Archaeological sites, however, can provide evidence of human adaption and climate change; sometimes even stratigraphically associated at the same location (Sandweiss and Kelley, 2012; Sandweiss et al., 2020; St. Amand et al., 2020). Remains of human activity, including food consumption choices, hunting and fishing technologies, changes in building style and function, and landscape modification (such as canal infrastructure) can be temporally constrained and compared between sites over time. AMS and other dating methods allows these correlations to be linked to specific periods of time, and in some instances, to discrete El Niño events (see St. Amand et al., 2020). Archaeological sites

along coastal Peru have contributed to a well-established timeline of human occupation spanning the Holocene.

Because El Niño events are discrete and can be recognizable due to their impacts on landscapes and in relation to human behavior, they can sometimes be identified in archaeological sites (Sandweiss et al., 2003; Sandweiss et al., 2020; St. Amand et al., *in press*). In other instances, stratigraphic context provides opportunities to identify change over time and associations can be made between cultural materials and changing environmental conditions. In this context, while long-term and continuous human occupations are ideal for examining changes in ENSO variability and human adaptation over time, it is sometimes necessary - and quite sufficient - to explore cultural change across multiple, shorter occupations, or to examine climate 'snapshots' in order to place these refined climate data in the broader context of ENSO and human behavior.

Marine bivalves as paleo-ENSO proxies

Marine bivalve geochemistry is one of the strongest proxies we have for studying the frequency and intensity of Eastern Pacific and Coastal El Niño events (Sandweiss et al., 2020). Peruvian species typically live less than a decade and thus individual bivalves lack the ability to directly measure long term ENSO event frequency. They do remain useful as short-term records of ENSO, nonetheless, because they directly track marine changes associated with ENSO (Carré et al., 2013). Bivalve assemblages, particularly those found in time-transgressive shell middens (such as the Chira Beach Ridges in northern Peru), can have great utility in reconstructing ENSO variability over hundreds of years to millennia.

Peruvian bivalves respond to changing environmental and climate conditions that affect their growth rates, biomineralization, and resulting isotopic shell carbonate compositions. Unlike fish or other marine species (Ñiquen and Bouchon, 2004), most adult bivalves cannot swim and are largely immobile (some exceptions, such as scallops, can move up to 5 m at a time using their abductor muscle). Individual mollusks do not migrate in response to short-term climate perturbations, though long-term

responses of entire populations to climate shifts may include a change in their habitat location (Rollins et al., 1986b). This means that they spend most their lives in one place and thus they offer climate records of ambient conditions in that spot. For this reason, shellfish can be used as local proxies of SST, salinity, and marine upwelling, as well as indicators of larger-scale changes such as varying marine currents (Rollins et al., 1986b).

As they grow, bivalves precipitate shell in equilibrium with their ambient marine environment and thus reflect the chemistry of local ocean water (Grossman and Ku, 1986). The relationship between bivalve growth and marine conditions is well established for many species (Carré et al., 2013; Gruver, 2018; Rollins et al., 1986; Rollins, Sandweiss, Brand, and Rollins, 1987; Sandweiss et al., 2001; Warner, DeLong, Chicoine, Wanamaker, and Thirumalai, 2016). As oxygen isotope fractionation in shell carbonate is temperature-dependent, geochemistry can yield insights into past SST and change in SST over time. Analysis of bivalve $\delta^{18}O$ available in the aragonitic growth rings of a shell's valve offer high resolution snapshots of ambient marine environments.

Some challenges for the use of bivalve $\delta^{18}O$ for SST reconstruction include uncertainties about the $\delta^{18}O$ of past ocean water as well as biases resulting from species-specific vital effects, which may impact metabolism, growth, and valve precipitation (Carré et al., 2005; Pérez-Huerta and Andrus, 2010). For instance, some species, such as *Mesodesma donacium*, are not tolerant of warmer SST and either stop precipitating new shell during high SST anomalies or die (Carré et al., 2014). In this manner, mass mortality events caused by anomalous SST during strong El Niño warming events can decimate local or regional populations (Sandweiss et al., 2001). *Choromytilus chorus* mortality is also a function of increasing SST: within 24 hours, half of a local *C. chorus* population will die at temperatures above 26.5°C. This lethal temperature, "LT-50", varies among species (Urban, 1994).

Studying assemblages of bivalves allows researchers to track spatial patterns in SST associated with ENSO (Carré et al., 2014). $\delta^{18}O$ variation in populations of bivalves track amplitude and allows for

evaluation of seasonal and interannual variation in SST of ambient marine conditions. (Carré et al., 2014). Coastal Peruvian SST anomalies manifest concurrent with those in the Eastern Pacific Niño1+2 region (Carré et al., 2013). Because of this, coastal SST anomalies are representative of larger-scale conditions linked to ENSO (Carré et al., 2013). Despite a number of challenges associated with the utility of marine bivalves as ENSO proxies, Peruvian bivalve assemblages are in broad agreement with other Holocene ENSO records throughout the Pacific basin, such as foraminifera, marine sediment cores and distant corals, as well as ENSO-related flood records (e.g. Fontugne et al., 1999; Keefer et al., 1998; Rein et al, 2005; Riedinger, Steinitz-Kannan, Last, and Brenner, 1998; Nesbit, 2016; Rodbell et al., 1999; Sandweiss, 2003; Sandweiss et al., 1996; Sandweiss et al., 2020). However, gaps in our ENSO chronology and questions regarding dramatic shifts in the frequency and intensity of EN events during the Mid-Holocene remain.

Reconstructing SST from Bivalve growth rings. Growth ring and stable isotope analysis can be effective methods of paleoclimate reconstruction because marine bivalves precipitate calcium carbonate shells in isotopic equilibrium with ambient ocean water (Grossman and Ku, 1986). The fractionation rate of the oxygen isotope in shell carbonate is temperature and salinity dependent, and is relatively well understood (Branscombe, Schulting, Lee-Thorp, and Leng, 2021; Dettman, Reische, and Lohmann, 1999; Grossman and Ku, 1986; White et al., 1999). In areas with little fluctuation in ocean salinity, such as in the nearshore of most of coastal Peru, the inverse relationship between $\delta^{18}O$ and SST is the primary driver behind the ratios of stable oxygen isotopes found in shells' aragonitic growth rings. This enables researchers to reconstruct SST during the lifespan of a bivalve (Branscombe, Schulting, Lee-Thorp, and Leng, 2021). Variation in salinity in the study areas was examined to assess potential impacts of salinity on $\delta^{18}O_{water}$: see Chapters 2, 3, and 4 for further discussion.

During El Niño events, $\delta^{18}O_{aragonite}$ values are more negative, reflective of ambient conditions (more negative $\delta^{18}O_{water}$) (Andrus et al., 2005; Branscombe, Schulting, Lee-Thorp, and Leng, 2021). Lower

salinity of ocean water (resulting from increased precipitation and surface water sources) also results in increased negativity of $\delta^{18}O_{aragonite}$ values (Andrus et al., 2002; Branscombe, Schulting, Lee-Thorp, and Leng, 2021). In this manner, bivalve $\delta^{18}O$ records track seasonal and interannual change in SST ($\triangle T$; thus ENSO variability over time, derived from variance in $\triangle T$) (Carré et al., 2013; Carré et al., 2014).

Relationships between $\delta^{13}C$ precipitation in shell carbonate material and the composition of dissolved inorganic carbon in ambient seawater are more complex (Andrus, 2011; Freitas, Clarke, Kennedy, Richardson, and Abrantes, 2005). Research indicates that $\delta^{13}C$ ($^{13}C/^{12}C$ ratios in shell carbonate material) is impacted by vital effects, including age, kinetic, and metabolic factors, as well as environmental drivers such as salinity, upwelling, and ocean stratification (Branscombe, Schulting, Lee-Thorp, and Leng, 2021; Freitas, Clarke, Kennedy, Richardson, and Abrantes, 2005). $\delta^{13}C$ values are explored in Chapter 3 and Chapter 4 as they relate to $\delta^{18}O$ as a proxy for SST; $\delta^{13}C$ annual cyclicity and correlation with $\delta^{18}O$ are discussed and simultaneous drops in $\delta^{18}O$ and $\delta^{13}C$ are identified as potential changes in salinity due to influx of freshwater. This research does not explore $\delta^{13}C$ further due to complexities of interpretation and the unknowns about environmental parameters at the study sites.

Microsampling consecutive growth rings builds a stable isotopic chronology during a bivalve's lifespan but understanding the corresponding timeline of these samples is important. Carré et al. note three types of incremental internal growth lines in Peruvian bivalves: first, second, and third order (2005). First order lines represent annual growth. These dark lines can be used as summer "biochecks" because they form during the period of slower growth during the austral summer (January through March). Second order lines have a periodicity equal to that of the lunar cycle (approximately 14.8 days), and form during extreme low tides corresponding to the new and full moon. Third order lines accrue daily. These growth increments are composed of paired light and dark bands. The lighter band results from calcium carbonate deposition formed from biomineralization during the period of immersion when the specimens' valves are open (Rollins et al., 1986a). The dark band forms during emersion, when the

shell is exposed at low tide and its valves are closed, and results from the anaerobic dissolution of the shell matrix (Carré et al., 2005; Rollins et al., 1986a). The visibility of second and third order lines varies between species. Furthermore, disruptions result in dark lines which form during strong wave action and heavy siltation, abrupt decreases in salinity due to freshwater influx, abrupt changes in SST, or other factors related to storms or seismic activity (Velarde et al. 2015). It is important to determine if a dark band is the result of a short-term perturbation or part of a long-term pattern of seasonal change (Carré et al., 2005).

Conclusion

ENSO proxies are scarce along Peru's North Coast, but the history of human occupation is rich and varied. We have much to learn about how humans have adapted to their environments, particularly to the disruptions and opportunities of El Niño (St. Amand et al., *in press*). While ENSO presents a powerful lens for studying changes in settlement patterns, subsistence strategies, and trade, it is also true that the remains of human occupations contain information about abrupt changes in climate during the Mid- and Late-Holocene. Marine bivalves, found in refuse piles known as shell middens, present some of the strongest evidence we have for reconstructing past climates along coastal Peru (Sandweiss and Kelley, 2012; Sandweiss et al., 2020). The following chapters explore two relatively understudied bivalves, *T. hians* and *A. tuberculosa*, in effort to increase our ability to understand ENSO in the past, and also examine the ability of high-resolution MUR satellite data to accurately measure SST variability during neutral, La Niña, and El Niño conditions.

CHAPTER 2
ASSESSING THE ACCURACY OF MUR HIGH RESOLUTION SATELLITE SST DATA

While the broader focus of this dissertation research is about the potential of *Tivela hians* and *Anadara tuberculosa* as marine paleoenvironmental proxies, this chapter addresses the need for calibration of bivalve SST records using local SST measurements. An important aspect of using marine bivalves as paleoENSO proxies is the comparison of modern species to modern SST records in order to assess the correlation of these specimens' isotopic SST records to ambient SST conditions. While some researchers periodically measure SST at bivalve collection locations, contiguous SST records spanning the entire lifespans of the bivalves would greatly improve the ability of researchers to correlate isotopic SST records to measured SST.

Monitoring ocean conditions along coastal Perú is important, as the country experiences abrupt changes in SST, marine upwelling, marine currents, atmospheric winds, and precipitation associated with ENSO events. Along the coastline, the Instituto del Mar del Perú (IMARPE) operates SST monitoring stations. SST records from ten of these stations are available for download in daily and monthly averages spanning the time period January 2000 to February 2020 at most stations. While this system is extremely important for tracking coastal changes in SST associated with El Niño and La Niña, ten stations simply cannot provide detailed coverage for the full 3,080 km expanse of the Peruvian coastline. However, higher resolution data are available in the form of high-resolution satellite SST to study the complexities of different types of ENSO events, as well as the regional and local impacts of SST anomalies in the nearshore coastal marine environment.

Whereas the ten IMARPE coastal monitoring stations record local SST, global satellite SST data have existed since 1981, and with full coverage along the Peruvian coast since 2002. High resolution SST data shows varying accuracy in the coastal Peruvian environment: environmental variables such as cloud coverage, precipitation, and aeolian dust appear to cause low correlation between some in-situ temperature measurements and satellite data. In some areas, particularly Paita, on the North Coast, the

correlation is extremely high, indicating that in this region, researchers could use satellite data to assess $\delta^{18}O$ SST records from bivalves harvested from locations without local SST records. This would enable researchers to evaluate bivalves' abilities to record information about the ambient marine environment, even when the specimens were not collected from a location immediately adjacent to an IMARPE station where long-term SST records are available. In this manner, archaeological bivalves of the same species from that region could be used with relative confidence to reconstruct past SST and ENSO patterns and/or variability during the Holocene.

Background and Literature Review

Global satellite SST data have been collected since 1981, but the spatial resolution of these data have typically been too coarse, or low resolution, for applications in coastal regions. The level of detail typically required for studying the dynamic coastal-marine interface and the more complex variations in SST have necessitated contiguous higher resolution products such as the Multi-scale Ultra-high Resolution (MUR) satellite-derived SST dataset.

The global MUR SST dataset, available from June 2002 to present, is available in 0.01° x 0.01° intervals, which are pixels of approximately $1km^2$. The dataset, produced by the Group for High Resolution Sea Surface Temperature (GHRSST), is derived from multiple sources including infrared and microwave data from low earth orbiting satellites, infrared data from geostationary satellites, and in-situ data (O'Carroll et al., 2019; GHRSST Science Team, 2010). These include Moderate Resolution Imaging Spectroradiometers (MODIS) on NASA's Aqua and Terra satellite platforms, several satellite or aircraft-based microwave radiometers (AMSR-E, WindSat, AVHRR), and in-situ measurements from NOAA's shipboard iQuam project for validation of SST data using SST measurements (GHRSST Science Team, 2010).

MUR SST is defined as the temperature of the water near the surface, and not the temperature of the water at the ocean-atmosphere interface (GHRSST Science Team, 2010). These data are available

in a range of formats from Level 1 (unprocessed, raw data) through Level 4 (L4) products, which have gridded, averaged variables that have been merged with other satellite data to remove gaps) (GHRSST Science Team, 2010). L4 MUR SST values are provided in Kelvin (K = C° + 273) with error estimates for SST data ranging from 0.38 - 0.42°C (see Figure 2.1) (GHRSST Science Team, 2010). As SST equations can produce $\delta^{18}O$-derived SST values with errors as large as 2°C, MUR SST are accurate enough to be useful for comparison against bivalve isotopic data. L4 MUR SSTs are available as daily averages from 6/1/2002 to present.

Figure 2.1 MUR SST data error, ranging from 0.38 - 0.42°C along the coast of Peru.

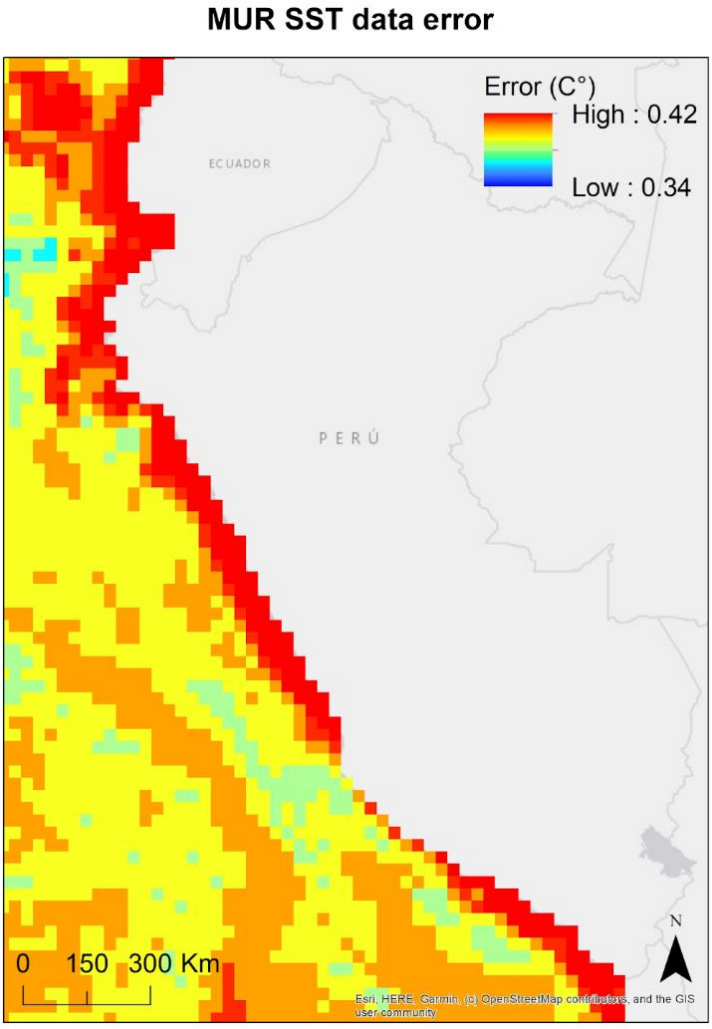

Challenges to measuring SST using satellites in the study area

Clouds

Satellites measure temperature at the earth's surface by detecting thermal energy in the infrared (IR) spectrum. In the case of SST, satellite instruments record details about the IR wavelengths reflected by the oceans and use algorithms to compute these data into SST values. A major challenge associated with satellite-derived SST measurements are obstructions of IR wavelengths by cloud cover (O'Carroll et al., 2019). Scattering and emission of energy wavelengths through clouds result in skewed and inaccurate temperature readings and thus algorithms are used to identify cloud cover and remove clouds from the dataset. In some environments, particularly coastal, misclassification of clouds is more likely, and uncertainty in SST values is larger (O'Carroll et al., 2019).

Satellite IR data are used to create SST datasets because of the relatively high resolution (1-4 km^2) of this format. However, IR data are very susceptible to cloud coverage and associated errors. Microwave data, on the other hand, are not impacted by cloud coverage except during instances of heavy rainfall but have a much coarser resolution (50-75 km^2) (O'Carroll et al., 2019). Blending IR and microwave data can partially address cloud coverage issues, but merged datasets result in other issues from in-filling of removed cloud data resulting from interpolation, including inaccuracies (over smoothing or patchiness) (O'Carroll et al., 2019). Viewing high resolution datasets like MUR over larger time periods can help address these issues (O'Carroll et al., 2019).

Other aerosols

Similar to clouds, aerosols closer to the surface of the earth can scatter - as well as absorb - IR radiation. This impacts the ability of satellites to measure infrared radiation and thus SST. One common aerosol along the Peruvian coast is fog, so pervasive in winters that it has its own name: Garúa. This fog is extremely dense and does not usually produce rain; it results from marine moisture blown over the land by trade winds, concentrating into thick fog of variable intensity and duration (Beresford-Jones et

al., 2015). Along the coast, garúa supports the growth of ephemeral fog oases known as lomas, stretching from ~6°S and 30°S (Beresford-Jones et al., 2015). A concentration of lomas from Huacho south (corresponding with the locations of the Huacho, Callao, Pisco, Ilo IMARPE stations), indicates the pervasiveness of this fog during winter months, August through November (Moat et al., 2021). Beresford et al. discuss archaeological evidence from lomas environments on the south coast of Peru, indicating the prevalence of these systems for at least five millennia (Beresford-Jones et al., 2015). Dust is also prevalent along the south coast of Perú due to intense winds and aeolian transport of fine-grained sediment. Mineral dust is particularly disruptive of IR-based SST measurements, and is airborne intermittently depending on wind direction, speed, and other factors. This variability results in non-systematic SST errors (O'Carroll et al., 2019). Other SST measuring platforms, such as microwave-based systems, are not affected by the presence of mineral dust (O'Carroll et al., 2019).

Spatial variability of pixels

Another challenge, as noted previously, is the resolution of individual satellite pixels, and understanding the spatial variability within each pixel. MUR pixels, approximately 1km^2, have associated uncertainty values published by GHRSST, but uncertainty is likely to change based on myriad factors, including environmental variations associated with the location of the pixel. In the case of coastal SST values, pixels are likely to have more variation than in the open ocean due to relative greater variability in atmospheric water vapor and aerosols, more variable SST due to complexities of currents, upwelling, and changes in mixing at the coastal interface, and freshwater flux from riverine or other sources which are too small to be identified by the satellite pixels (O'Carroll et al., 2019). Other anthropogenic factors include contamination of coastal waters which may modify surface emissivity, thus impacting SST measurements (O'Carroll et al., 2019). As noted, cloud cover and cloud detection of products varies based on methodologies and environmental factors. Some satellite platforms are known to systematically over-mask clouds during the spring and summer periods as temperatures are warming

(Crosman et al., 2017; O'Carroll et al., 2019), resulting in absences in the dataset which can skew SST averages. Platforms can also mistake cold, clear water for cloud cover, also resulting in systematic observation biases, as outlined by Crosman et al. (2017). Satellite data are screened to remove pixels with terrestrial features, so it is unlikely that SST data will be skewed by temperature of coastal landmasses.

Site Descriptions and data availability

The coast of Perú

Ocean

Off the coast of Peru, warm equatorial waters merge with the subtropical South Pacific Ocean, contributing to complex mixing of different water masses, each with distinct temperature (T) and salinity (S) profiles (Grados et al., 2018). These two variables, which directly control the density of seawater, impact ocean circulation. Ocean circulation in this region is controlled largely by the South Pacific subtropical anticyclone, which pushes the near-surface South Equatorial Current westward from approximately 20°S to about 5°N ($T > 20°C$ and $S > 35.1$ PSU) (Grados et al., 2018).

To the north, around 2-3°S, tropical SST is relatively warmer and fresher ($T < 23°C$ and $S > 33.5$) due to its proximity to the equator and to precipitation and freshwater from the Intertropical Convergence Zone (ITCZ) and rainfall and riverine flux (Grados et al., 2018). At times, this warmer water mass is transported south along the coast by the Ecuador-Perú Coastal Current. This creates a transition zone off the coast of northern Perú and southern Ecuador, sometimes referred to as the Paita Transition Zone, where the Peruvian currents and the equatorial currents meet before transporting surface waters westward (Rosales Quintana et al., 2021; Olsson, 1961). These two water masses have distinctive SST and salinity profiles. Strong SST and salinity gradients result in the top 100 m of the water column in the coastal swath between Paita and the Gulf of Guayaquil where these two currents meet (Grados et al., 2018). In addition to upwelled water from the Equatorial Undercurrent, mixing of water masses in this

transition zone defines the characteristics of the cold and saline Pacific Cold Tongue (T < 21°C and S > 34.5 PSU), which extends west to the Galapagos Islands (Grados et al., 2018).

Figure 2.2: Eastern Equatorial Pacific Ocean circulation from shipboard data. Figure modified from Chaigneau et al, 2013. White boxes show Paita and Tumbes study regions (Chapter 3 and 4).

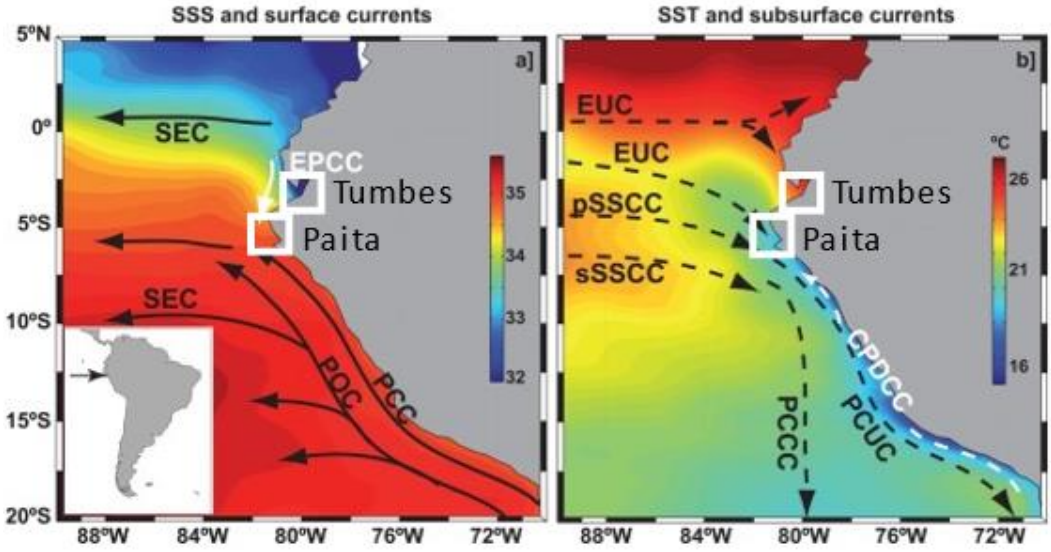

Strong upwelling along the Peruvian coast is wind driven. Easterly trade winds cross the Andes mountains, driving offshore transport of surface water west away from the coast (Rosales Quintana et al., 2021). Deeper, nutrient-rich water upwells along the coast to replace displaced surface water (Grados et al., 2018). In concert with Ekman transport, annually persistent alongshore winds moving north along the coast toward the equator fuel more rapid upwelling in the immediate coastal zone (Rosales Quintana et al., 2021; Grados et al., 2018). Upwelling along the Peruvian coast fluctuates throughout the year, seasonally, and is strongest during the austral summer (December, January, February) (Rosales Quintana et al., 2021). This results in a cold band of water and a productive ecosystem.

The location and mixing characteristics of the water masses along coastal Perú are driven by variations in atmospheric heat, pressure, and wind associated with the South Pacific subtropical anticyclone (Grados et al., 2018), as well as by seasonal and interannual basin-wide changes in

atmospheric pressure associated with ENSO. Eastern Pacific ENSO events impact circulation primarily along the northern half of the Peruvian coast. During an Eastern Pacific El Niño event, trade winds slow, stop entirely, or even reverse, and flattening of the thermocline results in a disruption of coastal upwelling, producing abnormally high SST (Rosales Quintana et al., 2021). During a La Niña event, trade winds can strengthen, reinforcing coastal upwelling and abnormally cool SST can develop in the normally cool nearshore. Central Pacific events, described in more detail in Chapter 1: Introduction, are defined as SST warming anomalies in the central Pacific and associated, slightly cooler waters along the Peruvian coast (Ashok et al., 2007).

Terrestrial environment

The coastal terrain is arid and generally lacking in vegetation along the windy coastal swath, except where westward flowing rivers cross the desert terrain. In far northern Peru, there is more rainfall and mangrove swamps grow in the Gulf of Guayaquil region near the border of Ecuador. In far southern Peru, the landscape shows increased aridity. The Paracas Peninsula (~13-15°S) is marked by natural, windblown aeolian deposits (Briceño-Zuluaga et al., 2017), and unusually strong winds in this area (known as the 'Paracas Winds') create clouds of aeolian dust. A concentration of mineral dust particles is also generated by the prominent mining industry in this area (including steelworks and tin smelters, iron ore mines, and zinc-lead mines) (Salvador, Arasa, and Codina, 2016). Salvador et al.'s study shows that the combination of natural and anthropogenic dust exceeds limits set by the Peruvian government for air quality measures (Salvador, Arasa, and Codina, 2016). Studies on air quality and dust are scarce elsewhere along the coast, but in other regions with concentrations of mining industries or particularly strong winds, aeolian dust is likely to be an issue.

Alongshore Paracas Winds, travel north along the coast toward the equator, creating intense dust storms 4-5 times a year, typically near the end of the winter (July through September) (Briceño-Zuluaga et al., 2017). While Paracas Winds create a cloud-free coastal zone reaching about 20-30 km

offshore, dust storms dramatically impact visibility (Briceño-Zuluaga et al., 2017), with the Pisco IMARPE monitoring station located in the heart of this region. However, aeolian dust storm modeling by Briceño-Zuluaga et al., coupled with analysis of satellite imagery, shows that particle plumes can spread up to 300 km from their source (see Figure 2.3).

Dust levels can increase uncertainty in satellite-derived SST measurements because particulates over the water column can increase total vertical heat flux from the ocean (Al-Shehhi, 2022). In turn, this impacts IR radiation from the ocean as well as the amount of solar radiation absorbed by the ocean's surface, resulting in increased or decreased SST at the ocean surface, depending on the circumstances (Al-Shehhi, 2022). Dust is also shown to absorb some wavelengths of IR radiation, resulting in low biases of SST by satellites (Al-Shehhi, 2022). To address the impacts of dust on the validity of SST data in some regions, satellite data corrections are implemented during seasons marked by biases.

Figure 2.3: Aeolian dispersion of fine mineral dust from mining operations located in the Paracas Penninsula. Strong 'Paracas Winds' can result in fine dust transport reaching nearly 10°S, impacting accuracy of satellite SST measurements. Figure modified from Briceño-Zuluaga et al., 2017 to show locations of IMARPE stations and thus corresponding MUR satellite data used in this research.

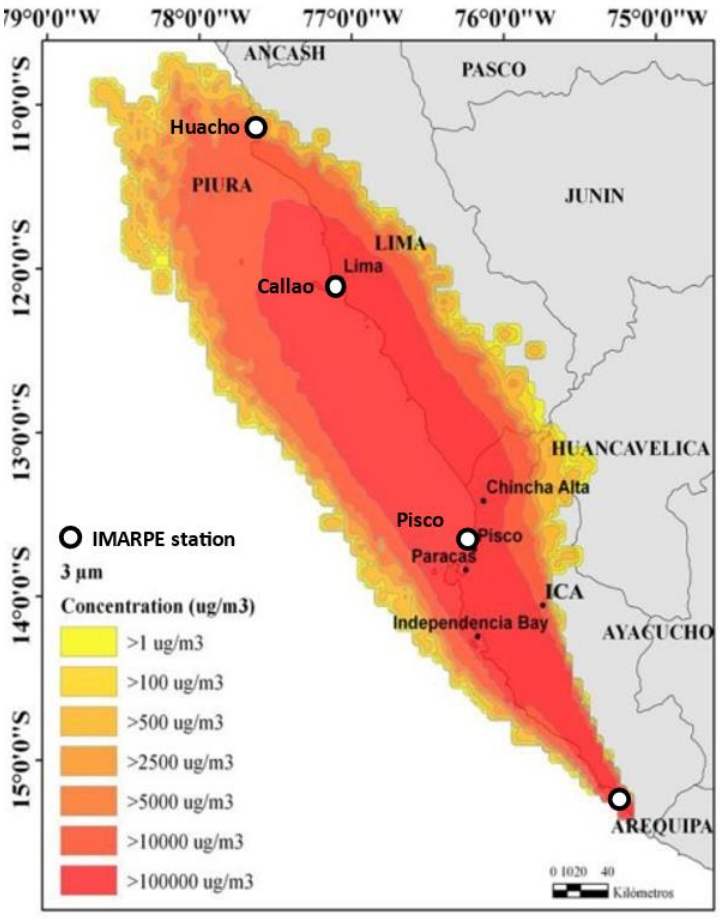

IMARPE monitoring stations

Ten coastal monitoring stations span the coast from Tumbes, on the far North Coast, to Ilo, near the border of Chile (for a distribution map, see Figure 2.4; for geographic coordinates, see Table 2.1). IMARPE provides access to their monthly SST data from these stations during the period January 2000 to February 2020, except for Huanchaco, where monthly records start in October 2008. Daily SST information has been collected at these stations since January 2018 and is data is available for download online from 2018 to February 2020.

According to the World Meteorological Organization (WMO), SST is defined as an essential climate variable, and formal meteorological protocols have been established by the Joint Committee for Guides in Metrology in order to ensure quality SST data is available globally (JCGM, 2008). Accordingly, estimates of uncertainty should always accompany in-situ SST data (JCGM, 2008). Uncertainties in SST records can result from non-systematic errors (improper use of equipment or differences in the methodologies used to obtain temperature readings between individual users) or systematic errors (such as incorrect calibration of a thermometer) (O'Carroll et al., 2019).

As indicated in Table 2.1, collection times vary by location but daily SST values consist of three averaged measurements taken during a ten to twelve hour period during daylight hours, with the exception of Callao, where temperature measurements are automatically taken every ten minutes during each 24-hour period. Daily values are used to produce monthly SST averages.

Figure 2.4: IMARPE stations showing various SST measurement methods (source of photographs: IMARPE).

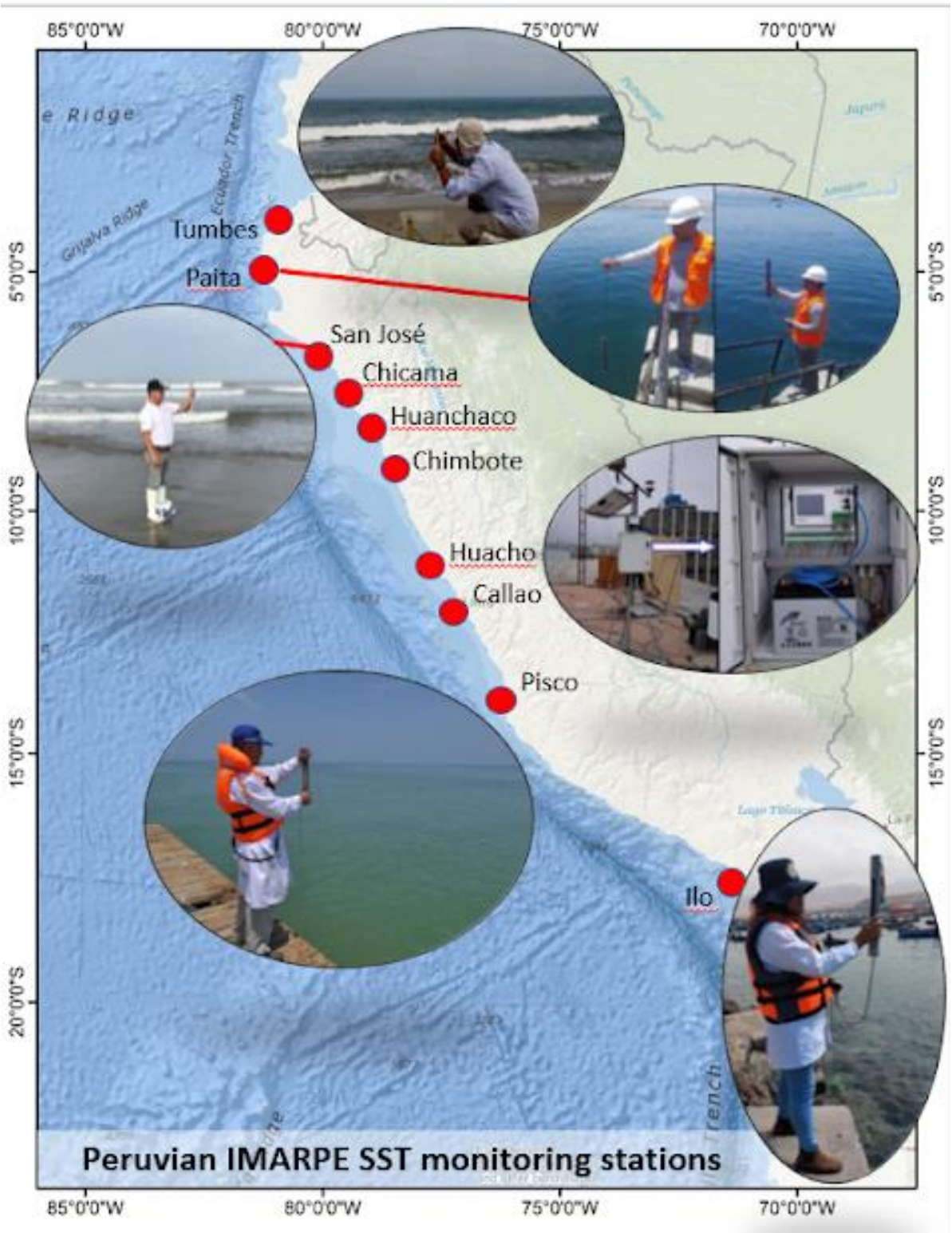

Table. 2.1 Information about IMARPE's coastal monitoring stations along the coast of Peru, including location and a description of the location, as provided by IMARPE. For all stations excepting Callao, temperature measurements are conducted using handheld thermometers three times a day. Times of measurements are specified. Instrument, as well as the range and error of the thermometer - when specified by IMARPE - is listed; otherwise, this information is listed as unsp. (unspecified). Coordinates, obtained from IMARPE, are also listed.

Location	Description	Time	Instrument (range; error)	Coordinates
Tumbes	Nueva Esperanza beach	8am, 12pm, 4pm	Hanna digital thermometer (unsp.; unsp.)	03°38'17.7" S 80°36'24.8" W
Paita	Artisanal Fishing Landing pier	8am, 12pm, 6pm	Alla France total immersion thermometer (ASTM/S63C) (-8°C to 32°C; unsp.)	05°04'37.98" S 81°07'13.98"W
San Jose	San José beach	8am, 1pm, 5:30pm	Alla France total immersion thermometer (ASTM/S63C) (-8°C to 32°C; 0.1°C)	06°46'15" S 79°58'00" W
Chicama	Puerto Malabrigo dock	8am, 12pm, 6pm	Alla France total immersion thermometer (90 ASTM 63C) (-8°C to 32°C; unsp.)	07°41'40.0" S 79°26'19.3" W
Huanchaco	Huanchaco Pier	8am, 12pm, 6pm	Alla France total immersion thermometer (90 ASTM 63C) (-8°C to 32°C; 0.1°C)	08°04'41.2" S 79°07'19.3" W
Chimbote	Port of Chimbote dock	8am, 12pm, 4pm	Kesler USA surface thermometer (total Immersion ASTM 63C-86 571118) (-8°C to 32°C; unsp.)	09°27'19.8" S 78°23'0.2" W
Huacho	National Ports Company wharf	8am, 12pm, 6pm	Alla France total immersion thermometer (ASTM 63C) (-8°C to 32°C; 0.1°C)	11°07'18.83" S 77°36'58.53"W
Callao	IMARPE dock	Every 10 min. Prior to 2010: 8am, 12pm, 4pm	After 2017: SEA-BIRD MicroCAT sensor, DA9000 data logger (unspecified; 0.01°C). Before 2017: unsp. (unsp.; unsp.)	12°03'57.78" S 77°09'30.54"W
Pisco	Pisco Playa Fiscal pier	7am, 12pm, 5pm	Ludwig Schneider total immersion thermometer (ASTM/S63C) (-8°C to 32°C; 0.1°C)	13°42'33.4" S 76°13'18.5" W
Ilo	Ilo dock	8am, 12pm, 6pm	Alla France thermometer (unspecified; unspecified)	17°38'38.4" S 71°20'45.6" W

When comparing satellite datasets to in-situ data, the associated error and uncertainty of the in-situ datasets must also be considered. Ten IMARPE stations use a variety of different handheld thermometers which are manually operated three times a day to measure SST in a designated location. The sample timing is generally in the morning, mid-day, and late afternoon or early evening, though variations exist at each of the ten stations (see Table 2.1). At Callao, IMARPE's headquarters, a temperature sensor and datalogger have been in operation since 2017, measuring SST data every 10 minutes and averaging the temperature readings to produce one daily value.

No information about the depth of water temperature sampling is provided. Instrumental calibration details are not provided, and while all but two stations provide information about the thermometer brands and models used, only five of the ten stations provide specifications about the temperature range and error or uncertainty of the thermometer used. General error range of the devices is 0.1^{o}C (0.01^{o}C in Callao), but differences in sampling techniques, water depth, and location may impart additional error to temperature readings, and inconsistencies in instrumentation (the use of digital, surface, and immersion thermometers) likely produces additional errors when making comparisons between datasets between different stations.

Methods

SST data was obtained from IMARPE's website (www.gob.pe/imarpe) and downloaded in monthly formats for each of IMARPE's ten coastal monitoring stations. Daily data was not used because of the relatively short time span of data availability (just over two years) and for reasons discussed throughout this paper (particularly the presence of cloud cover along most of the Peruvian coast and the biased impacts of cloud masking on daily SST datasets compared to monthly aggregated datasets). Monthly data was available and downloaded from 1/2000 to 2/2020 for all stations except for Huanchaco (10/2008 to 2/2020). Monthly IMARPE SST values are aggregated in the format of a full month, starting on the first day and ending on the last day of the month.

L4 MUR SST data was downloaded in 1km^2 increments that overlapped geographically with the IMARPE stations. These monthly SST averages, produced by GHRSST and aggregated by NOAA, were available from 6/2002 to present from NOAA's Coastwatch website (https://coastwatch.noaa.gov) (NOAA 2022). Because IMARPE records were not available after February 2020, MUR data was not obtained after that period. MUR SST data was displayed using the *NetCDF to raster tool* in ArcMap 10.8.1 and extracted using shapefile points in ArcMap with the geographic coordinates provided by IMARPE for each station.

The output was ten SST records spanning the period 6/2002 - 2/2020 in overlapping geographic locations where the IMARPE stations exist. The coverage period of the monthly mean SST product spans from the 16th of one month to the 16th of the next. Unlike the in-situ IMARPE records, the monthly MUR data period is not evenly spaced, but averages 30 days 10h 26m 37s (NOAA, 2022). Monthly SST averages from both datasets were compared for each of the ten IMARPE monitoring stations.

Results and Discussion

In general, satellite-derived MUR records do a good job of capturing SST variability seen in in-situ SST records along the coast of Perú (see Figure 2.5). Three broad trends are observed in the MUR datasets. In some areas, such as Paita, satellite records correlate extremely well with in-situ data. In other areas, there appear to be large, systematic temperature offsets. Callao, for example, has in-situ SST records across the period 2002-2020 average over 2.2°C lower than comparative satellite records for the same geographic location (16.1°C vs. 18.3°C). This offset is relatively consistent throughout the year (discussed in further detail below). In other areas, such as San Jose, MUR records correlate well with in-situ records seasonally, while other periods of the year are consistently marked by large offsets when compared to in-situ data. Possible reasons for annual and seasonal offsets are discussed below in further detail.

Figure 2.5 Scatter plots of monthly average IMARPE SST vs. MUR SST over the period 6/2002 - 2/2020 (except Huanchacho, 10/2008 - 2/2020).

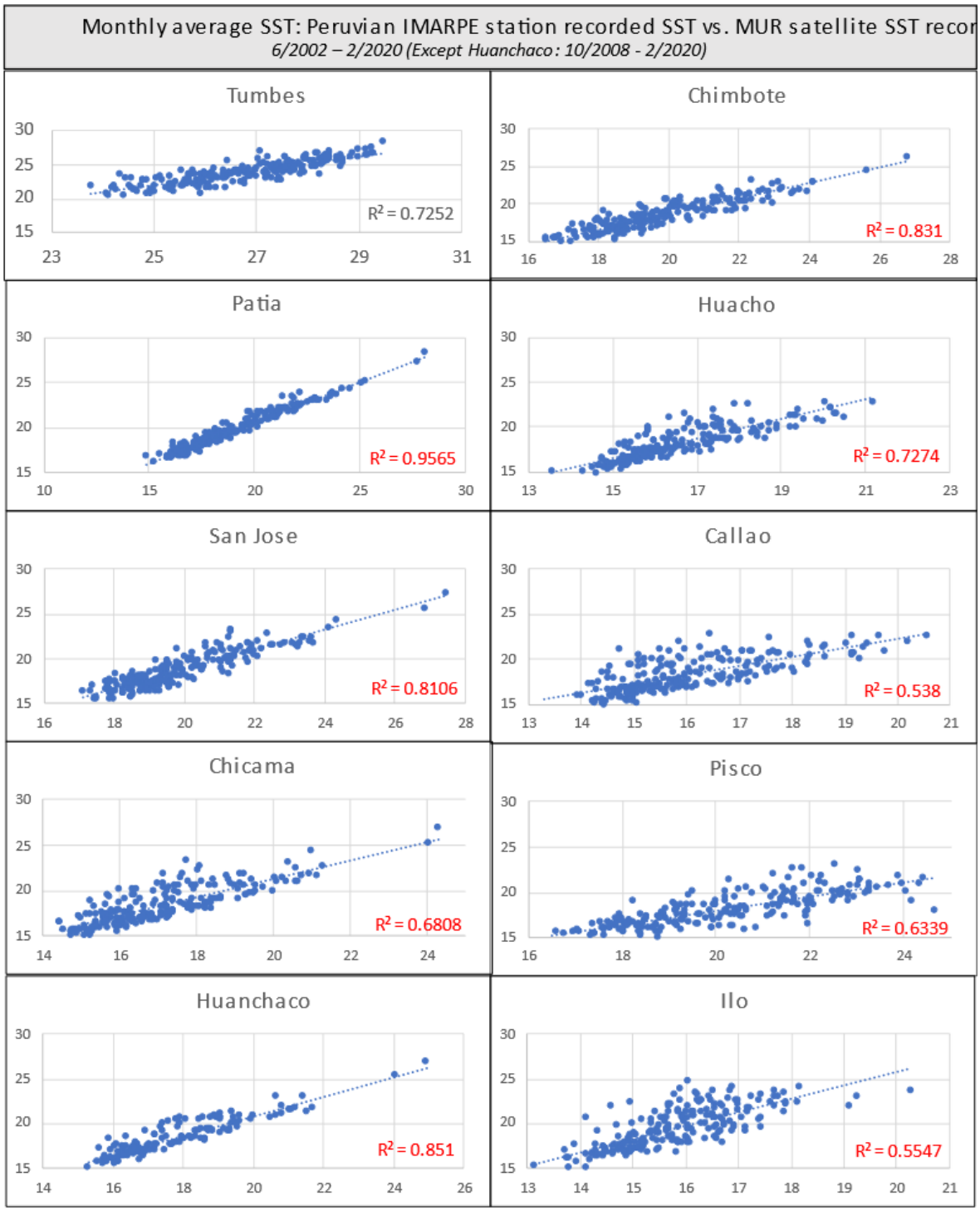

Figure 2.6: SST averages of in-situ and satellite SST measurements across the period 6/2002 - 2/2020 (except Huanchacho, 10/2008 - 2/2020). The blue boxes represent IMARPE SST, and the orange boxes represent MUR satellite data. The additional colored boxes for Tumbes and Paita represent MUR SST records from the harvest sites of each bivalve addressed in Chapters 3 (*T. hians*, from Paita) and Chapter 4 (*A. tuberculosa*, from Tumbes). A star over a box plot indicates a systematic offset of that SST record over the other record for that location.

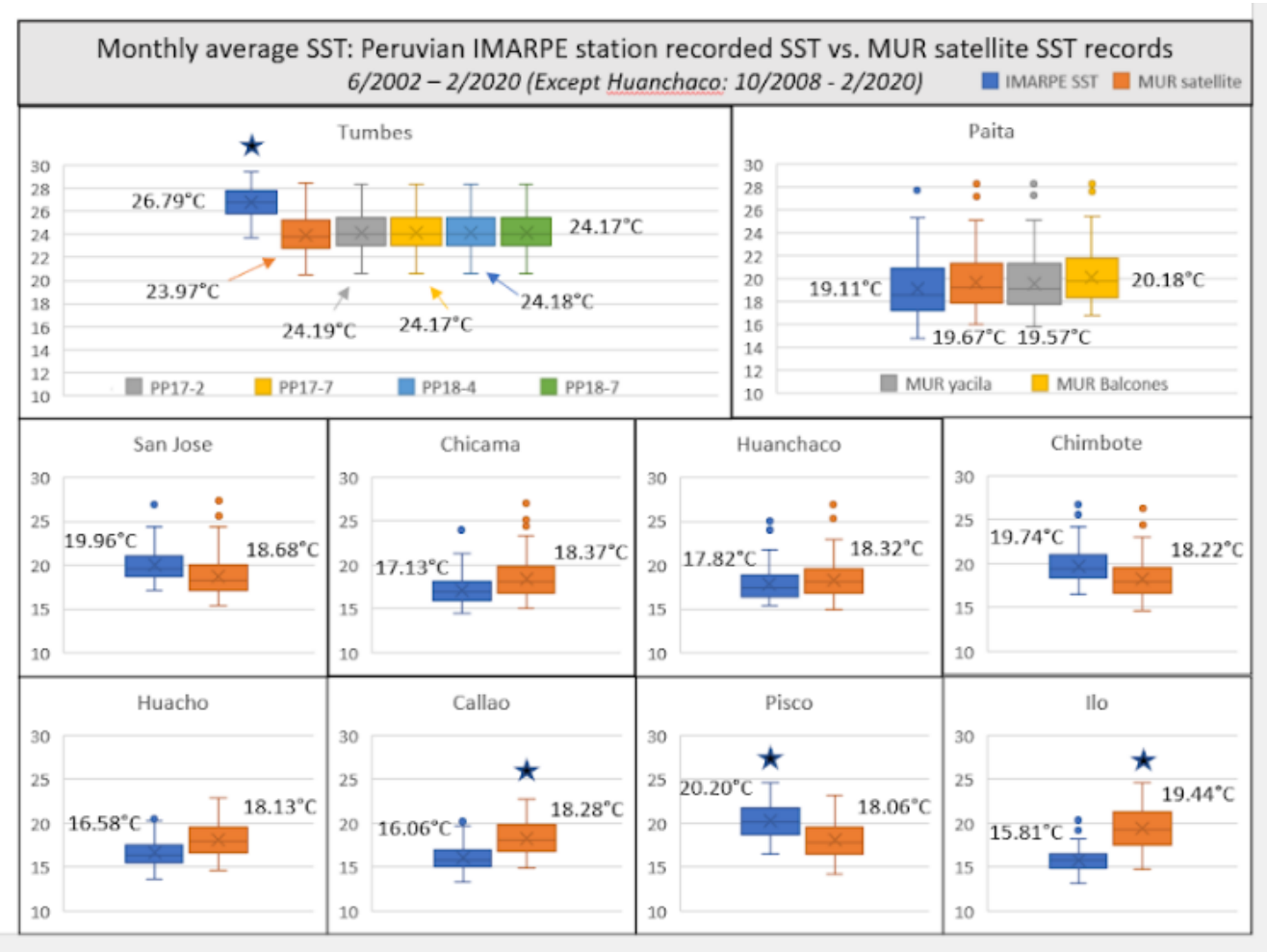

Comparing in-situ and satellite SST averages across the entire time period at each IMARPE station shows no consistent pattern in over- or under-estimation of in-situ SST by satellite data (see Figure 2.6). In Paita, San Jose, Huanchaco, and Chimbote, the locations with the highest correlation between in-situ and MUR data, MUR SST records overestimate, underestimate, overestimate, and underestimate (respectively) in-situ measurements.

Exploring the data in more depth, the author examined whether differences in the methods of in-situ measurement may explain some of the variation between SST datasets, or whether patterns in satellite-derived data could be explained by environmental variables that may result in less-accurate measurements. Paita, for example, has an extremely high R^2. IMARPE SST and satellite SST were positively correlated with $R^2 = 0.96$. Paita's SST measurements are conducted in Paita Harbor, off a pier, using an immersion thermometer. Average SST during the period 6/2002 - 2/2020 from in-situ measurements was 19.1°C, compared to 19.7°C from MUR records during this same period.

Figure 2.7: SST records at Paita during the period 6/2002 - 2/2020.

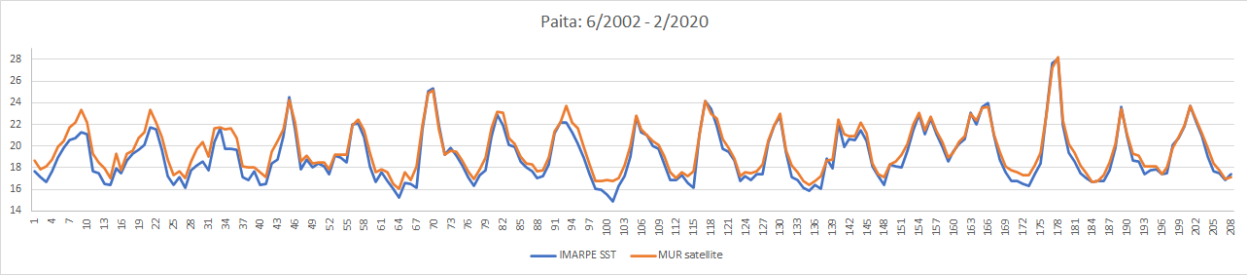

Comparing the two SST records, in general MUR records show high correlation with in-situ SST without an apparent lag or offset. While several summer periods, particularly December through February in 2002, 2003, and 2004, don't capture the full range of high SST values, subsequent summer SST peaks are captured. August (troughs) are consistently not captured by satellite-derived data, which doesn't capture the coldest winter SST values measured by in-situ devices (see Figure 2.7). This is interesting because historically, summer represents the cloudiest period along the coast of Peru, with February as the cloudiest month in Paita. During months with high cloud cover, some high-resolution satellite instrumentation is less accurate (sensors measuring IR radiation), resulting in data gaps that are filled with information from other platforms that may be lower resolution (O'Carroll et al., 2019). August, on the other hand, is the clearest month in this region, yet August is consistently when the satellite data doesn't capture the coldest SST temperatures. Comparing other IMARPE and MUR records

reaffirms this trend, indicating that cloud cover is not a major contributor to low correlation between in-situ and satellite records. Other aerosols, including dust, are known to impact the validity of satellite SST data. As noted above, concentrations of dust can result in underestimation of SST. However, because MUR data overestimates SST during winter months, and due to the distance between Paita and dustier southern regions of Peru, dust is not determined to explain small differences seen between in-situ and MUR data.

San Jose ($R^2 = 0.81$), Huanchaco ($R^2 = 0.85$), Chimbote ($R^2 = 0.83$) all have relatively high R^2, indicating moderately high correlation between the two datasets (see Figure 2.5). San Jose's SST measurements, made using an immersion thermometer, are taken from the beach, which might be expected to result in less-than accurate measurements. However, correlation in this dataset is among the highest. Huanchaco and Chimbote's records were also both produced with an immersion thermometer from a pier and a dock, respectively.

Looking at the SST data in series, differences emerge in the ability of the MUR dataset to capture the full annual range in SST variability at these locations (see Figure 2.8). In San Jose and Chimbote, MUR records appear to capture SST highs during summer months with relatively little offset, but winter SST lows from the satellite-derived records are lower than associated in-situ measurements. A possible explanation for this is that San Jose SST measurements were taken from the beach, while the MUR records were obtained across a $1km^2$ surface area of the coastal ocean. In this instance, solar heating and air mixing at the ocean interface could have resulted in higher SST in-situ measurements taken at this location. However, unlike at Tumbes, where beach measurements resulted in a consistent annual offset of 2.8°C (26.8°C in-situ and 24.0°C MUR; see Figure 2.9), San Jose SST records show a 1.3°C offset seen primarily during the winter months with MUR temperature readings lower than their in-situ counterparts.

In Huanchaco, a 0.5°C offset represents the overestimation of SST by MUR during the summer months. Both in-situ records were obtained from a pier or dock, respectively, and were measured with an immersion thermometer. Huanchaco and Chicama are the only two locations where overestimation of SST by MUR records occurs during the summer months only. In the other three locations where MUR overestimates SST (Huacho, Callao, and Ilo), this pattern is annually consistent).

A large-magnitude Coastal El Niño event in February and March 2017 is recorded in both in-situ and satellite-derived SST records from Paita to Chimbote where SST anomalies associated with the warming event lessen at stations located further south. This abrupt attenuation, typically at around 12°S, is characteristic of Coastal events, which helps distinguish them from Eastern Pacific events with impact further south along the coast (Sandweiss et al., 2020). The four outlier data points seen in the box plot for Chimbote (see Figure 2.6) all occurred during the 2017 event. In Tumbes, in-situ measurements did not register the coastal El Niño warming event, though satellite records show an anomalously high SST of 28.5°C compared to an average of 24°C for this location. Though both San Juan and Chimbote show low biases by MUR SST records during the winter months, Huanchacho does not, indicating that an environmental variable such as clouds or fog cannot systematically explain biases between SST records in this region of the coast.

Figure 2.8: SST records at San Juan, Huanchaco, and Chimbote.

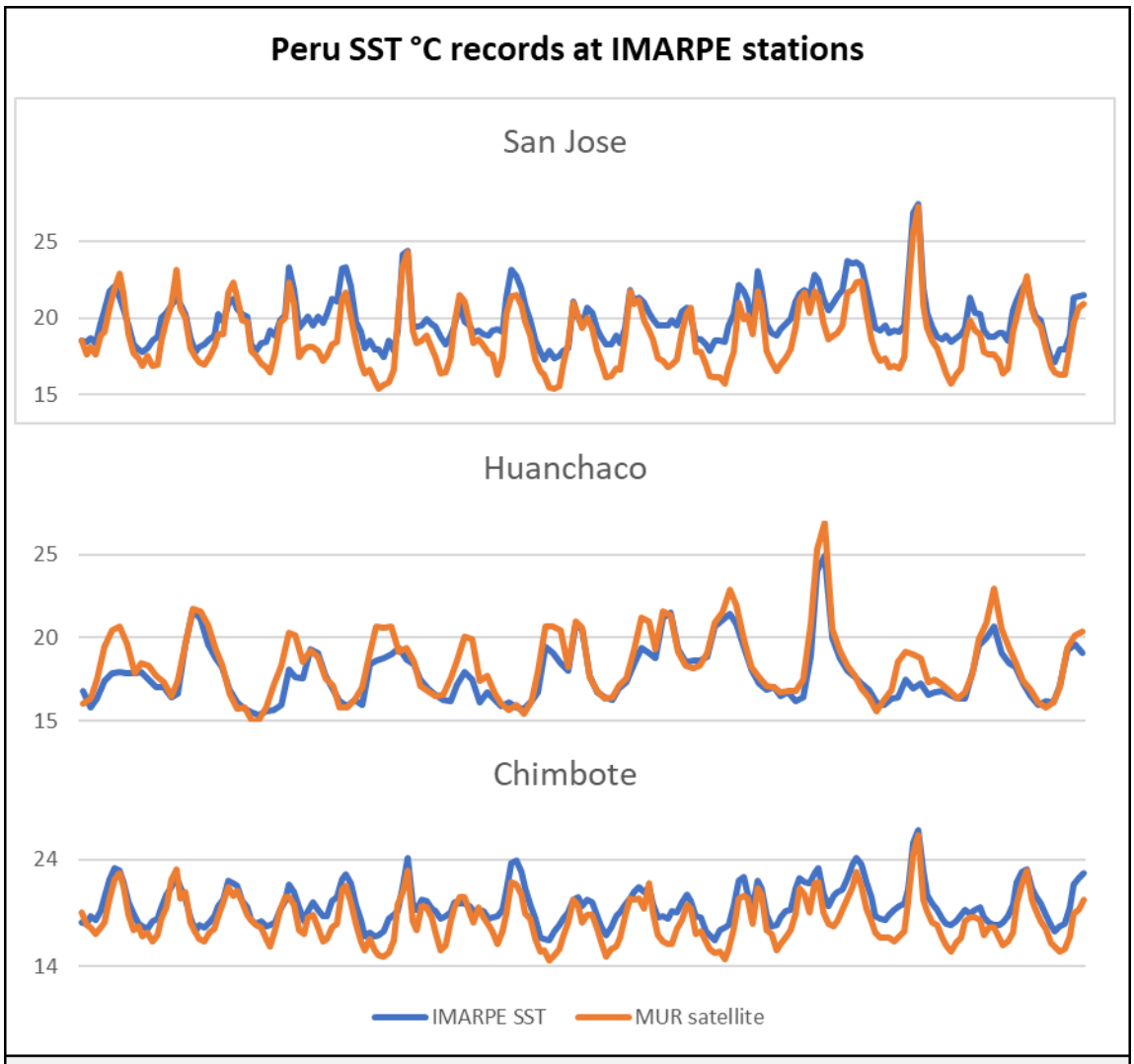

SST records from 6/2002 (left) to 2/2020 (right) except for Huanchaco (10/2008 – 2/2020).

Tumbes ($R^2 = 0.73$), Chicama ($R^2 = 0.68$), and Huacho ($R^2 = 0.73$) have moderately high R^2 values, indicating that other variables may account for a substantial amount of disagreement between in-situ and satellite SST. At Tumbes, in the far north, SST was recorded with a digital thermometer, which could produce variations in measurements since the device is not fully submerged in the water and the exact method of measurement may vary between individuals. Temperature was measured from the beach; as with San Jose, this could have resulted in warmer temperatures compared to satellite measurements. The offset at Tumbes is 2.8°C annually, with a smoothing of some peaks and lows by both records, while other fluctuations in high and low temperatures are captured by both records.

Correlation between the two SST records at Chicama (dock, immersion thermometer) is stronger during the winter than in the summer, when MUR overestimates SST. During February 2004, MUR SST is 5.5°C higher than in-situ records indicate (23.3°C vs. 17.8°C); this is higher than the average summer offset of 2-3°C, throughout the period 2002 - 2020. At Huacho (wharf, immersion thermometer), MUR overestimates SST primarily during temperature peaks in the summer months, while the majority of winter SST lows are also overestimated (represented as higher than in-situ values).

Callao ($R^2 = 0.54$), Ilo ($R^2 = 0.55$), and Pisco ($R^2 = 0.63$) have the lowest R^2 values. At Callao, IMARPE records (permanently submerged sensors attached to the Callao dock measure SST every 10 minutes) are systematically lower than MUR records. In Pisco (pier, immersion thermometer), in-situ records are higher than MUR SST, with rare points of correlation (2.1°C average difference across 6/2002 -2/2020 period). Tumbes is the only other location where in-situ records are systematically higher than MUR SST, but the difference at Tumbes could be explained by in-situ SST being measured from a beach, whereas in Pisco, measurements are taken from a pier; an area presumably with less solar heating than at the shore interface, and an area with less tidal range impacting SST measurements depending on the time of day they are collected. In Ilo, MUR SST is also systematically higher than in-situ records. Ilo's in-situ records are taken from the Ilo dock using an unspecified thermometer.

The southern coast of Perú is characterized by high concentrations of consistent winter fog, as well as intermittent dust storms during the period July through September (Briceño-Zuluaga et al., 2017). Dense lomas vegetation corresponds to the locations of IMARPE stations at Huacho, Callao, Pisco, Ilo (Moat et al., 2021). This is indicative of the impact that fog may have on satellite SST records during the austral winter. In some regions, such as Callao (in the greater Lima area), fog is persistent annually. Dust, shown in Figure 2.3, is concentrated in the Pisco region, and can spread as far north as Callao during winter months due to wind patterns. Anthropogenic mineral dust is present year-round, though overall levels of dust (natural and anthropogenic in source) may fluctuate seasonally.

Evaluating MUR records in this context, MUR SST systematically overestimates in-situ SST measurements at Huacho, Callao, and Ilo stations on an annual basis. Low correlation between SST records in Callao can likely be explained by consistent fog in this area which - unlike clouds - can cause SST overestimates, which could explain the pattern seen at this station. At Pisco, MUR SST shows a consistent underestimation bias, characteristic of the ways that annually persistent dust can skew satellite SST readings (Al-Shehhi, 2022). Because coastal high resolution SST measurements are based from IR satellite sensors, dust absorbing longwave IR radiation causes systematic underestimations of SST (Al-Shehhi, 2022). In Ilo, MUR shows a systematic overestimation of in-situ SST values; however, this pattern is more apparent during summer SST highs, when average differences can reach 6°C. Patterns like this can sometimes be explained by over-masking of clouds by satellite algorithms, particularly as ocean and air temperatures are warming during the spring and summer (Crosman et al., 2017). When over-masking happens, cold ocean SSTs are misidentified as clouds and also removed from the dataset, resulting in positive skewing and overall warmer satellite-derived SST averages, which could be the case in Ilo. This is particularly relevant since Ilo is located furthest from the equator in the study region and thus SSTs are on average, cooler than at other IMAPRE station regions examined in this research. This could result in more over-masking of clouds in satellite data than at other locations.

Exploring systematic offsets in IMARPE data

IMARPE SST monitoring stations are located on piers, beaches, and undefined coastal locations in urban areas. As noted above, systematic differences between in-situ and satellite-derived records can result from the location in which SST measurements are taken, particularly as in-situ measurements represent one point while satellite-derived records cover a larger area and SST values are averaged across the pixel. Particularly in the case of temperature measured from beaches, as in Tumbes, it is probable that a satellite-derived SST pixel will capture cooler water temperatures from the open, thus resulting in a cold bias in the MUR data.

San Jose in-situ measurements were also taken from a beach. Comparing each in-situ record to respective MUR data (Figures 2.9 and 2.10) shows that both records are systematically offset with underestimation of in-situ SST by MUR. The Tumbes record shows a systematic offset of 2.8°C (an underrepresentation of actual measured SST by MUR). When adjusted by 2.8°C across the full temporal span of the dataset, the MUR record more clearly overestimates the range of SST on both the high and low ends, but does capture the overall seasonal variability seen in the IMARPE dataset (see Figure 2.9).

Figure 2.9: Tumbes in-situ and MUR records (top) and in-situ and MUR records after MUR data was adjusted by 2.8°C (bottom).

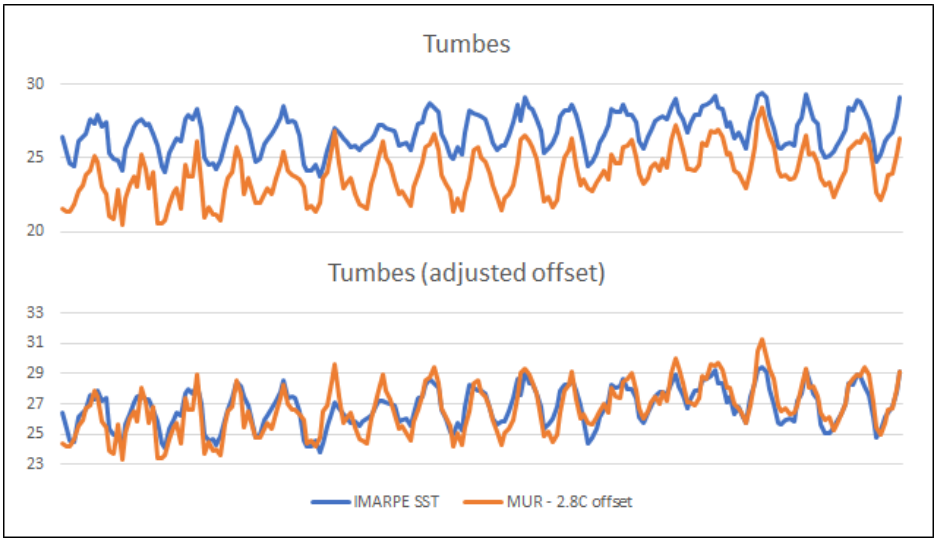

The MUR dataset from San Jose was adjusted by 1.1°C; a value equal to the average offset between the two datasets (see Figure 2.10). The resulting graph more clearly shows, as with Tumbes, the overestimation of SST range by the MUR dataset. Beach measurement location cannot explain all differences between the two datasets, however. For example, while both Tumbes SST records capture the 2007-2008 La Niña SST low in August, comparative datasets from San Jose show only the MUR dataset captures abnormally low SST during August 2007 (while in-situ measurements do not). These results, however, suggest that while satellite-derived records may show a systematic bias when compared to coastal in-situ measurements, the MUR records are nonetheless representative of the variability and range of the in-situ ones.

Figure 2.10: San Jose in-situ and MUR records (top) and in-situ and MUR records after MUR data was adjusted by 1.1°C (bottom). Vertical line indicates the 2007-2008 La Niña event.

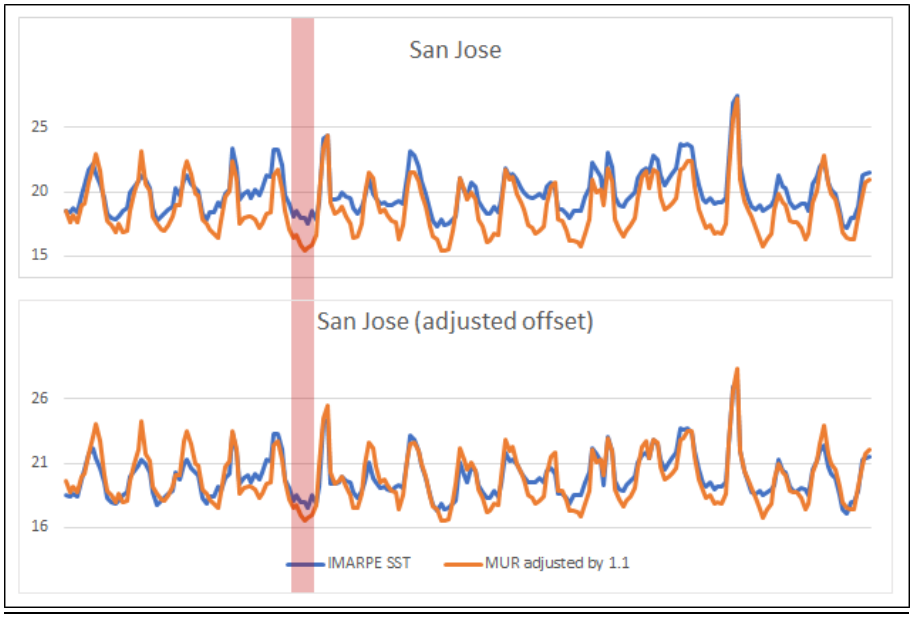

Other systematic offsets seen in the Pisco and Ilo datasets are less easily explained. In the case of Pisco, in-situ data was collected from a dock, and is generally systematically higher than MUR SST, with some exceptions seen in the first two summer periods captured by the datasets. Limited information is provided about the nature of the IMARPE dataset and changes that may have occurred in

the early years of this program. Was the designated measurement location changed after 2003, resulting in SST readings that were more representative of the Pisco region? In the case of Ilo, sufficient information about the location or method of measurement is not provided. IMARPE records indicate that measurements are taken from a "Point located in Ilo", and the geographic coordinates provided are not immediately located on the shore. The brand (Alla France) of the thermometer is specified but not the model, and no further information is given as to the capabilities of the instrument or the associated error of temperature readings.

The type of instrumentation used could also lead to systematic offsets in SST records, however, no correlations were established between type of measuring device and SST offsets at any of the ten study locations. Environmental factors (e.g., solar azimuth or cloud coverage) were also not identified that could consistently explain differences in in-situ and satellite-derived SST records across multiple sites. Other parameters that have been shown to impact the quality of satellite SST (e.g., wind speed or relative humidity) could also not be linked to correlations between SST datasets at each location.

Non-systematic offsets in IMARPE data

Non-systematic errors in both datasets could potentially result from a range of factors associated with both instrumentation or sampling strategies. Insufficient information is provided by IMARPE to assess these factors, including differences in sampling strategies at a single site over time such as immersion depth of the thermometer, actual time of day the measurement was taken, or the associated tidal range or high- or low-tide at sampling intervals.

Conclusion

In general, MUR datasets capture the variability seen in the in-situ SST records, with instances of annually systematic biases that can be addressed, such as at Tumbes. In these cases, the range of SST recorded by MUR can also be useful for coastal research. MUR datasets from other IMARPE station locations show seasonally specific variability and lower correlation with in-situ measurements, such as in

San Jose, Chicama, Huanchaco, Chimbote, Huacho, and Ilo. In some instances, such as in Huacho, these can be explained by environmental factors such as fog and dust dispersion during winter months. In the case of Ilo, environmental conditions (cold water) may lead to over-masking of clouds, thus impacting MUR records. In other regions, like Callao and Pisco, fog and dust (respectively) are environmental explanations for systematic biases in the data. Another challenge in assessing the validity of MUR high resolution SST data is the error associated with the in-situ records, which varies between IMARPE stations, and must not be overlooked (JCGM, 2008).

This research indicates that MUR SST records from the Peruvian coast accurately represent variability, but do not consistently accurately represent actual SST values or the range of SST over time. As in other areas of the world, corrections can be developed to account for biases in MUR SST measurements due to predictable environmental factors in the Peruvian coastal region, including cloud cover, fog, and dust (Al-Shehhi, 2022). Improvement of cloud screening algorithms, particularly in coastal regions, is currently a focus of climate and meteorological research and advances in this field will benefit the validity of satellite SST along coastal Peru. In particular, the use of IR bands used for SST measurements should be shifted to improve the ability of these radiometers to also detect cloud cover, as suggested by O'Carroll et al., (2019) as well as increased research into other methodologies used for cloud and other aerosols detection (2019).

Short of these advances, research using MUR SST data along coastal Perú should include a thorough examination of environmental and anthropogenic factors in the region of study that may impact satellite-derived SST datasets. In some cases, as demonstrated in the study regions discussed in this paper, corrections can be made to address systematic biases. In other cases, further exploration is needed to identify variables that may explain deviations between in-situ and satellite data. In dynamic environments such as coastal Peru, this process is iterative and satellite-based SST datasets are bound to keep improving.

CHAPTER 3
TIVELA HIANS AS NORTH COAST PERUVIAN PALEO-ENSO PROXIES

Marine bivalves have been used to reconstruct ENSO on the coast of Peru because their shell material can record changes in marine conditions during El Niño and La Niña events. Despite their relatively short lifespans, in an arid region devoid of other common paleoclimate proxies, bivalves provide a means of examining changes in SST and can be sourced from archaeological sites. This chapter examines the Peruvian clam *Tivela hians* (commonly known as concha blanca) as a potential paleoclimate proxy. Fortnightly growth rings were identified microscopically in four *T. hians* valves and used to guide sampling of the outer shells for stable isotope analysis. Oxygen isotope (δ18O) patterns from four shells were examined and translated to SST conditions during the bivalves' lifespans. These reconstructed SST records were compared to local in-situ SST measurements and all but one shell record was determined to represent local conditions well. This research indicates that well-preserved archaeological T. hians, found abundantly on the Chira Beach Ridges on the North Coast of Peru, may be used as environmental SST proxies and potentially as a source of information about past seasonal SST range and variation in this region. These findings are valuable given the dearth of other ENSO proxies in this region during the mid- to late-Holocene transition where abrupt changes in ENSO correlate with cultural changes on the North Coast.

Background and Literature Review

This research examines the potential of bivalve *T. hians* as an archive for marine environmental conditions. Of particular interest is determining if oxygen isotopes from shell material accurately reflect ambient SST conditions. By using growth data, isotopic data can be placed in time accurately in order to compare to instrumental data. Biomineralization processes of *T. hians* are similar to those of other marine carbonate bivalves in that their shell matrices precipitate in equilibrium with the $\delta^{18}O$ of ambient water (Dettman, Reische, and Lohmann, 1999; Grossman and Ku, 1986; White et al., 1999). Oxygen isotope fractionation in shell carbonate is temperature dependent, enabling the creation of SST

equations based on the relationship between ambient temperature of the marine environment and the isotopic fractionation in the shell's aragonitic growth rings, forming a chronological record (Epstein et al., 1953; Dettman, Reische, and Lohmann, 1999; Grossman and Ku, 1986; White et al., 1999). However, species-specific biological factors, known as vital effects, have been suggested to prominently affect processes of oxygen isotope fractionation (Carré et al., 2005; Pérez-Huerta and Andrus, 2010).

The goal of this research is to examine *T. hians* as a potential source of paleoenvironmental information through the comparison of modern samples to in-situ SST records. This is particularly meaningful because *T. hians* are abundant in archaeological shell middens found on North Coast beach ridges dating to the mid- to late-Holocene (Ortlieb, Fournier, and Macharé, 1993; Richardson III, 1983). Middens are repositories of paleoenvironmental data (Andrus, 2011). These refuse piles are formed through the collection and discard of local materials (in the case of shell middens; bivalves) from a local area (Andrus, 2011). Shell midden environments generally favor preservation. Thus, archaeological samples from past millennia may have utility as paleoENSO indicators. Identification of isotopic signatures in modern *T. hians* presents the potential for archaeological samples to be used as records of SST variability during periods lacking sufficient paleoclimate proxies (Sandweiss and Kelley, 2012). Use of this species as a climate analogue during a period where other paleoclimate records are limited on the North Coast of Peru could represent additional opportunities for the reconstruction of mid- and late-Holocene ENSO activity in this region (Sandweiss et al., 2001; Sandweiss et al., 2007).

On the North Coast, beach ridges are underutilized sources of data for ENSO chronologies. Beach ridges are prograding ridges of sand, gravel, or other material, that accrete parallel to the shoreline. Sequences of these ridges form time-transgressive sets (Shafer Rogers et al., 2004). Beach ridge formation in this region is due in part to the extreme seismicity of northern Peru, where tectonic activity produces unconsolidated sediments inland that become available for riverine transport to the coast (Sandweiss et al., 2009). During El Niño years, heavy rains provide a mechanism for transport of

this material and ENSO events following large earthquakes have been shown to transport large amounts of sediment to river deltas (Belknap and Sandweiss, 2014; Sandweiss et al 2009). Despite wave activity, longshore currents deposit sediment materials northward from stream or river mouths, which may be preserved as ridges as the shoreline progrades (Belknap and Sandweiss, 2014; Shafer Rogers et al., 2004). Because El Niño is a driver in this "earthquake–flood–ridge–sand incursion disaster cycle", beach ridges are associated with EN events (Belknap and Sandweiss, 2014; Sandweiss, Rollins, and Richardson, 1983; Sandweiss, 1986; Sandweiss et al., 2009). Due to these formation processes, North Coast beach ridges represent low resolution records of strong El Niño events (Sandweiss et al., 2007; Reid, 2007).

In northern Peru, remains of *T. hians* shells are common at the Chira Beach Ridges. This ridge set was formed during the mid- to late-Holocene, and the ridges of this set have been well-constrained by radiocarbon dates by previous researchers (Ortlieb, Fournier, and Macharé, 1993, Richardson III, 1983). PaleoSST reconstructions using *T. hians* from the Chira Beach Ridges would enhance our understanding of several millennia of marine conditions on the North Coast during a period marked by a scarcity of paleoclimate records (Sandweiss et al., 2007; Sandweiss and Kelley, 2012).

T. hians examined in this paper were harvested in October 2019. These modern samples were not alive during the 2017 El Niño, but further research could identify whether *T. hians* continue growing during high SST anomalies, making their utility as climate indicators even greater. Despite having a limited distribution, they are nonetheless valuable because of their potential for paleo-reconstruction in this well-studied beach ridge sequence.

Site Description

North Coast of Peru and ENSO

Strong oceanic upwelling reinforces aridity along the North Coast of Peru, except in the Gulf of Guayaquil in the far north at the border with Ecuador (Ramos, 2010). This study focuses on two sites in the Paita region, Playa Grande, in Yacila, and Playa de Punta Balcones, Negritos (referred to as Yacila and

Punta Balcones, respectively), where natural sandbanks provide habitat for *T. hians*. Clams grow in abundance in these banks, as they have throughout the Mid-Holocene, demonstrated by their density in nearby archaeological shell middens. South of Punta Balcones, beach ridges span a long expanse of beach, located approximately 30 km to the *Rio Chira* (4°50'S).

Figure 3.1: Map of Paita study region, indicating the Paita IMARPE station location, which has the same coordinates as the MUR satellite SST data. The two collection locations of *T. hians* are also indicated: Punta Balcones, at the far north, located proximate to the Chira Beach Ridges, visible as strips of a lighter color radiating down the coast from Punta Balcones, and Yacila, south of the IMARPE station.

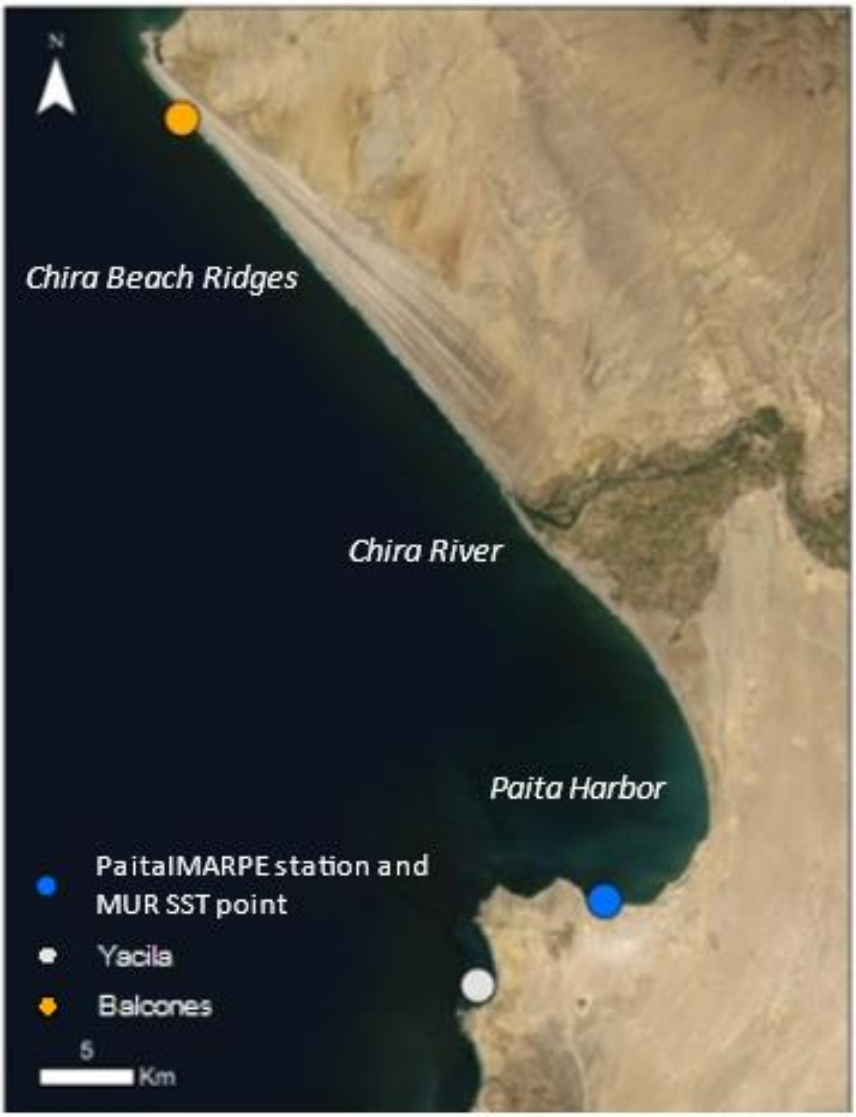

Location	Location
Paita IMARPE station and MUR point	-5° 4' 24.63", -81° 7' 12.32
Yacila	-5° 7' 27.07", - 81° 9' 41.13
Balcones	-4° 43' 39.50", - 81° 17' 1.48

Both Punta Balcones and Yacila are within the vicinity of Paita Harbor and the Instituto del Mar del Peru (IMARPE) monitoring station. Yacila has the closest natural banks of *T. hians* to the SST-monitoring IMARPE station, thus allowing a more confident assessment of the shells' record of SST conditions that these shellfish grew in. Punta Balcones, while somewhat further from the IMARPE station, is adjacent to the Chira Beach Ridges. Here, different environmental parameters may have affected growth of *T. hians* found at the archaeological site. Comparing bivalves from both locations can help identify any changes in metabolic processes resulting from differences in environmental conditions between the two collection sites.

Oceanic transition zone: Equatorial and Peruvian Currents

As described in Chapter 2, two major ocean currents meet between 4 - 6°S, forming an oceanic transition zone (Barahona, Vélez-Zuazo, Santa-Maria, and Pacheco, 2019). The Equatorial Counter Current moves tropical waters further from the equator, where they mix with cooler waters which are traveling toward the equator by means of the Peruvian Current. Both currents are deflected westward into the open Pacific (Olsson, 1961). Changes in the strength of these currents can cause the oceanic transition zone to shift along the northwest coast of Peru. For example, during El Niño events, the Equatorial stream becomes stronger, driving warmer tropical waters into the normally cooler Peruvian nearshore region (Olsson, 1961).

Chira Beach Ridges

Near the mouth of the Chira River (see Figure 3.1) is a set of nine major beach ridges that stretch approximately 20 km parallel along the coast (Ortlieb, Fournier, and Macharé, 1993; Richardson III, 1983; Shafer Rogers et al. 2004). These ridges are composed of sand and shells and contain signs of human activity such as archaeological middens, fire pits, and artifacts (Richardson III, 1983, Belknap and Sandweiss, 2014). The largest ridges stand 6 m high and were accumulated during alternating periods of

seismic activity, El Niño-induced high flow events, and subsequent transport of sediments down the Chira River to the coast (Shafer Rogers et al., 2004).

The top 20 – 50 cm of these ridges contain dense layers of shell deposits resulting from anthropogenic accumulations (Belknap and Sandweiss, 2014). *T. hians* and *Donax obesulus* are major components of shell refuse in the Chira Beach Ridge sequence (Belknap and Sandweiss, 2014; Richardson III, 1993; Ortlieb, Fournier, and Macharé, 1993; Shafer Rogers et al., 2004). At Chira, harvesters utilizing the ridges and discarding shellfish remains moved seaward as new ridges formed with the progradation of the coast (Reid, 2007; Richardson, 1983). Belknap and Sandweiss argue that these discarded shells formed an 'armor' which holds the otherwise mobile ridge sand in place in the face of persistent onshore southwest winds (Belknap and Sandweiss, 2014). Not only has human modification of the landscape at the Chira Beach Ridges helped preserve these paleoENSO records, but the deposition of archaeological artifacts stratigraphically associated with shells and other datable materials also provides an opportunity to date each ridge, thus developing a chronology for the formation of ridge sets over time (Sandweiss and Kelley, 2012).

The time-transgressive Chira ridges are well-constrained by radiocarbon dating to the mid- to late-Holocene, ca. 5180 – 414 cal yr BP (Ortlieb, Fournier, and Macharé, 1993, Richardson III, 1983, Shafer Rogers et al., 2004). Their formation correlates with an abrupt late-Holocene ENSO transition that is reported to have occurred on the North Coast of Peru ca. 2.9 ka (and on the south coast between 4.5-3 ka) (Carré et al., 2013; Sandweiss et al., 2020). Radiocarbon dates of charcoal and bivalves show that the oldest ridges, dating to 5141 cal yr BP, formed farthest east (Belknap and Sandweiss, 2014). As the beach ridge plain prograded, progressively more recent ridges formed westward during major EN events, adjacent to the shoreline, with the most recent ridge dating to 414 cal yr BP (AD 1547) (Belknap and Sandweiss, 2014). Each ridge represents multiple El Niño events, with a preservation rate of one ridge per every ~500 years (Shafer Rogers et al., 2004).

The largest inter-ridge depression dates to ca. 2800 cal yr BP, corresponding to a period of major transition from lower to modern-frequency EN behavior on the North Coast (ca. 2900 cal yr BP) indicated by bivalve assemblages as well as other proxies throughout the Pacific basin (Sandweiss et al., 2001). Some researchers suggest the lack of ridges dating to this transitionary period is attributed to the sudden increase in EN frequency and subsequent depopulation of the Chira region (Belknap and Sandweiss, 2014; Shafer Rogers et al., 2004). During periods of lower EN frequency, ca. 5800 – 3000 cal yr BP, major beach ridges separated by larger depressions may have formed because greater lengths of time between EN-induced flooding would have resulted in less transport of tectonically-dislodged sediments to the coast, allowing these materials more time to accumulate, thus resulting in larger transport events and subsequent ridge formation (Shafer Rogers et al., 2004; Sandweiss et al., 2001). As EN frequency increased, the style of deposition shifted to smaller beach ridges because sediment accumulation time between EN floods was far less (Shafer Rogers et al., 2004; Sandweiss et al., 2001). This pattern is noted on the North Coast plains of Chira, Piura, and Santa (Shafer Rogers et al., 2004). Also noted is an overall trend of high nearshore wave action for at least the past 5200 years (Shafer Rogers et al., 2004; Sandweiss, 1986). The abundance of intact *T. hians* on these well-dated ridges creates the opportunity for the reconstruction of SST during this period.

Tivela hians

T. hians are filter feeding clams that bury themselves in depths of 5-20 cm of sand, occupying the intertidal and infralittoral zones. They grow in sand banks that typically remain submerged in 0.2 to 0.5 m of water during low tide (Carrasco De La Cruz, 2012). The geographic distribution of this species in Peru is limited to the Piura Region on the north coast (Carrasco De La Cruz, 2012). Heavy exploitation of this marine resource limits its size distribution; not much information is available about the *T. hians* fishery, but average valve lengths are noted to be between 21 - 76 mm at San Pedro and San Pablo beaches in the Bay of Sechura, just south of the Paita region (Carrasco De La Cruz, 2012).

Factors impacting *T. hians* growth. Peruvian bivalves respond to changing environmental and climate conditions that affect their growth rates, biomineralization, and resulting shell carbonate material. In addition to SST, environmental parameters such as salinity and marine upwelling can impact precipitation of carbonate shell. Species-specific factors, including increased age, can cause slower growth rates (Tanabe et al., 2020).

Age. As bivalves age, their growth rate slows, which effectively smooths the climate records contained in their shell matrices (Tanabe et al., 2020). In early age, bivalve growth is faster, resulting in the precipitation of more shell in shorter periods of time. Growth rates need to be accounted for so that $\delta^{18}O$ values from periods of faster growth don't bias results. To account for this, sampling methods were guided by lunar growth patterns in the shell matrix, each sample represents approximately 28 days. To compensate for further unknowns in growth rates of *T. hians*, $\delta^{18}O$ compositions of the samples were assessed for maximum, minimum, and mean values during the bivalves' lifespans. Averaging helped reduce biases that result from unequal weight given to isotope data during periods of faster growth. *T. hians* examined in this research are relatively young (<3 years) and likely have relatively consistent growth rates throughout their lifespans since they died as a result of harvesting rather than natural causes associated with changes in growth and biomineralization. The methods outlined in this paper are applicable for archaeological samples when the exact date of death is unknown.

Salinity. Seawater salinity, related to freshwater flux in the ocean, is linked to changes in $\delta^{18}O_{water}$ (Conroy et al., 2017). Seasonal variations in salinity impact $\delta^{18}O_{water}$ range (minimum and maximum $\delta^{18}O_{water}$) and must be accounted for in SST equations (Conroy et al., 2017; Wanamaker, Kreutz, Schöne, and Introne, 2011). Changes in salinity in the study area were examined to assess the impact of salinity on $\delta^{18}O_{water}$ and the impacts were determined to be minimal. Along most of the arid coast of Peru, limited freshwater flux via precipitation and riverine sources means that ocean $\delta^{18}O_{water}$ and salinity do not vary dramatically during normal, non-El Niño conditions (Carré et al., 2013; Grados et

al., 2018). To confirm this, the author examined moderate-resolution satellite records (2.5-minute resolution WorldClim data) across the study region, which show average monthly precipitation at 25 mm or less during non-El Niño years, with rainfall heaviest in January through April during El Niño events, as expected (Fick and Hijmans, 2017).

Along the far northern coast, however, equatorial tropical surface water is driven southward by the Ecuador-Peru Coastal Current, bringing warmer (T > 23°C) water of relatively lower salinity (S < 33.5) toward the Paita region (Chaigneau et al., 2013). The lower salinity of this water mass results from freshwater flux from rainfall and riverine sources nearer the equator (Grados et al., 2018). From the south, the Perú Coastal Current and Perú Oceanic Current bring colder and higher salinity surface water T < 13°C and S < 34.3 water equatorward, toward the Gulf of Guayaquil near the border of Ecuador, which is then deflected westward, forming the Pacific Cold Tongue (Rosales Quintana et al., 2021; Grados et al., 2018). In the transition zone formed by the confluence these distinct water masses, a seasonally dependent salinity gradient forms in the coastal region. This salinity gradient is more latitudinally stratified in the summer (see Figure 3.2). This transition zone was explored in further detail to identify the range of seasonal salinity that might impact $\delta^{18}O_{water}$, as well as changes in salinity that may occur during ENSO events.

Figure 3.2: Patia salinity gradients in summer (left) and winter (right) in the study region. Modified from Grados et al., 2018.

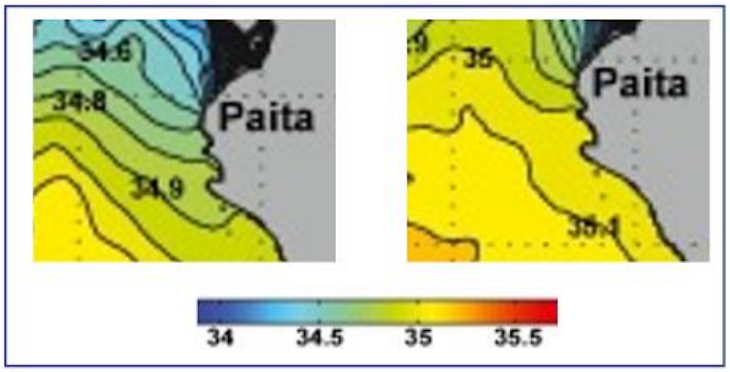

In the Paita region, seafloor salinity data from the three areas of interest (Paita Harbor IMARPE station, Yacila, and Punta Balcones) were examined at a resolution of 0.01° x 0.01° (1 km^2). 8-day averages are available from August 2011 to present from the Multi-Mission Optimally Interpolated Sea Surface Salinity Global Dataset (Melnichenko, 2021). Salinity was examined over the data availability period during summer and winter periods. During non-ENSO years, average annual salinity between the three locations was 34.8 $\pm$ 0.1 PSU. Salinity was consistently marginally higher at the Paita IMARPE station and Yacila locations than at Balcones, with only several exceptions. According to previous research on seawater salinity in the eastern tropical Pacific, this amount of seasonal variation translates to a standard deviation of 0.03‰ for $\delta^{18}O_{water}$, or approximately 0.1°C (Carré et al., 2013).

Complex currents in the Paita nearshore transition zone result in some changes to expected salinity characteristics during ENSO events, though Grados et al. (2018) note that this may also be related to a lack of in-situ salinity data in this region. In the Paita nearshore, El Niño events are associated with increased salinity of surface waters which are pushed equatorward, as well as less latitudinal stratification in the immediate area (Grados et al., 2018). During the strong 2015 Eastern Pacific El Niño event, for example, salinity values were statistically similar between the locations, with an annual average of only 0.04 PSU difference between the Paita Harbor, Yacila, and Punta Balcones. La Niña events, on the other hand, result in steeper latitudinal stratification of salinity in the Paita region and increased negative salinity anomalies (Grados et al., 2018). Decreases in salinity from the surface to 50-100 m deep in the water column during La Niña events in the nearshore coastal region are linked to increased upwelling of deep, colder and fresher waters compared to normal conditions (Grados et al., 2018).

Marine upwelling. Marine upwelling along the coast is generally strong and consistent except during an ENSO warming event. During an El Niño year, trade winds over the equatorial Pacific weaken, the thermocline deepens off the coast of Peru, and upwelling weakens. During a La Niña event,

upwelling is reinforced due to strengthening of the trade winds, causing cold SST anomalies in the coastal region (Grados et al., 2018). Because *T. hians* examined in this research were not alive during an ENSO event, it is unlikely there were large-scale changes in marine upwelling and primary production that would have impacted their growth and biomineralization.

Tidal range. Peru has a semidiurnal tidal cycle consisting of two high and two low tides of approximately equal size each lunar day. In Yacila and Punta Balcones, in far northern Peru, tidal range averages 2 m. Because this species remains buried and submerged at low tide (twice a day), solar heating or other environmental factors impacting regularly- or periodically- exposed bivalves will have less of an impact on *T. hians* than bivalves that are exposed to the air during low tide.

Location. The beach in Yacila is just under 7 km from the IMARPE station and the collection location in Punta Balcones is ~46 km from the station (see Figure 3.1). Punta Balcones, located closer to the equator, can be expected to have warmer average SST, despite its exposed coastline. MUR high resolution satellite SST records, shown to be highly consistent with in-situ measurements from the Paita Harbor IMARPE station when compared to in-situ measurement for the period 6/2002 - 2/2020 (R^2 value of 0.95; see Chapter 3), do show that Yacila, located further south, averages cooler SST than Punta Balcones (see Figure 3.3).

Figure 3.3: Paita IMARPE in-situ SST record compared to MUR satellite-derived SST during the same period at the same location. MUR SST records from two adjacent locations, *T. hians* harvest sites at Yacila and Punta Balcones, are also displayed. See Figure 3.1 for map.

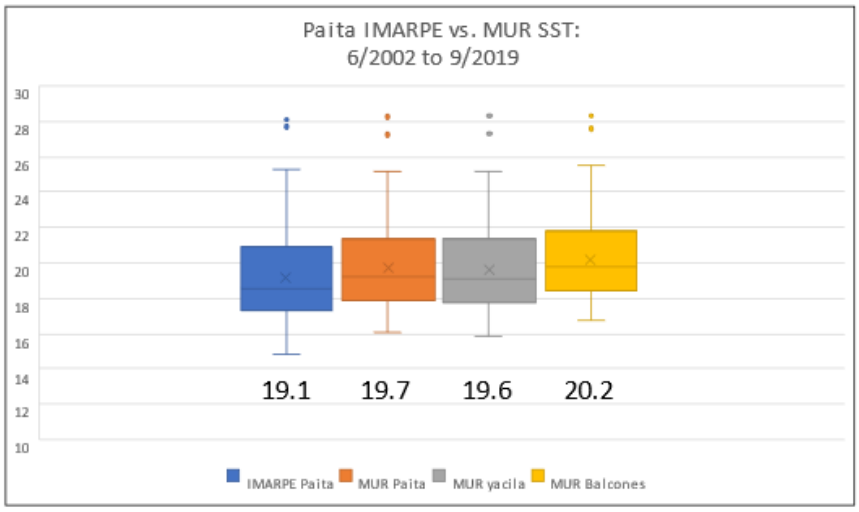

An examination of satellite SST data over nearly 20 years for the Yacila and Punta Balcones areas show that while temperatures in Punta Balcones are warmer than in Yacila, SST variations and anomalies occur concurrently at the two sites, increasing confidence in using the satellite-derived SSTs to build isotopic SST equations for the sample *T. hians*.

Table 3.1: Paita average aggregated monthly SST (°C) during period 6/2002 - 9/2019 from in-situ SST measurements (IMARPE) and remotely sensed SST (MUR high resolution satellite-derived data) for Paita Harbor, Yacila, and Punta Balcones.

Average monthly SST in °C during period 6/2002 - 9/2019		
Record type	**Location**	**SST in °C**
In-situ: IMARPE station	Paita Harbor	19.1
Remote: MUR satellite	Paita Harbor	19.7
Remote: MUR satellite	Yacila	19.6
Remote: MUR satellite	Punta Balcones	20.2

Methods

Sample collection

In October 2019, the author collected *T. hians* from two locations along the coast immediately after they were harvested and shucked by local fishermen: Playa Grande, Yacila (October 17), and Playa de Punta Balcones, Negritos (October 18). Approximately six complete (intact valves and hinges) bivalves were collected from fishermen at each site. These specimens had been harvested at low tide from a water depth of less than 0.5 m.

Sample preparation

Samples were cleaned with a toothbrush to remove soft material and were transported to the laboratory in Ziploc bags wrapped in bubble wrap to prevent breakage. In the laboratory, four valves were selected: two valves from two different *T. hians* bivalves from Yacila (Yacila 1 and 2) and two valves from two *T. hians* from Punta Balcones (Punta Balcones 1 and 2). Valves were further cleaned using deionized water (DI) and prepared in resin casts. The resin molds were polished using DI water on a Pace Technologies Nano 1000T Grinder Polisher and cut using a Buehler IsoMet 1000 Precision Cutter with DI water to an average width of 1.5 mm. The resulting resin profiles were polished using 1200 grit and 4000 grit paper and then mounted on microscope slides.

Valve cross-sections were examined using a binocular microscope with reflected light. Each profile was photographed and then visually evaluated for growth lines (see Figure 3.4). Fortnightly growth cycles of approximately 14 days were clearly identifiable on each of the cross sections (reflecting the lunar period of the new to full moon, 13.5 lunar days, and full to new moon, 15 days) (Tanabe et al., 2020). These cycles were marked on the photographs and used to guide sample collection at monthly resolution via microdrilling.

Figure 3.4: Microscopic photograph of thin section of *T. hians* (Yacila 2 specimin). Growth rings are visible in the enlarged section showing lunar periods used to guide microdrill sampling or carbonate material.

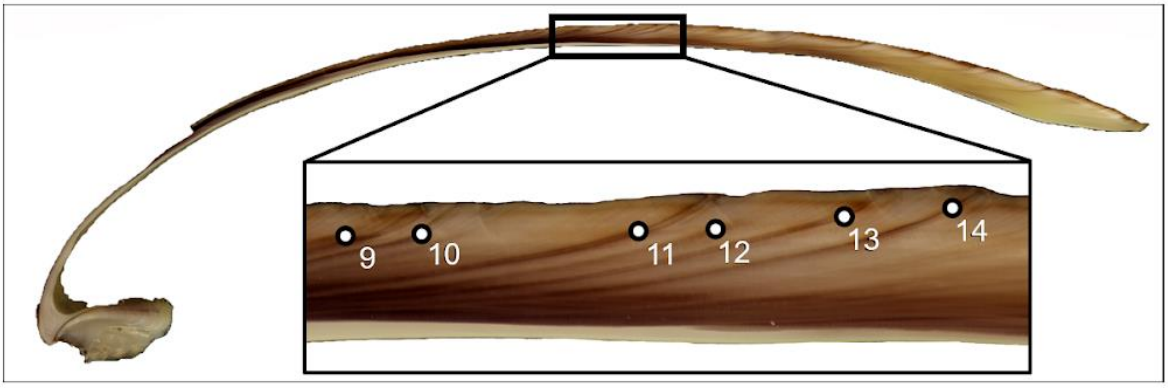

Collection of powder samples from the outer shell layer was completed using a MicroMill using methods outlined in Carré et al. (2013) and Carré et al. (2014), see Appendix A. Contiguous microsampling was performed from the umbo toward the ventral margin of each sample as far as growth lines were clearly identifiable. This yielded samples of approximately lunar monthly resolution, based on guidance from the visual identification of fortnightly growth lines associated with fortnightly lunar periods. Once drilled, powder samples were collected using a razor blade under a microscopic lens to aid sample collection. Compressed air was used to remove any remaining powder before the next sample was drilled.

Powdered carbonate samples were sent to the Stable Isotope Laboratory at Iowa State University for oxygen and carbon isotope analysis. Continuous flow mode analyses were performed using a ThermoFinnigan Delta V Plus mass spectrometer coupled to a GasBench with a CombiPal autosampler. Isotopic corrections (regression method) were performed using reference standards NBS-18 and IAEA 603. Isotope results were reported in parts per thousand (per mil, ‰). Analytical uncertainty (1σ) of isotopic results can be found in Table 3.2.

Table 3.2: Analytical uncertainty (1σ) associated with isotopic values of $\delta^{18}O$ and $\delta^{13}C$ produced in laboratory analyses at the Stable Isotope Laboratory at Iowa State University. All uncertainties are reported with respect to the Vienna Pee Dee Belemnite (VPDB) scale. * denotes that samples from Yacila 1 specimen were analyzed on two separate occasions, resulting in two different values of uncertainty resulting from separate calibrations.

Analytical uncertainty (1σ) of $\delta^{18}O$ and $\delta^{13}C$				
	Punta Balcones 1	**Punta Balcones 2**	**Yacila 1***	**Yacila 2**
Samples (monthly interval)	16	18	26	23
δ13C uncertainty	± 0.09‰	± 0.08‰	± 0.08‰ and ± 0.04‰	± 0.04‰
δ18O uncertainty	± 0.10‰	± 0.06‰	0.06‰ and 0.06‰	± 0.06‰

Results and Discussion

Bivalve SST Calculations

The relationship between SST and $\delta^{18}O$ records of the *T. hians* samples were examined using a modified version of Grossman and Ku's 1986 SST equation. Dettman, Reische, and Lohmann (1999) made minor corrections to Grossman and Ku's fractionation equation, which assesses shell aragonitic $\delta^{18}O$ in order to infer SST. In their modified equation,

$$T(C°) = 20.60 - 4.34 \times (\delta^{18}O_{aragonite} - (\delta^{18}O_{water} - 0.27))$$

$\delta^{18}O_{aragonite}$ represents the oxygen isotopic composition of shell material (VPDB), and $\delta^{18}O_{water}$ is the oxygen isotopic composition of the ocean (VSMOW) in which the bivalves grew. The $\delta^{18}O_{aragonite}$ is a function of seawater temperature and the isotopic composition of the water (Epstein et al., 1953). For past times, both SST and the isotopic composition of seawater are generally unknown, thus it is common to use a nominal value for $\delta^{18}O_{water}$. In the case of the above equation, 0 is often used as an assumed

value if $\delta^{18}O_{water}$ cannot be measured. Globally, some ocean regions, especially coastal areas, experience large fluctuations in both salinity and $\delta^{18}O_{water}$, thus paleoSST reconstructions can be difficult in these regions because the value that should represent $\delta^{18}O_{water}$ in the equation is unknown, or difficult to estimate. The above equation with an assumption of $\delta^{18}O_{water} = 0$ was used to initially calculate average monthly SST based on $\delta^{18}O_{aragonite}$, for each of the four specimens.

To assess *T. hians* ability to track ambient marine conditions, their $\delta^{18}O$-derived SST monthly averages were compared to measured SST during each shell's lifespan. To create comparative SST averages from IMARPE daily records, daily IMARPE records were obtained from https://www.gob.pe/imarpe. Starting from the day of collection, daily values were aggregated into 28-day increments and then averaged. This increment approximately represents two lunar periods of approximately 14 days, on which microdrill sampling was based (Carré et al., 2013). Box and whisker plots (Figure 3.5) show calculated maximum, minimum, and mean SST during the lifespan of the *T. hians* specimens compared to in-situ SST measurements.

Figure 3.5: Average IMARPE SST and $\delta^{18}O$-derived average SST with $\delta^{18}O_{water}$ value of 0. Yacila 1 & 2 reconstructions systematically underestimate average SST by 2.3°C. Punta Balcones 1 reconstructed SST overestimates SST by 0.7°C and Punta Balcones 2 underestimates SST by 2°C when using unmodified SST equation with $\delta^{18}O_{water}$ value of 0. Of note: the length of the SST record for the Yacila samples is shorter than the lifespan of the bivalves because daily SST records are not available from IMARPE before 1/1/2018.

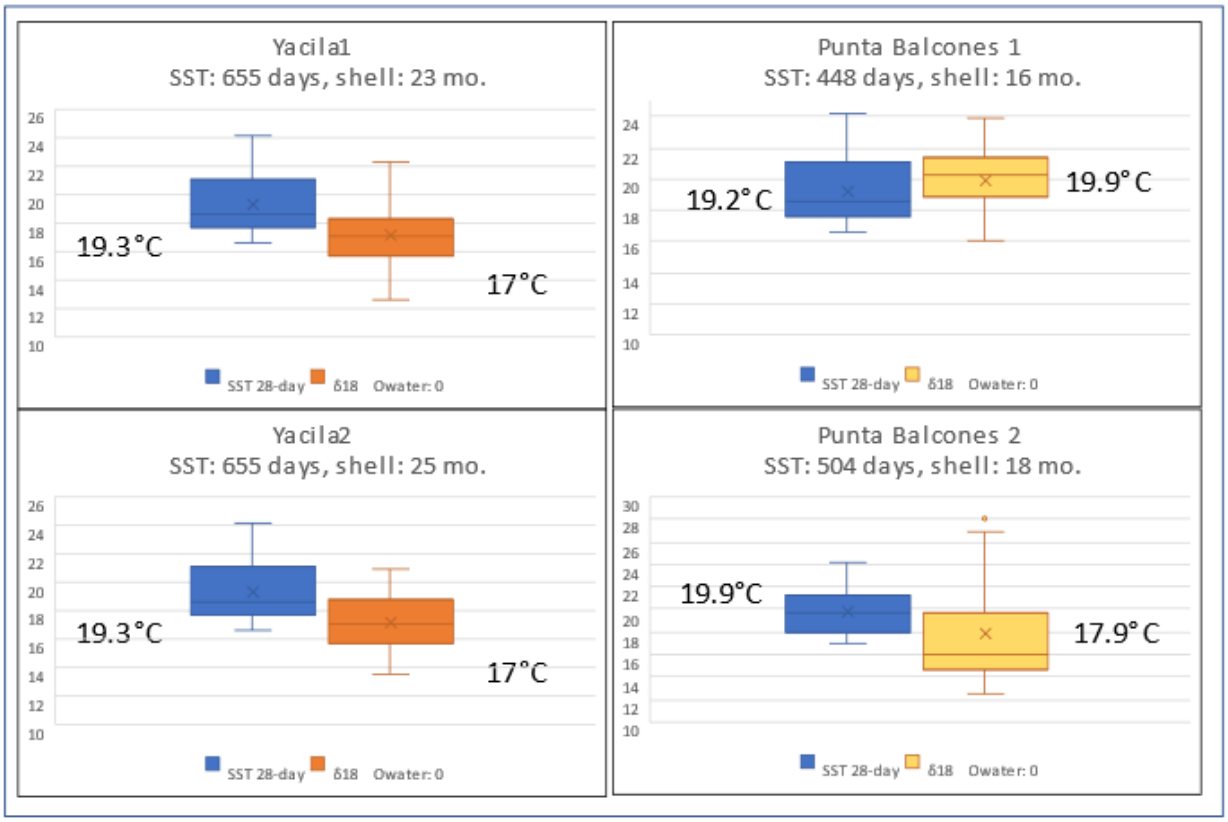

Shell reconstructed SST was systematically lower than in-situ measured SST values in three out of four of the *T. hians* samples. As seen in Figure X, both Yacila SST reconstructions show the mean value of SST throughout the shell's lifespans as systematically lower than measured SST. The Punta Balcones shells were different: one overestimated and one underestimated SST values. Punta Balcones 1 shell SST was higher than measured SST while Punta Balcones 2 underestimated measured SST during its lifespan.

Modification of $\delta^{18}O_{water}$ value in SST equation

Given that three of the four bivalve $\delta^{18}O$-derived SST records systematically underestimated SST, $\delta^{18}O_{water}$ in the Dettman SST equation was adjusted so that the overall means of the in-situ and $\delta^{18}O$-derived SST for the Yacila samples were the same. This value was $\delta^{18}O_{water} = 0.52$:

$$T(C°) = 20.60 - 4.34 \times (\delta^{18}O_{aragonite} - (0.52 - 0.27))$$

Prior to modifying $\delta^{18}O_{water}$ in the SST equation, Punta Balcones 1 SST overestimated measured SST, while Punta Balcones 2 underestimated it similarly to the pattern seen in the Yacila samples. Using the same $\delta^{18}O_{water}$ value (0.52) with the Punta Balcones 2 bivalve isotope data adjusted the mean of the reconstructed SST, bringing it much closer to that of the measured SST (19.9°C in-situ average SST vs. 20.2°C bivalve isotope-derived SST mean) (see Figure 3.6). For Punta Balcones 1, however, this equation produced an average reconstructed SST of 22.2°C across the shell's lifespan, while the IMARPE record indicates a mean SST of 19.2°C during the same 18-month period. A water value of -0.16 was required to adjust the mean values of Punta Balcones 1 reconstructed SST to reflect measured SST. However, true average SST at Punta Balcones may be higher than 19.2°C, as indicated by MUR records of Punta Balcones, which indicate average SSTs of 19.9°C during the shell's lifespan, about 0.72°C higher than SST recorded in Paita harbor, further south. It may also be possible that different adjustments need to be made to the SST equation for samples from Punta Balcones due to different environmental conditions at the two harvest locations. Differences in $\delta^{18}O_{water}$ in Yacila and Punta Balcones are possible, but it is also possible that differences in salinity between the sites may impact $\delta^{18}O$ precipitation in bivalve carbonate.

Figure 3.6: Average IMARPE SST and $\delta^{18}O$-derived average SST with $\delta^{18}O_{water}$ value of 0.52. Adjusted Yacila 1 & 2 reconstructed average SST equals in-situ SST during both bivalves' lifespans. Punta Balcones 1 adjusted reconstructed average SST overestimates SST by 3°C. Modification of the bulk water value to -0.16 adjusts SST to the same average values. Punta Balcones 2 overestimates average SST by only 0.3°C when using $\delta^{18}O_{water}$ 0.52.

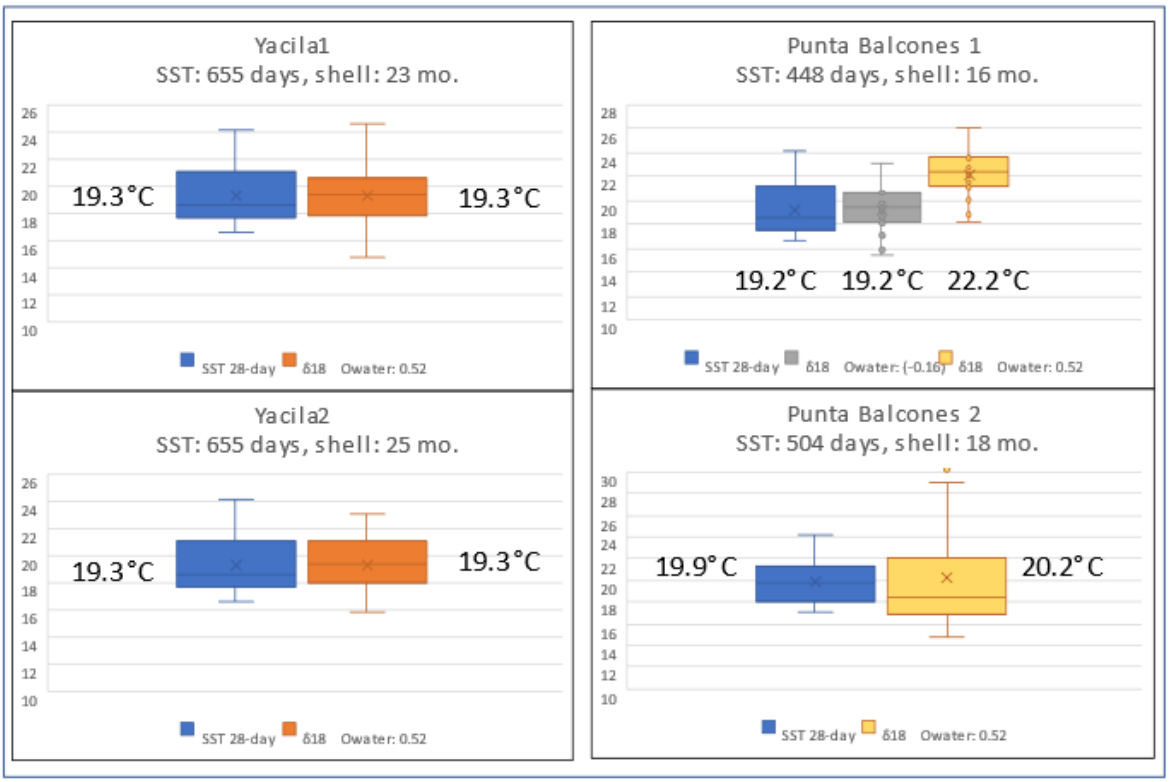

While both shells were harvested from the same location in Punta Balcones, numerous factors could be responsible for the differences in these shells' isotope values, including environmental factors impacting growth as well as errors made during isotope sampling. Overall, results indicate that systematic offsets of the shells are similar across different locations and can be compensated for in SST equations. A water value of 0.52, when used in the modified Grossman and Ku equation, did systematically adjust the reconstructed mean SST values to be the same as the measured SST for three of the four measured samples.

This $\delta^{18}O_{water}$ value does not agree with other recorded $\delta^{18}O_{water}$ values from Peru. According to the Global Seawater Oxygen-18 Database, $\delta^{18}O_{water}$ from Peru is -0.5 $\pm$ 0.2 (Schmidt, Bigg, and Rohling, 1999). The reference source for these data comes from four measurements obtained by Andrus et al.

from the Chicama region (2002). Nonetheless, more $\delta^{18}O_{water}$ measurements are needed from the coast to understand if there is a discrepancy between the $\delta^{18}O_{water}$ values in the Paita and Chicama regions.

Reasons for offset

Yacila shells show a systematic offset from measured SST. The bivalve isotope data suggest that temperatures in Yacila during the shell's lifespan were 2.3°C celsius lower than the SST recorded by the station in Paita Harbor. A possible explanation for this is that SST is higher within the protected harbor where the station is located and about 2°C cooler on the beach in Yacila outside of the harbor. While this temperature discrepancy is not confirmed by the MUR SST data, there are no in-situ measurements available from other locations within the study area which could shed more light on the actual differences between temperatures in and outside of the harbor. Importantly, the potential error for the isotopic SST reconstructions is 2°C. This should also be taken into consideration when considering systematic offsets in the Yacila samples and in one of the Punta Balcones samples.

Examining the range of the bivalve-derived SST for each shell (Figure 3.6) does show that seasonal variation is captured by two specimens: Yacila 2 and Punta Balcones 1. Yacila 1's estimated SST has a range of 2.3°C higher than that indicated by in-situ records from the same time period. Punta Balcones 2, the specimen with an isotopic record that does not appear to match ambient conditions, has an SST range of more than twice that of in-situ records, and an isotopic range of 3.57, which is unlikely high for a bivalve growing during non-ENSO conditions.

Table 3.3: Range of bivalve-derived SST, IMARPE measured SST, and $\delta^{18}O$.

	Yacila 1	**Yacila 2**	**Punta Balcones 1**	**Punta Balcones 2**
Range: bivalve °C	9.8	7.4	7.8	15.5
Range: IMARPE °C	7.5	7.5	7.5	7.1
$\delta^{18}O$ Isotope range	2.26	1.67	1.79	3.57

Stable carbon Isotopes

As noted in Chapter 1, the relationship between seawater $\delta^{13}C$ and precipitation of $\delta^{13}C$ in bivalve carbonate material is more complex (Andrus, 2011; Branscombe, Schulting, Lee-Thorp, and Leng, 2021; Freitas, Clarke, Kennedy, Richardson, and Abrantes, 2005). Bivalve specemines Balcones 1 and Yacila 1 show a moderate and weak negative correlation, respectively, between $\delta^{13}C$ and $\delta^{18}O$, while Balcones 2 and Yacila 2 show weak positive correlations. Annual cyclicity of $\delta^{13}C$ is not observed in any of the four *T. hians* stable carbon isotope records. Comparison of stable isotope records from the four valves also doesn't show any clear drop in both $\delta^{13}C$ and $\delta^{18}O$ values, which might indicate an influx of freshwater from a sudden increase in river discharge or heavy precipitation event (Carré et al., 2013). $\delta^{13}C$ records were not examined further for the specimens due to unknown variables at the collection locations (e.g. salinity, SST, dissolved inorganic carbon) and due to the complexity in interpreting stable carbon isotope records (Branscombe, Schulting, Lee-Thorp, and Leng, 2021).

Challenges in the use of bivalves as paleoenvironmental proxies

Caution must be taken when using archaeological bivalves as paleoenvironmental proxies for a number of reasons. Diagenesis, the transformation of the shell matrix into inorganic material post-death, must be identified in archaeological specimens, as this process will impact the isotopic records that were stored within the carbonate shell matrix. When shell valves are adequately preserved and there are limited signs of diagenesis, relative or absolute dating is necessary to fit these data into a long-term ENSO chronology. The marine reservoir effect can also pose challenges for radiocarbon dating marine carbonates because of cycling of older carbon through the water column that precipitates in carbonate shell material can make the specimen appear older than it actually is. This can be addressed by independent dating of stratigraphically associated, short-lived terrestrial materials. Another concern is the short lifespan of Peruvian bivalves. Even when assigned to a time period when dated, the short lifespan of Peruvian bivalves means that a single valve provides a brief snapshot of environmental

conditions, spanning – at most – several years. Cross-species reconstructions or comparisons are one way to expand the utility of these brief windows of information. There are challenges involved with cross-species comparisons due to the impact of vital effects on isotope fractionation, and caution must be used when creating a paleorecord from multiple species. Ensuring an adequately large sample size will help create more confidence in statistical analyses and recreations of SST variability.

Conclusion

Based on evaluation of reconstructed SST values and environmental parameters possibly related to the offset between measured and isotopic SST, it appears that *T. hians* does have value as a paleoENSO proxy. When the isotopic composition of water is adjusted, the SST equation accurately reconstructs average measured SST throughout the lifespan of each bivalve, seventy five percent of the time. Differences in environmental conditions between the two locations may help explain some of the differences between the Yacila and Punta Balcones bivalve isotope records data. Furthermore, SST variability appears to be well captured by this small sample set, which is of more value than reconstructing SST when using archaeological bivalves due to unknown isotopic water values. Overall, this preliminary research indicates that *T. hians* are promising candidates for paleoenvironmental reconstruction of SST range and variability associated with ENSO events and building on these findings should enable researchers to draw conclusions about climate conditions and about ENSO during the shells' lifespans. However, additional research is needed to identify whether *T. hians* are temperature tolerant enough to continue growth during warming anomalies. To accomplish this, specimens need to be collected that were alive during an Eastern Pacific or Coastal El Niño.

The methods used here to examine average reconstructed SST can be applied to archaeological *T. hians* sourced from the Chira Beach Ridges. Accumulations of *T. hians* remains along time-transgressive and temporally constrained beach ridges should provide a record of ENSO variability during the mid- to late-Holocene. Using the methods outlined in this paper would allow climate

reconstruction during this period, where few other records exist. These analyses will be of utility in the fields of archaeology and paleoclimatology, particularly for research on the mid- to late-Holocene transition period ca. 4200 and 2900 cal yrs BP when changes are observed in the processes of beach ridge formation that are coincident with abrupt shifts in ENSO frequency and intensity (Shafer Rogers et al., 2004).

CHAPTER 4

EXAMINING ANADARA TUBERCULOSA AS RECORDS OF ANOMALOUSLY HIGH SST

A. tuberculosa is a common mangrove cockle known locally as concha negra. Harvested for millennia (Diriger et al., 2019), archaeological specimens may have utility for helping us reconstruct paleoenvironments during the Holocene. Here, the author explores four *A. tuberculosa* bivalves harvested by a colleague, Matthieu Carré, in 2017 and 2018. Two of these bivalves were alive during both the 2015-2016 and 2017 El Niño events, and two were alive during the 2017 event. This species precipitates shell in isotopic equilibrium in the same way that the similar aragonitic mangrove species *Senilia senilis* does (Carré et al., 2019). Growth ring and $\delta^{18}O$ analyses indicate that *A. tuberculosa* capture average SST and seasonal fluctuations in SST throughout the year, but these four samples' oxygen isotope patterns do not accurately represent the range of ambient marine temperature. Factors impacting oxygen isotope fractionation in shell carbonate, including salinity, are explored, and potential growth breaks and changes in biomineralization patterns are identified as potential causes of misalignment between isotope-derived and measured SST. More research is needed to determine if *A. tuberculosa* are temperature sensitive enough to systematically close their valves during anomalously high SST, halting shell precipitation and causing breaks in their isotopic records.

Study area

Tumbes, Peru (~3.5°S), located approximately 20 km south of the border of Ecuador, is the southernmost range of *A. tuberculosa*. Tumbes is home to the largest mangrove forests in Peru and coastal marine conditions are influenced by the confluence of two major ocean currents, the southward Ecuador-Perú Coastal Current and the northerly Peruvian Coastal Current (Barahona, Vélez-Zuazo, Santa-Maria, and Pacheco, 2019). North of 4–5°S, the equatorial front separates tropical and relatively fresh water from cooler, more saline waters moving north along the coast (Grados et al., 2018). This junction is home to steep seasonal SST and salinity gradients that form due to the mixing of equatorial

and subtropical surface water (Gandy Maria Rosales Quintana et al., 2021; Olsson, 1961). These gradients have marked seasonal patterns, and are also influenced by ENSO events, as discussed in Chapters 2 and 3.

Under neutral ENSO conditions described in Chapters 1-3, Tumbes, at the southern mouth of the Gulf of Guayaquil, is located within the lower range of the tropical water mass dominated by relatively warm ($T > 23°C$) and fresh ($S < 33.5$ PSU) tropical surface water (Grados et al., 2018). The salinity gradient in this region is more apparent than SST gradients associated with the equatorial front. This is because the Gulf of Guayaquil is influenced by precipitation from the Inter Tropical Convergence Zone (ITCZ) as well as the mixing of lower salinity river water into the gulf (Grados et al., 2018).

SST and salinity gradients are seasonal due to the displacement of the equatorial and tropical surface waters during the summer (Grados et al., 2018). In the summer, no apparent SST gradient forms along the coast of the Gulf of Guayaquil in the equatorial front region; however, a salinity gradient does exist (see Figure 4.1) (Grados et al., 2018). Both salinity and SST gradients are more apparent in the austral winter months, when the subtropical anticyclone is stronger and located further north, displacing more saline and cooler coastal waters north by 2-3° (Grados et al., 2018). SST follows a clear seasonal pattern (see Figure 4.2).

Figure 4.1: Temperature and salinity gradients along coastal Peru in summer (top) and winter (bottom). Image modified from (Grados et al., 2018)

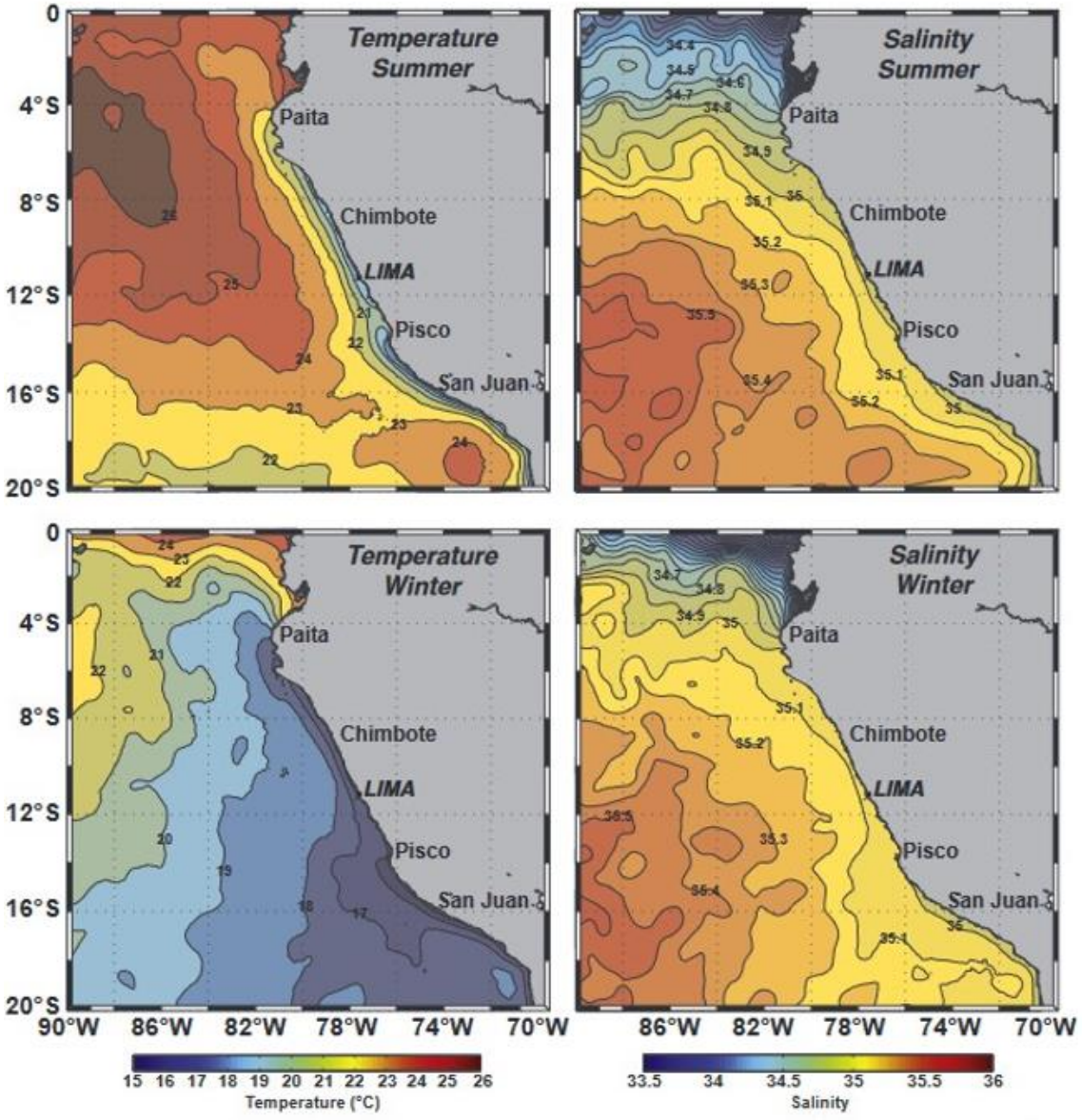

During moderate to strong Eastern Pacific or Coastal El Niño events, the thermocline deepens in the nearshore and upwelling of deep, cold water weakens, resulting in warmer surface water (Grados et al., 2018). Grados et al. reconstructed the distributions of SST anomalies between 4°S and 18°S using decades of data from IMARPE coastal monitoring station and shipboard measurements (2018). Results from SST anomaly distributions compiled by Grados et al. are not reliable north of ∼2–3°S, due to a scarcity of data in this region (2018). Temperature anomalies of up to 4 °C can be observed in the top 50 m of the water column between 2°S and 14°S (Grados et al., 2018). Salinity profiles in the Gulf of Guayaquil during El Niño events are more complex; lower salinity surface water would be expected during poleward depression of the equatorial current, but this is not observed (Grados et al., 2018). Between 0–2°S, increases of salinity between 0.2–0.3 PSU are present in the top 30 m of the water column. These anomalies are attributed to limited salinity data in this region requiring broad interpolations, as well as to meandering patterns of the equatorial front which might allow saline intrusions in equatorial surface waters (Grados et al., 2018). In contrast, during moderate to strong La Niña events, the coastal region experiences an influx of anomalously cold SST (15–16 °C) and fresh water (Grados et al., 2018). Near-coastal upwelling is enhanced, attributed in part to the deepening of the thermocline, as well as the strengthening of trade winds.

Because of the complex marine conditions in the Gulf of Guayaquil, understanding the impact of environmental variables on bivalve growth in this region is difficult. The lack of SST and salinity measurements poses additional challenges to understanding how bivalve shell isotopic compositions are impacted by their ambient environment.

Figure 4.2: Monthly average SST in-situ SST measurements from Caleta Cruz, Tumbes during the period January 2000 to February 2020 (26.7°C). Caleta Cruz is located almost 30 km from Puerto Pizarro, the collection site of *A. tuberculosa* discussed in this paper. Data source: IMARPE.

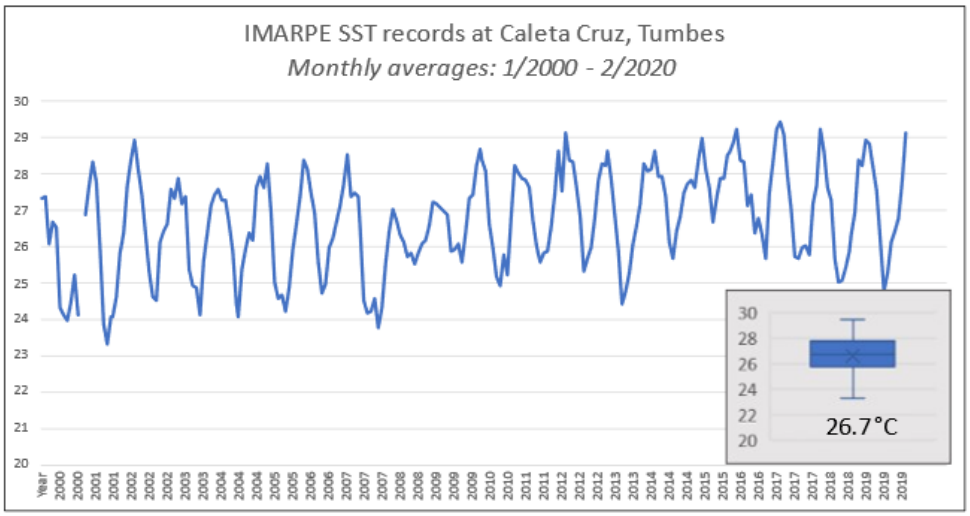

A. tuberculosa

A. tuberculosa grows in natural banks submerged approximately 15 cm deep in mud in mangrove swamps (MacKenzie, 2001). These mangrove environments are characterized by *Rhizophora mangle*, red mangroves, which grow along the shores and island peripheries of lagoons (MacKenzie, 2001). The majority of *A. tuberculosa* grow near to or amongst prop roots and canopies of mangrove trees, though some live in intertidal mud flats and up to the low tide line in proximity to trees (MacKenzie, 2001). The extent of this range is 50 to 100 m wide, on average (MacKenzie, 2001). Peru's diurnal tides mean that every 24-hour period, some *A. tuberculosa* are exposed for approximately four hours, twice a day (MacKenzie, 2001).

A. tuberculosa have been harvested for millennia by coastal communities (Diriger et al., 2019). In the Tumbes region, *A. tuberculosa* are overharvested by local fishermen who have a preference for larger-sized individuals. The species is also under pressure due to the process of conversion of mangroves into shrimp farms (Diriger et al., 2019). *A. tuberculosa* are reported to grow rapidly during their first few months of life; fisherman state that they grow from seed to a harvestable size within

several months, and experimental research confirms that the species can reach harvestable sizes between 3-8 months of age (MacKenzie, 2001). Research on this species in northern Mexico indicates that they can reach 60 mm within 1 year (Felix-Pico et al., 2011). In Costa Rica, natural populations have been shown to grow rapidly during the first 2 years of life and to attain their full length (average of 81 mm) at 5 years of age (Borda and Cruz, 2004). *A. tuberculosa* average under 55 mm long in heavily harvested areas such as Peru (MacKenzie, 2001). Other research has indicated slower growth in various distribution areas, likely related to the effects of varied SST (see discussion in Borda and Cruz, 2004). *A. tuberculosa* are reported to grow faster when consistently submerged in water (MacKenzie, 2001). This suggests that a single population, dispersed between prop roots and the low tide zone, may demonstrate variable growth rates due to location.

A. tuberculosa spawn when they reach a minimum length of 23-26 mm (MacKenzie, 2001). May through September is the season marked by spawning activity of this species, though some researchers note spawning can occur throughout all seasons (MacKenzie, 2001). Borda and Cruz (2004) note a correlation between spawning and warmer temperatures; increased spawning is also correlated with increased precipitation associated with El Niño events. Reproductive cycle is known to impact growth rates of bivalves, but further research is needed to understand its impact on *A. tuberculosa* growth rates. Other factors affecting growth include changes in seasonality linked with SST and salinity gradients in the study region, as well as primary productivity in the water column.

The isotopic compositions of *A. tuberculosa* valves can be expected to reliably reflect temperature and salinity changes during their lives, according to research on similar aragonitic mangrove species such as *Senilia senilis* (Carré et al., 2019). However, it is unknown if *A. tuberculosa* close their valves during high SST anomalies and stop precipitating new shell material, creating a break in their isotopic records that must be identified and accounted for when constructing $\delta^{18}O$-derived SST chronologies. Alternatively, the species may die during periods of extremely high SST (personal

communication with Matthieu Carré). The four *A. tuberculosa* examined in this research, provided by Carré, each lived through one or two El Niño event and were examined to test these possibilities.

Data used for study

A. tuberculosa

Sample collection. *A. tuberculosa* specimens examined in this paper were harvested from Puerto Pizarro by Matthieu Carré and students on two different dates (see Table 4.1). Four valves total were prepared for stable isotopic analysis.

Table 4.1: Information about Puerto Pizzaro *Anadara tuberculosa* shells harvested near Tumbes in Northern Peru by Mattheiu Carré and team. The naming convention is: PP = Puerto Pizarro, 17 = collected in 2017, 18 = collected in 2018. The final, hyphenated number represents the sampling site. The shell harvest coordinates (provided by Carré) are also specified. The number of monthly growth periods identified in microscopic images is indicated. One month equals 28 days, or approximately two lunar periods, which were used to guide sampling. While power samples were obtained for each growth period, not all samples produced viable $\delta^{18}O$ data. The number of $\delta^{18}O$ values produced (one $\delta^{18}O$ value equals one month) is also specified.

Puerto Pizzaro *A. tuberculosa* bivalves				
	PP17-2	**PP17-7**	**PP18-4**	**PP18-7**
Harvest date	September 5, 2017	September 5, 2017	April 11, 2018	April 11, 2018
Shell harvest location	-3.48493, -80.363922	-3.514404, -80.42153	-3.495972, -80.38461	-3.5015, -80.42167
Number of monthly growth periods identified	31	24	24	20
$\delta^{18}O$ data obtained (months)	26	16	19	19

Sample preparation. Thin sections from four *A. tuberculosa* valves were prepared by Matthieu Carré and students in his laboratory at the Universidad Peruana Cayetano Heredia in Lima, Peru using methods outlined in Carré et al., 2013 and 2014. Thin sections from PP17-7, PP18-4, and PP18-7 were

photographed by the author using a binocular microscope with reflected light and photographs were visually examined for growth lines. Carré and team photographed and identified growth lines for valve PP17-2 and subsequently obtained shell powder samples using the same methods outlined below.

Lunar growth cycles of approximately 14 days were clearly identifiable on each of the cross sections and were used to guide sample collection at monthly resolution via microdrilling (see methods in Carré et al., 2013). Sample collection via microdrill was completed using methods outlined in Carré et al. (2013) and Carré et al. (2014).

Contiguous microsampling of the outer shell was performed from the umbo toward the ventral margin. All but one bivalve produced at least two years of monthly isotopic samples, which were evaluated at the Stable Isotope Laboratory at Iowa State University for $\delta^{18}O$ and $\delta^{13}C$. Isotopic corrections were performed using reference standards NBS-18 and IAEA 603. Isotope results were reported in parts per thousand (per mil, ‰). Analytical uncertainty (1σ) of isotopic results can be found in Table 4.2.

Table 4.2: Analytical uncertainty (1σ) associated with isotopic values of $\delta^{18}O$ and $\delta^{13}C$ produced in laboratory analyses at the Stable Isotope Laboratory at Iowa State University. All uncertainties reported with respect to the Vienna Pee Dee Belemnite (VPDB) scale

Analytical uncertainty (1σ) of $\delta^{18}O$ and $\delta^{13}C$				
	PP17-2	**PP17-7**	**PP18-4**	**PP18-7**
δ18O uncertainty	± 0.05‰	± 0.16‰	± 0.16‰	± 0.10‰
δ13C uncertainty	± 0.04‰	± 0.12‰	± 0.12‰	± 0.09‰

Assessing the validity of SST records for Puerto Pizzaro

There are no SST measurements from within the mangrove forest at Puerto Pizzaro. Therefore, SST proxies were examined to identify a dataset to be used to assess correlations between isotope-

derived SST and measured SST at the harvest locations. IMARPE SST from Caleta Cruz, MUR satellite data from Puerto Pizzaro, and Senahmi air temperature records from Puerto Pizzaro were compared.

IMARPE

The IMARPE SST series from Caleta Cruz is approximately 30 km south of the harvest location and exists for the full lifespan of the *A. tuberculosa* samples. Environmental conditions inside the mangrove forest can be different from the open coastline, so IMARPE records were evaluated to discern whether these measured temperatures are representative of mangrove SST further north within the Gulf.

MUR

Monthly averaged satellite-derived SST was obtained for each of the four harvest locations in Puerto Pizzaro within the mangrove (see Table 4.3). It was previously determined that MUR records are systematically 2.8°C lower than in-situ temperature measurements taken in Caleta Cruz, but when adjusted for this offset, these satellite-derived SST records capture the overall annual and seasonal variability of SST at Caleta Cruz as well as anomalies associated with ENSO events (see Chapter 2). Therefore, all MUR data were adjusted by +2.8°C.

Table 4.3: Location of downloaded MUR SST records. One satellite-derived SST dataset was obtained for the IMARPE coastal monitoring station location in Caleta Cruz, and four datasets were downloaded according to the harvest locations in Puerto Pizzaro where *A. tuberculosa* were harvested by Matthieu Carré and team. Locations of the coastal monitoring station and harvest sites are more precise while MUR coordinates have only two significant digits due to the size of the pixels (0.01° x 0.01°).

Tumbes, Peru MUR SST data locations				
	Shell harvest location		MUR SST record location	
	Latitude	Longitude	Latitude	Longitude
IMARPE station			-3.63	-80.60
PP17-2	-3.48493	-80.363922	-3.48	-80.37
PP17-7	-3.514404	-80.42153	-3.50	-80.39
PP18-4	-3.495972	-80.38461	-3.49	-80.38
PP18-7	-3.5015	-80.42167	-3.50	-80.42

Senamhi

Air temperature is the primary control of SST within mangrove forest ecosystems via interactions at the air-sea interface (Zhang, Meng, Xia, and Li, 2021). As there are no SST monitoring stations located in the Puerto Pizzaro mangroves, daily air temperature records were obtained from Senamhi as a possible alternative source of SST data (https://www.senamhi.gob.pe/?&p=estaciones). Daily Senamhi records from Caleta Cruz and Puerto Pizzaro were aggregated into monthly averages for the period February 2018 - February 2020 (see Figure 4.3). Because these records are only available during the period February 2018 to present, falling outside of the majority of the lifespans of the four *A. tuberculosa*, air temperatures were compared to IMARPE and MUR SST to examine correlation between these records (see Table 4.4).

Table 4.4. Environmental data examined as potential sources of SST records within the mangrove forest at the harvest locations of *A. tuberculosa* (SST and air temperature). Precipitation and hydrological flow data examined to assess possible fluctuations of salinity within the study area.

Source	Data	Location	Measuring device (range; error)	Date range
IMARPE	SST	Caleta Cruz	Hanna digital thermometer (unspecified; unspecified)	January 2000 to February 2020
MUR	SST	Puerto Pizzaro	Satellite-derived platforms (unspecified; 0.38-0.42°)	June 2002 to present
Senamhi	Air temperature, precipitation	Puerto Pizzaro	Unspecified (unspecified; unspecified)	February 2018 to present
Senamhi	Hydrologic flow	Tumbes River	Unspecified (unspecified; unspecified)	August 2017 to present

Identifying a measured SST record to compare to bivalve SST

Monthly average air temperature during the period February 2018 to February 2020 was 25.1°C in Caleta Cruz and 26.8°C in Puerto Pizzaro. Temperature ranges during this same period were 6.1°C and 4.1°C, respectively. There appears to be less temperature fluctuation within the mangrove forest compared to the more open coastline in Caleta Cruz (see Figure 4.3). There are similar seasonal patterns at both locations, with air temperature highs during the austral summer months. Winter temperature lows are not as extreme in Puerto Pizzaro, with an average minimum of 24.1°C compared to 21.5°C at Caleta Cruz. Given that air temperature is the dominant control of water temperature within mangrove forests, this indicates that Puerto Pizzaro is likely to share the characteristics with Caleta Cruz, but is probably warmer for much of the year, especially in the winter, and with less seasonal variability

Figure 4.3: Senamhi air temperature records over a two-year period (February 2018 to February 2020) were compared to assess differences in air temperature variability between Caleta Cruz and Puerto Pizzaro.

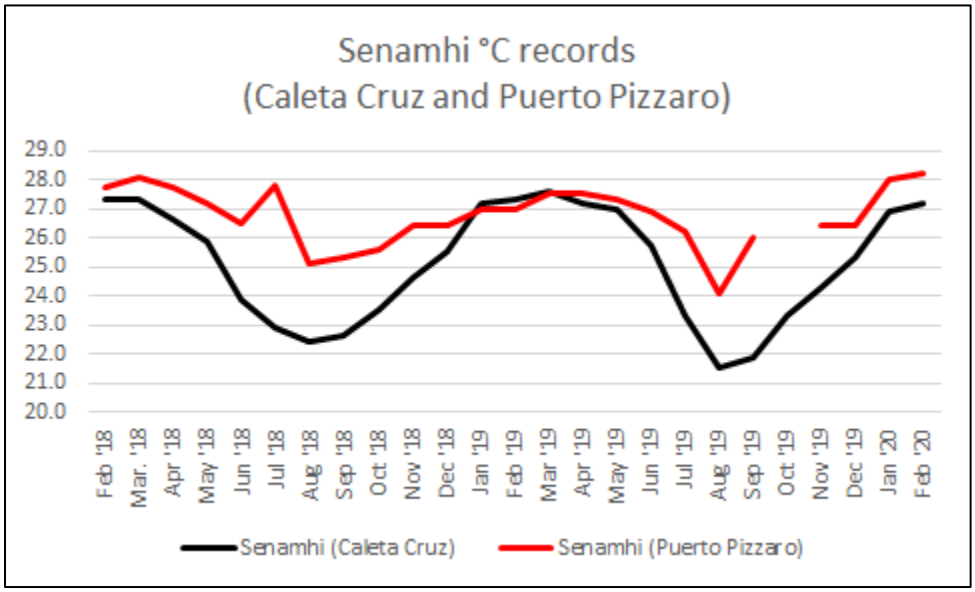

Because Senamhi records don't exist during the lifespans of bivalves examined in this research, Senamhi data were compared to IMARPE and MUR records to identify a suitable proxy for Puerto Pizzaro SST. MUR records were adjusted by +2.8°C (Figure 4.4).

Figure 4.4: All available sources of SST records (IMARPE in-situ and MUR satellite-derived) were compared to air temperature records (Senamhi) for Caleta Cruz and Puerto Pizarro. Adjusted satellite SST data (MUR) was also included in this comparison (+2.8°C, based on Chapter 2).

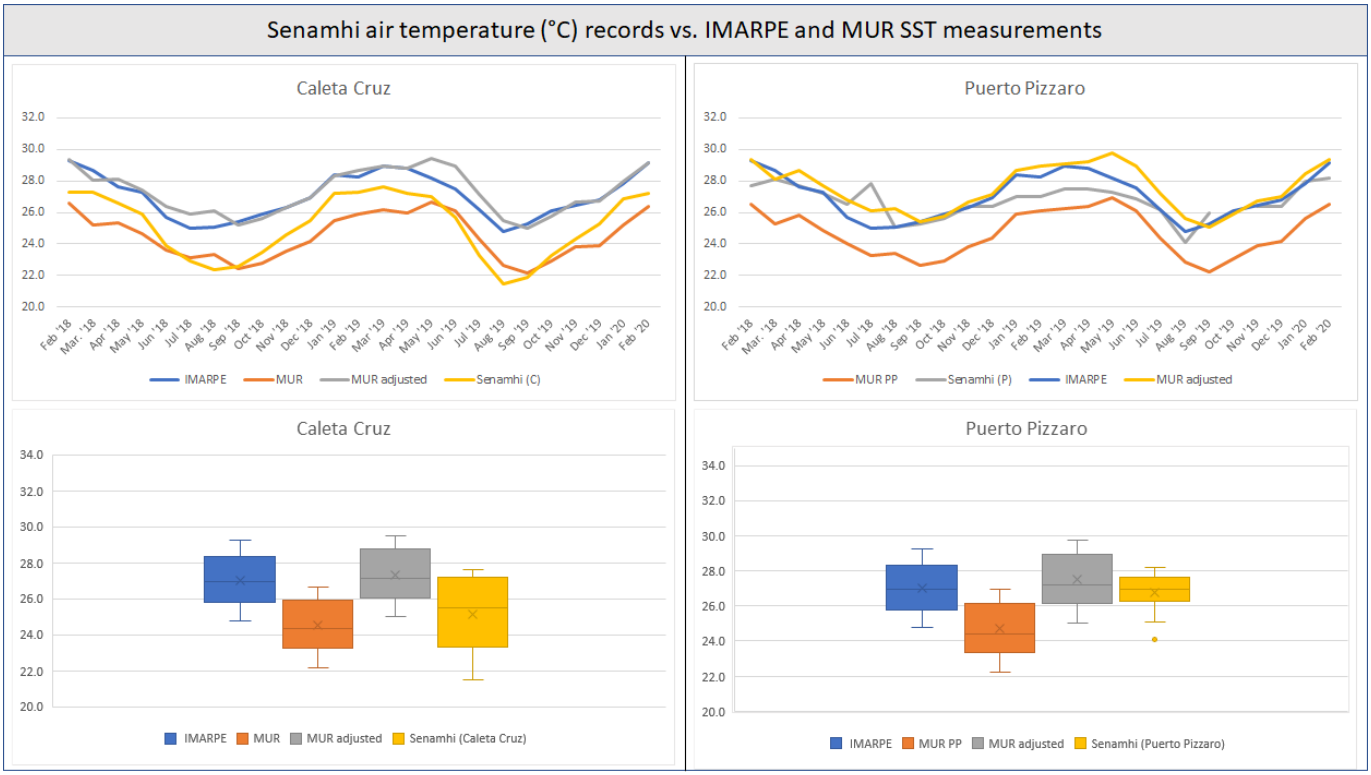

IMARPE and MUR records do not consistently provide accurate representations of average temperature or variability at both locations (see Figure 4.4). While MUR shows a general agreement with Senamhi average temperature (24.5°C vs 25.1°C, respectively) and range (4.5°C and 6.1°C) at Caleta Cruz, MUR SST monthly averages during the period 2/2018-2/2020 are 2.1°C lower than corresponding Senamhi air temperature records from Puerto Pizzaro (24.7°C vs 26.8°C, respectively). Furthermore, MUR records show only a 0.2°C difference in water temperature between the two locations, while Senamhi air temperature measurements show a 1.7°C discrepancy. Since the Senamhi data result from direct measurements, these can be considered more representative of actual mangrove water temperatures. MUR records were therefore not considered for use as a SST proxy in the mangrove

environment. Further consideration into the satellite biases, including exploring the impacts of cloud coverage, precipitation, and textual complexity of satellite pixels, is warranted.

Caleta Cruz IMARPE records are in better agreement with Senamhi temperature averages from Puerto Pizzaro (27°C vs. 26.8°C, respectively), despite their geographic distance. Overall variability of air temperature in Puerto Pizzaro (a range of 4.1°C) is also captured relatively well by IMARPE data (corresponding range of 4.5°C). For this reason, Caleta Cruz IMARPE records were used to represent SST in Puerto Pizzaro and for comparison with *A. tuberculosa* isotope-derived SST records.

Bivalve δ^{18}O SST records

A standard SST equation, developed by Grossman and Ku (1986) and modified by Dettman et al. (1999) was used to calculate bivalve δ^{18}O-derived SST records from each of the four *A. tuberculosa* valves (see Chapter 3 for a complete discussion of the use of this SST equation):

$$T(C°) = 20.60 - 4.34 \times (\delta^{18}O_{aragonite} - (\delta^{18}O_{water} - 0.27))$$

The resulting SST values are shown in Figure 4.5.

Comparison of bivalve and measured SST values

Bivalve and measured SST were compared during each specimens' lifespan (see Figure 4.5). All *A. tuberculosa* isotope records have missing data (see Table 4.1) resulting from insufficient sample sizes or other sampling errors, including storage and transport of samples wrapped in tinfoil and stored in plastic vials, which created difficulties removing samples in the lab. Despite these challenges, many powdered samples did produce viable δ^{18}O data, and isotope-derived SST was compared to measured SST as well as to each shells' growth rings, potential growth breaks, and possible identified changes in biomineralization patterns related to environmental stress.

Monthly averages and overall variability, including minimum and maximum SST as well as range, were examined for each dataset. ANOVA tests were used to statistically compare the datasets as some isotope-derived SST values are missing and thus the two datasets are not equal in size. Monthly averages were compared for the full span of each bivalve's lifespan. A discussion of the results of these analyses follows.

Results and Discussion

Figure 4.5: δ^{18}O-derived SST records from four *A. tuberculosa* harvested in Puerto Pizzaro and corresponding IMARPE SST measurements from nearby Caleta Cruz. Some isotope-derived SST values are displayed as colored dots for visibility. Black boxes indicate potential growth breaks during anomalously high SST. Two El Niño events are indicated by red boxes outlining periods of anomalously high SST in Niño regions 1 & 2. A strong warming event in 2015-2016 displayed characteristics of both an Eastern Pacific and Central Pacific El Niño (L'Heureux et al., 2017), followed by a Coastal El Niño warming event during January through March of 2017 (Rodríguez-Morata et al., 2019).

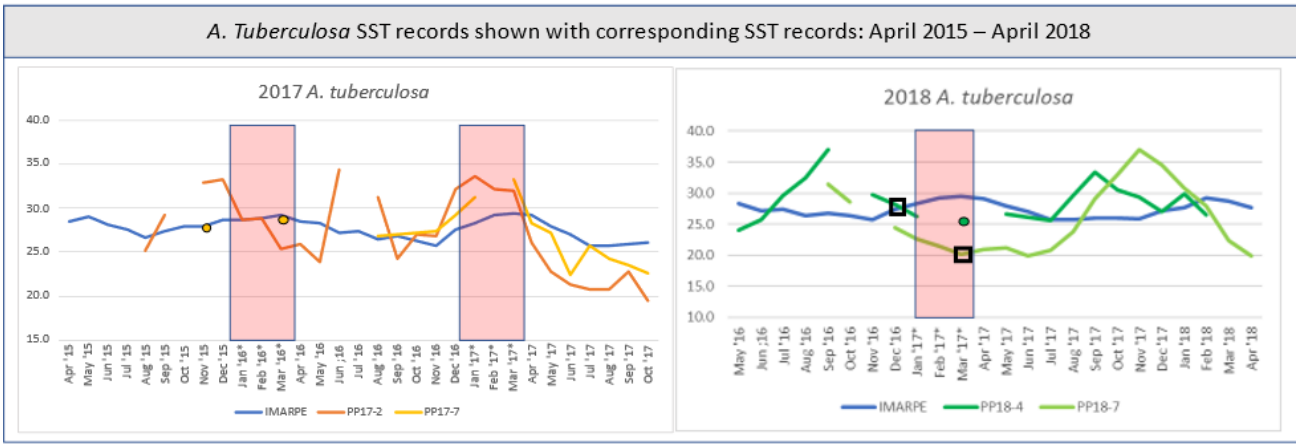

PP17-2

Overall, PP17-2s δ^{18}O record does reflect average ambient SST during its lifespan. Isotope-derived SST is not statistically significantly different from measured SST. However, the range of measured SST is only 3.8°C, while isotope-derived SST shows much greater variability, with a range of 14.9°C. It is unlikely that SST within the mangrove varied that much. Air temperatures range during the period February 2018 to February 2020 is 3.9°C. Missing isotope data cannot explain differences in variation between the two datasets, though some discrepancy could possibly be explained by tidal cycles and solar heating of mud flats in the relatively shallow environment.

Of the four primary divergences of $\delta^{18}O$ SST from measured SST, two correlate to El Niño warming events, indicating that temperature stress may play a role in aragonite oxygen isotope precipitation for this species. It is also possible that SST in the mangroves was higher than SST measured at Caleta Cruz during the El Niño events. The period of anomalously low isotope SST immediately follows the 2017 El Niño event. It is possible that slowed shell growth during this period and/or changes in aragonite precipitation following temperature stress are responsible for this isotopic signature. One other diversion from measured SST occurred during June-August of 2016; further examination is needed to ascertain the cause for this isotopic diversion, which may be best explained by sampling error, including contamination during sampling. The author did not conduct microscopic photographing or sampling of PP17-2 and does not have access to a photograph of this bivalves' thin section in order to examine the profile for further evidence of stress.

PP17-7

Powdered samples from PP17-7 produced 24 viable $\delta^{18}O$ monthly averages, correlating to the period November 2015 to October 2017. PP17-7's isotope-derived SST record also reflects ambient SST during its lifespan and there are no statistically significant differences from measured SST. PP17-7's SST reflects a range is 10.7°C, compared to the measured range of 3.8°C during the shell's lifespan. However, $\delta^{18}O$ SST values that are anomalously higher than measured SST do fall within the 2017 El Niño, indicating that environmental stressors may have impacted precipitation and isotope ratios within the shell's aragonitic growth rings. It is also possible that SST values within the mangroves at Puerto Pizzaro were higher than at the IMARPE station at Caleta Cruz due to shallower waters and tidal cycle in the mangrove forests. The period of anomalously low $\delta^{18}O$ SST occurred during June 2017, following the Coastal El Niño event. Slowed growth during this period, or possibly changes in aragonite precipitation following temperature stress, may be responsible for this isotopic signature.

Shell microscope images were examined for indications of growth breaks associated with temperature stress. Closer to the umbo, corresponding to the 2015-2016 El Niño, seven bivalve samples did not produce $\delta^{18}O$ values (see Figure 4.5). This period does correspond with evidence of stress along the outer edge of the shell, indicated by grooves and discoloration, which are not seen along the rest of the shell's outer profile. PP17-7 does not have any visually identified growth breaks within the internal structure of the shell. Further evaluation is needed to determine if there were changes in shell precipitation due to temperature stress related to El Niño events. The two isotope-derived SST values corresponding with a warming event do correlate with measured SST during that time: the November 2015 $\delta^{18}O$-derived SST was 27.5°C while measured SST was 27.9°C. The March 2016 $\delta^{18}O$-derived SST was 28.9°C while measured SST was 29.2°C. It is important to note that while no growth breaks were visually identified, the shell may still have stopped precipitating during higher SST, meaning that the shell SST timeline would need to be shifted according to the length of the period of stopped growth.

PP18-4 and PP18-7

PP18-4 isotope-derived SST is statistically similar to measured SST, with an average of 28.6°C and 27.3°C, respectively. The same is true when comparing PP18-7's $\delta^{18}O$-derived SST and measured SST averages (27.3°C and 25.8°C, respectively). However, neither bivalve's $\delta^{18}O$-derived SST record correlates with measured SST on a month-by-month basis even though the averages are similar (see Figure 4.5). Variability between the two $\delta^{18}O$-derived SST datasets is not in alignment with measured SST during the bivalves' lifespans. PP18-4 and PP18-7 indicate SST ranges of 12.9°C and 17.1°C during their lifespan, compared to 3.8°C indicated by IMARPE records. SST variations of this scale are unlikely, despite solar heating of mud flats that could impact $\delta^{18}O$ ranges for *A. tuberculosa* living in the intertidal zone. $\delta^{18}O$-derived SST trends are in relative agreement with one another, however, with a possible lag in recorded temperature by two months (PP18-7's SST record lags behind PP18-4's). Reasons for a lack of correlation between $\delta^{18}O$-derived and measured SST could stem from a number of issues, including

systematic sampling errors, differences in growth rates, and unidentified growth breaks causing a disconnect between calendar year SST records and the isotope chronologies.

Potential biomineralization breaks were visually identified in microscope photos of both samples (as in Veralde, Flye-Sainte-Marie, Mendo, and Jean, 2015). These are indicated by black boxes in Figure 4.5 and correlate with the onset and duration of the 2017 Coastal El Niño event. PP18-4 has a potential break at the beginning of the 2017 El Niño during increasingly high SST anomalies, followed by a period of fast growth indicated by a subsequently wider growth ring relative to the average growth ring width for this specimen. The inner carbonate structure is markedly different before and after the identified potential biomineralization break. PP18-7 has a potential break in growth during anomalously high SST in April 2017 near the end of the 2017 Coastal El Niño (see Figure 4.6). SST recorded by IMARPE in Caleta Cruz at this time was 29.1°C. Shifting the isotope records accordingly could help address the disconnect between the SST records. Further analyses, including biomineral evaluation of growth rings, could help identify the duration of potentially identified growth breaks to guide adjustment of $\delta^{18}O$ records.

Figure 4.6: PP18-7 with closeup of shell growth during peak temperature anomalies in the Niño 1&2 region during the 2017 Coastal El Niño. The dark line (indicted by dashed line in closeup) may represent slowed growth during this period of anomalously high SST, or possibly a period when growth stopped entirely.

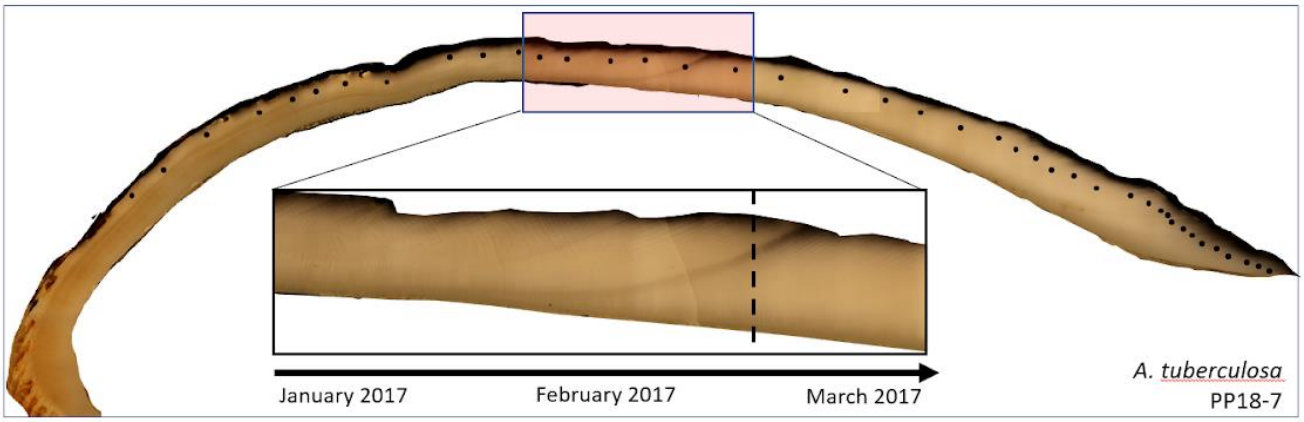

Figure 4.6 shows a closeup of PP18-7's outer shell and internal growth rings corresponding to the 2017 Coastal El Niño. During periods of high stress, shell biomineralization can slow or stop; this is often attributed to environmental stressors, including abnormally high or low SSTs (Velarde, Flye-Sainte-Marie, Mendo, and Jean, 2015). The dark growth line (indicted by a dashed line in Figure 4.6) may be a result of slowed growth or a growth break during anomalously high SST (Velarde, Flye-Sainte-Marie, Mendo, and Jean, 2015). A gap in isotope data resulting from sampling errors correlates with a period of anomalously high SST in the Niño 1&2 region. Missing data make it difficult to confirm a break in growth or to correct for differences in growth rate.

Salinity

Riverine flux can impact salinity by creating more negative $\delta^{18}O$ seawater values in the immediate coastal area (Branscombe, Schulting, Lee-Thorp, and Leng, 2021). Because $\delta^{18}O$ is inversely correlated to SST, increased input of freshwater from rivers into the ocean could help explain some of the anomalous stable oxygen isotope patterns in shell growth rings formed during Eastern Pacific and Coastal El Niño warming events, which are correlated with increased coastal precipitation and river flow (Branscombe, Schulting, Lee-Thorp, and Leng, 2021). Central Pacific events, not discussed in detail in this

dissertation because they are largely unimpactful along Peru's coast, do correlate with decreased precipitation in the highlands and less riverine flow to the coast, resulting in increased salinity during the austral summer at the coast when Peruvian rivers normally have their highest rates of flow (Sandweiss, A, 2019). On the far northern coast of Peru, the ITCZ also controls precipitation patterns.

To assess fluctuations in salinity, Senamhi flow data from the neighboring Tumbes River were downloaded and examined (see Table 4.3). Increased discharge of the Tumbes River, measured by river level in meters (see Figure 4.7), occurred in November 2017, which correlates with anomalous $\delta^{18}O$-derived SST peaks in PP18-4 and PP18-7 during this time (September 2017 and November 2017, respectively). Because water depth in the mangroves is very shallow and probably has less rapid exchange with the ocean, an influx of fresh water from river discharge should alter salinity much more than it would in deeper water along open coastlines (for instance where *T.* hians live).

Figure 4.7: Changes in discharge of the Tumbes River, measured in river level (meters). The Tumbes River is proximate to the harvest locations of *A. tuberculosa* in Puerto Pizzaro and may have an impact on local salinity.

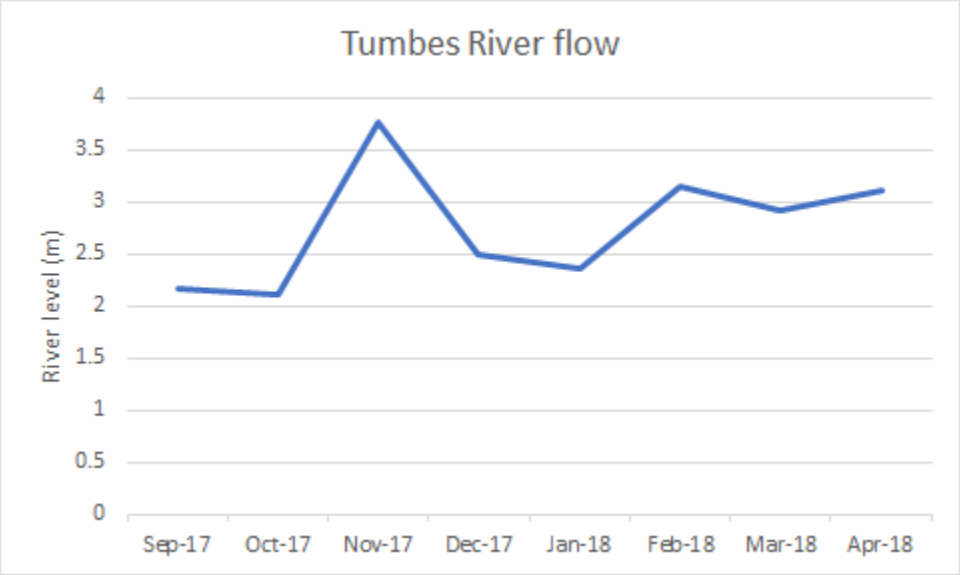

Additional data is needed to test this hypothesis. Systematic salinity measurements from within the mangrove would be ideal to understand potential impacts of salinity on $\delta^{18}O$ precipitation in carbonate bivalves. Short of this, addressing the lack of data in this region, identified by Grados et al. (2018), could help build confidence in salinity interpolations throughout the Gulf of Guayaquil. Obtaining $\delta^{18}O$ measurements from water in the Tumbes River would also help explain the potential impact of riverine flux on mangrove ocean $\delta^{18}O$. Longer-term records of river discharge and precipitation, correlating to the lifespans of the bivalves, would also be helpful. Current records from the Tumbes River only go back as far as August 2017. Continuing these monitoring efforts and expanding them along the coast is an important component of understanding environmental changes in response to climate perturbations such as ENSO. Finally, without more precise information about these issues, it is not possible to confirm the impact of salinity on *A. tuberculosa* $\delta^{18}O$ records.

Another explanation of unexpectedly negative $\delta^{18}O$ values (and thus warmer reconstructed $\delta^{18}O$ SSTs) could be the steep salinity gradients observed in the Tumbes study region. Though gradients are steeper during the austral winter (approximately June through September), overall annual salinity variation in the Gulf of Guayaquil is far greater than that discussed in the Paita region (Chapter 3) due to intrusion of fresher equatorial surface waters. Although this isn't observed in interpolations of salinity between 0-2°S (salinity increases of 0.2–0.3 PSU are actually observed in surface waters during winter months), Grados et al. (2018) suggest that these anomalies may be the result of a lack of data and inaccurate salinity interpolations. More high-resolution salinity data are needed in the Tumbes study region of approximately 3.5°S in order to identify the variation in salinity during summer and winter months and the possible impact on precipitation of carbonate bivalve $\delta^{18}O$.

Bivalve $\delta^{13}C$ Results

Stable isotope records from all four *A. tuberculosa* show weak positive correlations between $\delta^{13}C$ and $\delta^{18}O$. PP17-2 and PP17-7 show clear seasonal $\delta^{13}C$ variation; in these two specimens, annual

cyclicity is more apparent than that of $\delta^{18}O$, associated with water temperature. Seasonal $\delta^{13}C$ variation is more difficult to assess for PP18-4 due to missing samples, but appears to be weaker, and relatively unidentifiable for PP18-7. During several periods of time, both $\delta^{13}C$ and $\delta^{18}O$ values drop in unison, suggesting that intrusion of freshwater may have impacted salinity and thus $\delta^{18}O$ values (Carré et al., 2013). During the 2017 Coastal El Niño, both PP17-2 and PP17-7 show simultaneous drops in both stable isotope records from December 2016 to March 2017 (PP17-2) and February 2017 to April 2017 (PP17-7) during a period of anomalously high SST along far northern Peru and heavy precipitation associated with the strong Coastal El Niño.

PP18-4 shows the strongest simultaneous drops in both stable isotopes during a two-month period correlating to September and October 2017, and PP18-7 shows a corresponding drop in both $\delta^{13}C$ and $\delta^{18}O$ values around the same time (October and November 2017). There are no SST anomalies during this time that might have impacted fractionation of stable oxygen isotopes during precipitation of carbonate shell material. However, the records from the Tumbes River indicate a near doubling of river levels during this period, from approximately 2 to 3.75 meters. Senamhi precipitation records don't extend back this far, but increased river height is likely attributed to increased precipitation, which could additionally create fresher conditions within the Gulf of Guayaquil, providing a possible explanation for the disconnect between $\delta^{18}O$ and measured SST records during that time.

Conclusion

While *A. tuberculosa* samples appear to capture average ambient SST during their lifespans, the relationship between $\delta^{18}O$ and SST is not straightforward. More information is needed to identify how environmental factors influence carbonate shell precipitation before it can be determined if this mangrove species has utility as a paleoENSO proxy. Some of the misalignment between measured and isotope-derived SST records may result from growth breaks during high SST anomalies. Growth breaks are potentially identified in two of the three available microscope images of specimens. These appear to

occur during the 2017 strong Coastal El Niño event. Further research, including the analysis of minerals in growth rings, is needed to identify changes in biomineralization patterns associated with temperature stress, as well as to help confirm visual evidence of growth breaks. Should *A. tuberculosa* stop precipitating during anomalously high SST, it is utility as an ENSO proxy would be reduced because it would not be able to record high SSTs experienced during warming events. However, evidence of growth breaks is inconclusive at this point, necessitating further research.

Some $\delta^{18}O$ variability in the *A. tuberculosa* valves can likely be explained by seasonal salinity fluctuations in the Gulf of Guayaquil. Shipboard and other monitoring stations, including satellite instruments, show steep salinity gradients at the confluence of the Equatorial and Peruvian Currents. As the study region is largely lacking in salinity data, more contiguous records are needed to clarify the potential impacts of salinity on *A. tuberculosa* growth. It is well known, however, that salinity and temperature are primary drivers of oxygen isotope fractionation in shell carbonate material, leading to a likely conclusion that the impacts of salinity on shell growth result in some of the unexplained variability in bivalve-derived SST discussed in this chapter.

CHAPTER 5

CONCLUSIONS AND FUTURE RESEARCH

In large part, the coast of Peru is arid, with little precipitation or river discharge during neutral ENSO conditions. Periodically, Eastern Pacific and Coastal El Niño events cause intense rainfall and flooding events. Coupled with extreme seismic activity in Peru, El Niño flooding and erosion result in transport of sediments to the coast, where some of these materials accumulate in the form of beach ridges (Sandweiss, Rollins, and Richardson III, 1983; Sandweiss, 1986; and Shafer Rogers et al., 2004). Humans have taken advantage of the relative diversity of flora and fauna in coastal floodplains throughout the Holocene. Many coastal occupations have been characterized by a reliance of marine resources, and shellfish harvesting appears to have been a key subsistence strategy for millennia (Dillehay et al. 2017; Reitz and Sandweiss 2001; Reitz, Sandweiss, and Cannarozzi 2019).

Throughout changes in the frequency and intensity of ENSO events during the Holocene, humans demonstrated adaptive capacity, flexibility, and a reliance on traditional ecological knowledge that included both short- and long-term responses to disruptive El Niño events. During the mid- and late-Holocene, abrupt changes in the behavior of ENSO are indicated across archaeological sites, via changes in human behavior, as well as in the geological record (Sandweiss and Kelley, 2012; Sandweiss et al., 2020; St. Amand et al., 2020).

Bivalves are plentiful in coastal Peruvian archaeological sites, and despite some challenges outlined in this dissertation associated with using them as short-term records of environmental conditions, they are among the best paleoENSO proxies available (Sandweiss and Kelley, 2012; Sandweiss and Maasch, 2020; Carré et al., 2013). This research has focused on enhancing our knowledge of two bivalve species, *T. hians* and *A. tuberculosa*. Both are found in archaeological sites on the North Coast of Peru, and are found to represent average SST during their lifespans. The goal of this research is to identify correlations between variations in their carbonate $\delta^{18}O$ and ambient marine environment so

that archaeological specimens may serve as additional sources of information about past marine conditions associated with ENSO.

T. hians

T. hians are abundant on the well-studied Chira Beach Ridges in the Paita region. Individual ridges in this set have been dated and their formation spans the period ca. 5180 – 414 cal yr BP during the Mid- to Late-Holocene (Ortlieb, Fournier, and Macharé, 1993; Richardson III, 1983; Shafer Rogers, 2004). This research demonstrates that archaeological *T. hians*, sourced from the Chira Beach Ridges and elsewhere, can provide information about ENSO during key periods of change in the Mid- to Late-Holocene, particularly during transitional periods in ENSO's behavior ca. 5800 and 2900 cal years BP. *T. hians* appear to have utility as records of average SST and temperature variability during their lifetimes; overall, 75% of specimens examined in this research statistically reflect measured SST of their ambient environment. 50% of these samples also accurately reflect SST variability during their lifespans. Inconsistencies in *T. hians* specimens' isotopic records may be associated with seasonal changes in salinity in the Paita region, which is located at the southern extent of the oceanic transition zone and confluence of two major Peruvian currents. Discrepancies in one of these two samples (Punta Balcones 2) when compared to local SST or seasonal variations in temperature may result from sampling error or contamination, as discussed in Chapter 3. Additional information about salinity and $\delta^{18}O$ of water at the harvest locations could help explain unexpected variations in $\delta^{18}O$. In the absence of high-resolution, continuous salinity data from the Paita region, working with local Peruvian researchers or government staff to obtain river discharge records from the Chira River and local precipitation records would help identify if major changes in salinity in the study region occurred during the specimens' lifespans.

In the past, *T. hians* were likely under less harvesting pressure, meaning they had overall longer average lifespans before they were harvested and discarded in coastal middens. Therefore, archaeological specimens would have recorded more annual cycles than modern *T. hians*. Thus, the use

of archaeological valves could allow for a more comprehensive analysis of seasonal variation from a single individual. The collection of valves from each beach ridge would allow for the examination of average temperatures associated with periods during the Mid- and Late-Holocene as well as variation in SST from single valves as well as across sample sets.

Future research should also examine *T. hians* individuals which survived an Eastern Pacific or Coastal El Niño event to determine if this species continues carbonate precipitation during anomalously high SST, or if the bivalves stop growing or die. *T. hians* examined in this research lived in water temperatures of 19.0-19.3°C on average, with a maximum monthly average of 24.2°C. Laboratory research on lethal temperatures (LT-50; the temperature at which half a local population of bivalve will die within a 24-hour period) is another possible way to determine the temperature sensitivity of *T. hians* in order to assess its utility as a record of El Niño events (Sandweiss et al., 2001). In the case of *Choromytilus chorus*, a temperate giant mussel inhabiting the southern Peruvian and Chilean coasts, this temperature is 26.5°C (Gosselin, Lazareth, and Ortlieb, 2013; Sandweiss et al., 2001; Urban, 1994). It would be expected that tropical bivalve species living closer to the equator, such as *T. hians,* would be less sensitive to higher temperatures, with a higher LT-50 threshold. Collecting well preserved *T. hians* valves, therefore, with visual evidence of growth breaks on their outer shell, would help ensure that specimens examined in future research did experience and survive temperature or other environmental stress and thus serve as records of anomalously high SST during their lifetime.

A. tuberculosa

A. tuberculosa bivalves examined in this dissertation lived in greatly different circumstances than the *T. hians* specimens. All four *A. tuberculosa* lived through at least one El Niño event, and two of the samples were alive during both the 2015-2016 and 2017 El Niños. This provided a unique opportunity to study their $\delta^{18}O$ and $\delta^{13}C$ records and the impacts of warming events on the precipitation of their carbonate shell material. These mangrove bivalves grew in considerably warmer water than

recorded in Paita. Average SST during their lifespans was 27.3 - 27.6°C, over 8°C warmer than the ocean habitat of *T. hians,* approximately 1.5° further south. Some of this difference is attributed to the fact that air temperature is a dominant control of mangrove SST, the Gulf of Guayaquil is located closer to the equator, and the equatorial water mass mixes with the Peruvian current creating an overall warmer ocean environment (Grados et al., 2018; Zhang, Meng, Xia, and Li, 2021). Warmer average SST can also be attributed to the El Niño warming events that occurred during the *A. tuberculosa*'s lives. The maximum average monthly temperature experienced by these bivalves was 29.5°C, indicating this species is not as temperature sensitive as some other Peruvian bivalves used as ENSO proxies. This bodes well for the potential of archaeological *A. tuberculosa* as faithful records of temperature variability, particularly during anomalously high temperatures associated with El Niño events.

All *A. tuberculosa* samples have missing isotope values resulting from insufficient sample sizes or other sampling errors. Despite these challenges, many powdered samples did produce viable isotope data. The two specimens harvested in September 2017 have $\delta^{18}O$ records that statistically reflect average temperatures during their lifespans. PP17-7 shows no statistically significant difference from monthly in-situ measured temperatures. The other two *A. tuberculosa*, harvested in April 2018, show visual evidence of growth disruption during the strong 2017 Coastal El Niño. As discussed in Chapter 4, more research is needed to identify whether these lines and apparent changes in growth patterns represent actual breaks in growth, or simply slowed growth in response to temperature stress. That *A. tuberculosa* lived through anomalously high temperatures is strong evidence that this species is capable of capturing information about their ambient marine environments during similarly strong ENSO events during the Mid- and Late-Holocene. While the two specimens harvested in 2018 (PP18-4 and PP18-7) have $\delta^{18}O$ records that do reflect overall average temperatures during their lifespans, neither bivalve reflects monthly or seasonal SST variation. However, the two records are in agreement with one another, suggesting there may be a systematic factor influencing their carbonate $\delta^{18}O$. This could most

likely be explained by unidentified growth breaks causing a disconnect between calendar year SST records and the isotope chronologies, but heavy precipitation and river discharge, as discussed previously, relative to the 2015-2016 El Niño, could also explain these valves' $\delta^{18}O$ records.

Additional information is needed to understand seasonal changes in salinity in mangroves, as well as seawater freshening related to heavy rainfall and river discharge. While there is a clear lack of salinity and SST temperature data, particularly along the north coast of Peru (Grados et al., 2018), the use of high-resolution MUR data shows promise as a source of SST in areas lacking coastal monitoring stations, as discussed in Chapter 2. Salinity variation in the Gulf of Guayaquil is greater than in Paita because the former is closer to the equator and ITCZ where there is increased precipitation and river discharge. The primary impact of these factors on salinity in the immediate coastal area examined here is the more negative $\delta^{18}O$ of ocean water. The inverse correlation between $\delta^{18}O$ and SST could explain some anomalous carbonate $\delta^{18}O$ values in *A. tuberculosa* growth periods corresponding to Eastern Pacific and Coastal El Niño warming events. The corresponding drops in both $\delta^{18}O$ and $\delta^{13}C$ during a period of increased discharge of the Tumbes River provides a likely explanation for the disconnect between both $\delta^{18}O$ and measured SST.

MUR dataset

This research also examined the correlation between MUR satellite-derived SST data and in-situ SST measurements to determine if high-resolution satellite SST records have utility for calibrating bivalve-derived SST chronologies. In general, MUR data do a good job of capturing SST variability along the coast of Peru. Three broad trends were observed in the satellite datasets. In some areas, such as Paita, satellite records correlate extremely well with in-situ data. While the collection of *T. hians* in this research was guided by their proximity to the IMARPE coastal monitoring station in Paita Harbor, the use of MUR records to calibrate *T. hians* $\delta^{18}O$-derived SST in future research would allow for more

confident collection and analysis of bivalves that didn't grow directly near an IMAPRE station in the Paita region.

In other areas, there appear to be large, systematic temperature offsets between MUR and IMARPE records. In Tumbes, a systematic offset of 2.8°C resulted from MUR measurements underestimating actual in-situ SST. When adjusted, MUR records do appear to capture annual average and season changes in SST, though not as well as in Paita. MUR records from the harvest location within the mangrove forests in Puerto Pizzaro are likely less accurate due to reasons discussed in Chapter 2, including textural variability of pixels, terrestrial and cloud masking, and precipitation. Without a clearer understanding of which factors impact systematic offsets, researchers could not use these data as confidently for calibrating bivalve-derived SST records. As discussed in Chapter 4, air temperature records are likely most reflective of SST within mangrove areas and would thus be most useful for comparison with harvested specimens in the future.

The third trend observed is non-systematic offsets between the MUR and IMARPE data, such as in Ilo, where MUR satellite-derived records skew warmer, particularly during the spring and summer months. There are various explanations for non-systematic offsets. In the case of the more southern records such as Ilo, over-masking of clouds by satellite algorithms occurs more often as ocean and air temperatures are warming during the spring and summer. When this happens, areas of cold ocean are misidentified as clouds and removed from the dataset, resulting in positive skewing and overall warmer satellite-derived SST. In addition to cloud masking errors, aerosols, including mineral dust transported from the Paracas region northward, can explain some other non-systematic offsets between MUR and IMARPE datasets. Correcting for errors in IR-derived satellite SST datasets is one way to adjust for non-systematic biases caused by aerosols. Continued improvements in remotely sensed datasets from coastal regions will address challenges posed by aerosols such as those seen in and around the Paracas Peninsula. In the meantime, these datasets are still useful, particularly when environmental parameters

such as wind speed that impact aerosol dispersion and result in less-accurate satellite-derived SST records are observed independently. This allows for researchers to identify periods during which SST records are likely inaccurate and should be discarded. Lastly, complex textures of pixels at the coastal interface are known to interfere with satellite SST accuracy, meaning that MUR data from areas with complex coastlines such as Tumbes must be used with caution and compared to independent records when available, such as air temperature, river discharge, or precipitation data. Fortunately, the accuracy of satellite SST measurements in coastal areas is a major focus of advances in satellite instrumentation, and it can be expected that the accuracy of these large-scale datasets will continue to improve as new technologies and methods are developed.

Overall, this research identifies next steps in the search for additional accurate and reliable paleoENSO proxies. It confirms that archaeological *T. hians* can be used to reconstruct average SST as well as seasonal SST variability and that *A. tuberculosa* survive anomalously high SSTs associated with El Niño events. This research also confirms that with some exceptions, MUR high-resolution satellite data can serve as a reliable alternative to in-situ SST measurements for calibrating averages and ranges of bivalve-derived SST. As technologies and methods for tracking changes in SST and salinity in the equatorial Eastern Pacific improve, we will no doubt increase our ability to understand the complex and shifting dynamics of ENSO throughout the Holocene.

BIBLIOGRAPHY

Andrus, C. F. T., Hodgins, G. W., Sandweiss, D. H. and Crowe, D. E. (2005). Molluscan radiocarbon as a proxy for El Niño-related upwelling variations in Peru. *Special Papers – Geological Society of America*, *395*, 13.

Andrus, C. F. T. (2011). Shell midden sclerochronology. *Quaternary science reviews*, *30*(21-22), 2892-2905.

Andrus, C. F. T., Crowe, D. E., Sandweiss, D. H., Reitz, E. J. and Romanek, C. S. (2002). Otolith $\delta^{18}O$ record of Mid-Holocene sea surface temperatures in Peru. *Science*, *295*(5559), 1508-1511.

Al-Shehhi, M. R. (2022). Uncertainty in satellite sea surface temperature with respect to air temperature, dust level, wind speed and solar position. *Regional Studies in Marine Science*, *53*, 102385.

Ashok, K., Behera, S.K., A. Rao, S., Weng, H., and Yamagata, T. (2007). "El Niño Modoki and Its Possible Teleconnection." *Journal of Geophysical Research: Oceans* 112 (C11). https://doi.org/10.1029/2006JC003798.

Barahona, S. P., Vélez-Zuazo, X., Santa-Maria, M. and Pacheco, A. S. (2019). Phylogeography of the rocky intertidal periwinkle Echinolittorina paytensis through a biogeographic transition zone in the Southeastern Pacific. *Marine Ecology*, *40*(4), e12556.

Belknap, D. F. and Sandweiss, D. H. (2014). Effect of the Spanish Conquest on coastal change in Northwestern Peru. *Proceedings of the National Academy of Sciences*, *111*(22), 7986-7989.

Beresford-Jones, D., Pullen, A. G., Whaley, O. Q., Moat, J., Chauca, G., Cadwallader, L., ... and French, C. (2015). Re-evaluating the resource potential of lomas fog oasis environments for Preceramic hunter–gatherers under past ENSO modes on the south coast of Peru. *Quaternary Science Reviews*, *129*, 196-215.

Branscombe, T., Schulting, R., Lee-Thorp, J. and Leng, M. J. (2021). The potential of marine bivalve Spisula sachalinensis as a marine temperature record. *Palaeogeography, Palaeoclimatology, Palaeoecology*, *582*, 110634.

Briceño-Zuluaga, F., Castagna, A., Rutllant, J. A., Flores-Aqueveque, V., Caquineau, S., Sifeddine, A., ... and Cardich, J. (2017). Paracas dust storms: Sources, trajectories and associated meteorological conditions. *Atmospheric Environment*, *165*, 99-110.

Caramanica, A., Quilter, J., Huaman, L., Villanueva, F. and Morales, C. R. (2018). "Micro-Remains, ENSO, and Environmental Reconstruction of El Paraíso, Peru, a Late Preceramic Site." *Journal of Archaeological Science: Reports* 17 (February): 667–77. https://doi.org/10.1016/j.jasrep.2017.11.026.

Caramanica, A., Mesia, L.H., Morales, C. R., Huckleberry, G., Castillo B., L. J. and Quilter, J. (2020). "El Niño resilience farming on the north coast of Peru." *Proceedings of the National Academy of Sciences* 117 (39): 24127-24137. https://doi.org/10.1073/pnas.2006519117

Carrasco De La Cruz, P. M. (2012). Dinamica Poblacional De Tivela hians “Concha Blanca” En La Zona Submareal De Punta Balcones Al Sur De Negritos, Talara. August 2011-July 2012.

Carré, M., Azzoug, M., Zaharias, P., Camara, A., Cheddadi, R., Chevalier, M., ... and Wade, M. (2019). Modern drought conditions in western Sahel unprecedented in the past 1600 years. Climate Dynamics, 52(3), 1949-1964.

Carré, M., Bentaleb, I., Blamart, D., Ogle, N., Cardenas, F., Zevallos, S., Kalin, R. M., Ortlieb, L. and Fontugne, M. (2005). Stable isotopes and sclerochronology of the bivalve Mesodesma donacium: potential application to Peruvian paleoceanographic reconstructions. Palaeogeography, Palaeoclimatology, Palaeoecology 228, 4–25.

Carré, M., Sachs, J. P., Schauer, A. J., Rodríguez, W. E. and Ramos, F. C. (2013). Reconstructing El Niño-Southern Oscillation activity and ocean temperature seasonality from short-lived marine mollusk shells from Peru. *Palaeogeography, Palaeoclimatology, Palaeoecology*, *371*, 45-53.

Carré, M., Julian P. S., Purca, S., Schauer, A. J., Braconnot, P., Falcón, R. A., Julien, M. and Lavallée, D. (2014). “Holocene History of ENSO Variance and Asymmetry in the Eastern Tropical Pacific.” *Science* 345 (6200): 1045–48.

Chaigneau, A., Dominguez, N., Eldin, G., Vasquez, L., Flores, R., Grados, C. and Echevin, V. (2013). Near-coastal circulation in the Northern Humboldt Current System from shipboard ADCP data. *Journal of Geophysical Research: Oceans*, *118*(10), 5251-5266.

Crosman, E., Vazquez-Cuervo, J. and Chin, T. M. (2017). Evaluation of the multi-scale ultra-high resolution (MUR) analysis of lake surface temperature. *Remote Sensing*, *9*(7), 723.

Conroy, J. L., Thompson, D. M., Cobb, K. M., Noone, D., Rea, S. and Legrande, A. N. (2017). Spatio temporal variability in the δ^{18}O-salinity relation-ship of seawater across the tropical Pacific Ocean, Paleoceanography, 32, 484–497, doi:10.1002/2016PA003073.

Dettman, D. L., Reische, A. K. and Lohmann, K. C. (1999). Controls on the stable isotope composition of seasonal growth bands in aragonitic fresh-water bivalves (union- idae). Geochimica et Cosmochimica Acta 63 (7–8), 1049–1057.

Dillehay, T. D., Goodbred, S., Pino, M., Vásquez Sánchez, V. F., Rosales Tham, T., Adovasio, J. and Collins, M. B. (2017). "Simple technologies and diverse food strategies of the Late Pleistocene and Early Holocene at Huaca Prieta, Coastal Peru." *Science Advances* 3, no. 5: e1602778.

Epstein, S. and Mayeda, T. (1953). Variation of O18 content of waters from natural sources. *Geochimica et cosmochimica acta*, *4*(5), 213-224.

Fick, S. E. and Hijmans, R. J. (2017). WorldClim 2: new 1km spatial resolution climate surfaces for global land areas. International Journal of Climatology 37 (12): 4302-4315.

Fontugne, M., Usselmann, P., Lavallée, D., Julien, M.,= and Hatté, C. (1999). El Niño variability in the coastal desert of southern Peru during the Mid-Holocene. *Quaternary research*, *52*(2), 171-179.

Freitas, P., Clarke, L. J., Kennedy, H., Richardson, C. and Abrantes, F. (2005). Mg/Ca, Sr/Ca, and stable-isotope (δ18O and δ13C) ratio profiles from the fan mussel Pinna nobilis: Seasonal records and temperature relationships. *Geochemistry, Geophysics, Geosystems*, *6*(4).

GHRSST Science Team (2010). The Recommended GHRSST Data Specification (GDS) 2.0, document revision 4, available from the GHRSST International Project Office, 2011, pp 123.

Goodbred Jr, S. L., Dillehay, T. D., Galvéz Mora, C. and Sawakuchi, A. O. (2020). "Transformation of Maritime Desert to an Agricultural Center: Holocene Environmental Change and Landscape Engineering in Chicama River valley, northern Peru coast." *Quaternary Science Reviews* 227: 106046. https://doi.org/10.1016/j.quascirev.2019.106046.

Gosselin, M., Lazareth, C. E. and Ortlieb, L. (2013). Sclerochronological studies in the Humboldt current system, a highly variable ecosystem. *Journal of Shellfish Research*, *32*(3), 867-882.

Grados, C., Chaigneau, A., Echevin, V. and Dominguez, N. (2018). Upper ocean hydrology of the Northern Humboldt Current System at seasonal, interannual and interdecadal scales. *Progress in Oceanography*, *165*, 123-144.

Grossman, E. L. and Ku, T. L. (1986). Oxygen and carbon isotope fractionation in biogenic aragonite: temperature effects. *Chemical Geology: Isotope Geoscience Section*, *59*, 59-74.

Gruver, S. M. (2018). *Occupational seasonality and paleoenvironmental reconstruction at Quebrada Jaguay 280*. Northern Illinois University.

Hu, Z-Z., Huang, B., Zhu, J., Kumar, A. and McPhaden, M. J. (2019). “On the Variety of Coastal El Niño Events.” *Climate Dynamics* 52 (12): 7537–52. https://doi.org/10.1007/s00382-018-4290-4.

Keefer, D. K., DeFrance, S. D., Moseley, M. E., Richardson III, J. B., Satterlee, D. R. and Day-Lewis, A. (1998). Early maritime economy and EL Niño events at Quebrada Tacahuay, Peru. *Science*, *281*(5384), 1833-1835.

Melnichenko, O. 2021. Multi-mission L4 Optimally Interpolated Sea Surface Salinity. Ver. 1.0. PO.DAAC, CA, USA. Dataset accessed [2022-5-29] at https://doi.org/10.5067/SMP10-4U7CS

Moat, J., Orellana-Garcia, A., Tovar, C., Arakaki, M., Arana, C., Cano, A., ... and Whaley, O. Q. (2021). Seeing through the clouds–Mapping desert fog oasis ecosystems using 20 years of MODIS imagery over Perú and Chile. *International Journal of Applied Earth Observation and Geoinformation*, *103*, 102468.
NOAA Satellite Oceanography & Climatology Division. (n.d.). *Coastwatch*. Retrieved July 2, 2022, from https://coastwatch.noaa.gov

Nesbitt, J. (2016). “El Niño and Second-Millennium BC Monument Building at Huaca Cortada (Moche Valley, Peru).” *Antiquity* 90 (351): 638–53.

Ñiquen, M., and Bouchon, M. (2004). “Impact of El Niño Events on Pelagic Fisheries in Peruvian Waters.” *Deep Sea Research Part II: Topical Studies in Oceanography*, Oceanography of the Eastern Pacific: Volume III, 51 (6): 563–74. https://doi.org/10.1016/j.dsr2.2004.03.001.

Olsson, A. A. (1961). *Mollusks of the tropical eastern Pacific: particularly from the southern half of the Panamic-Pacific faunal province (Panama to Peru); Panamic-Pacific Pelecypoda*. Paleontological Research Institution.

Ortlieb, L., Fournier, M. and Macharé, J. (1993). Beach ridge series in Northern Peru: Chronology, correlation and relationship with major Late-Holocene El Niño events. *Bulletin de l'Institut Français d'Études Andines*, (1), 191-212.

O'Carroll, A. G., Armstrong, E. M., Beggs, H. M., Bouali, M., Casey, K. S., Corlett, G. K., ... and Wimmer, W. (2019). Observational needs of sea surface temperature. *Frontiers in Marine Science*, *6*, 420.

Pérez-Huerta, A. and Andrus, C. F. T. (2010): Vital Effects in the Context of Biomineralization. "Biominerals and Biomineralization Processes." Seminarios de la Sociedad de Española de Mineralogía, 07, p. 35-45. ISSN 1698-5478.

Prieto, G. (2015). "Gramalote: Domestic Life, Economy and Ritual Practices of a Prehispanic Maritime Community." Ph.D. dissertation, Yale University, New Haven, CT.

Ramos (2010) Encyclopedia of the world's coastal landforms, ed eric e.f. bird. Ramos chapter 4.2 called Peru.

Reid, D. A. (2007). Peruvian Beach Ridges: Records of Human Activity and Climate Change.

Rein, B., Lückge, A., Reinhardt, L., Sirocko, F., Wolf, A. and Dullo, W-C. (2005). "El Niño Variability off Peru During the Last 20,000 years." *Paleoceanography* 20 (4).

Reitz, E. J. and Sandweiss, D. H. (2001). "Environmental Change at Ostra Base Camp, A Peruvian Preceramic Site." *Journal of Archaeological Science* 28 (10): 1085–1100.

Reitz, E. J., Sandweiss, D. H. and Cannarozzi, N. R. (2019). "Fishing on the Frontier: Vertebrate Remains from Amotape, Siches, and Honda Phase Occupations at Sitio Siches (Pv 7-19), Perú." *Bulletin of the Florida Museum of Natural History* 56 (4): 109–81.

Richardson III, J. B. (1983). The Chira Beach Ridges, sea level change, and the origins of maritime economies on the Peruvian coast. Ann. Carnegie Mus. 52, 265–276.

Riedinger, M., Steinitz-Kannan, M., Last, W. and Brenner, M. (1998). A 6100 yr El Niño record from the Galapagos Islands. In *Geological Society of America Abstracts with Programs* (Vol. 30, No. 7, pp. 161-162).

Rodbell, D. T., Seltzer, G. O., Anderson, D. M., Abbott, M. B., Enfield, D. B. and Newman, J. H. (1999). An~ 15,000-year record of El Niño-driven alluviation in southwestern Ecuador. *Science*, *283*(5401), 516-520.

Richardson III, J. B. (1983). The Chira Beach Ridges, sea level change, and the origins of maritime economies on the Peruvian coast. Ann. Carnegie Mus. 52, 265–276.

Rollins, H. B., Richardson III, J. B. and Sandweiss, D. H. (1986). "The Birth of El Niño: Geoarchaeological Evidence and Implications." *Geoarchaeology* 1 (1): 3–15.

Rollins H. B., Sandweiss D. H., Brand U., Rollins J. C. (1987). Growth increment and stable isotope analysis of marine bivalves: implications for the geoarchaeological record of El Niño. *Geoarchaeology* 2:181–87.

Rosales Quintana, G. M., Marsh, R., and Icochea Salas, L. A. (2021). Interannual variability in contributions of the Equatorial Undercurrent (EUC) to Peruvian upwelling source water. *Ocean Science*, *17*(5), 1385-1402.

Salvador, A., Arasa, R. and Codina, B. (2016). Aeolian dust forecast in arid and semiarid regions of Peru and Chile and their contribution over particulate matter concentration. *Journal of Geoscience and Environment Protection*, *4*(01), 128.

Sandweiss, A. (2019). El Niño Modoki: A Diagnostic Study for Peru and Beyond. In The Emirates Center for Strategic Studies and Research (Author), *Climate Change and the Future of Water* (pp. 133-152). The Emirates Center for Strategic Studies and Research.

Sandweiss, D. H. (1986). The beach ridges at Santa, Peru: El Niño, uplift, and prehistory. *Geoarchaeology*, *1*(1), 17-28.

Sandweiss, D. H. (2003). Terminal Pleistocene through Mid-Holocene archaeological sites as paleoclimatic archives for the Peruvian coast. *Palaeogeography, Palaeoclimatology, Palaeoecology*, *194*(1-3), 23-40.

Sandweiss, D. H. and Maasch, K. A. (2022). Climatic and Cultural Transitions in Lambayeque, Peru, 600 to 1540 AD: Medieval Warm Period to the Spanish Conquest. *Geosciences*, *12*(6), 238.

Sandweiss, D. H. and Quilter, J. (2012). "Collation, Correlation, and Causation in the Prehistory of Coastal Peru**."** In *Surviving Sudden Environmental Change: Answers from Archaeology*, edited by P. Sheets and J. Cooper, 117–41. Boulder: University of Colorado Press.

Sandweiss, D. H. and Kelley, A. R., (2012). "Archaeological Contributions to Climate Change Research: The Archaeological Record as a Paleoclimatic and Paleoenvironmental archive." *Annual Review of Anthropology* 41: 371–91.

Sandweiss, D. H., Andrus, C. F. T., Kelley, A. R., Maasch, K. A., Reitz, E. J. and Roscoe, P. B. (2020). Archaeological climate proxies and the complexities of reconstructing Holocene El Niño in coastal Peru. *Proceedings of the National Academy of Sciences*, *117*(15), 8271-8279.

Sandweiss, D. H., Maasch, K. A., Andrus, C. F. T., Reitz, E. J., Richardson III, J. B., Riedinger-Whitmore, M., and Rollins, H. B. (2007). "Chapter 2 - Mid-Holocene Climate and Culture Change in Coastal Peru." In *Climate Change and Cultural Dynamics*, edited by David G. Anderson, Kirk A. Maasch, and Daniel H. Sandweiss, 25–50. San Diego: Academic Press.

Sandweiss, D. H., Maasch, K. A., Burger, R. L., Richardson III, J. B., Rollins, H. B. and Clement, A. (2001). Variation in Holocene El Niño frequencies: Climate records and cultural consequences in ancient Peru. *Geology*, *29*(7), 603-606.

Sandweiss, D. H., Richardson III, J. B., Reitz, E. J., Rollins, H. B. and Maasch, K. A. (1996). Geoarchaeological evidence from Peru for a 5000 years BP onset of El Niño. *Science*, *273*(5281), 1531-1533.

Sandweiss, D. H., Rollins, H. B. and Richardson III, J. B. (1983). Landscape alteration and prehistoric human occupation on the north coast of Peru. *Annals of Cornegie Museum.*, *277*, 297.

Sandweiss, D. H., Solís, R. S., Moseley, M. E., Keefer, D. K. andOrtloff, C. R. (2009). Environmental change and economic development in coastal Peru between 5,800 and 3,600 years ago. *Proceedings of the National Academy of Sciences*, *106*(5), 1359-1363.

Schmidt, G. A., Bigg, G. R. and Rohling, E. J. (1999). "Global Seawater Oxygen-18 Database - v1.22" https://data.giss.nasa.gov/o18data/

Shafer Rogers, S., Sandweiss, D. H., Maasch, K. A., Belknap, D. F. and Agouris, P. (2004). Coastal change and beach ridges along the northwest coast of Peru: Image and GIS analysis of the Chira, Piura, and Colan beach-ridge plains. *Journal of Coastal Research*, *20*(4), 1102-1125.

St. Amand, F, Childs, S. T., Reitz, E. J., Heller, S., Newsom, B., Rick, T. C., Sandweiss, D. H. and Wheeler, R. (2020). “Leveraging Legacy Archaeological Collections as Proxies for Climate and Environmental Research.” *Proceedings of the National Academy of Sciences* 117 (15): 8287–94. https://doi.org/10.1073/pnas.1914154117.

St. Amand, F., Leclerc, E. L., Blackwood, E., McGinn, A., Landazuri, H., Sandweiss, D. H., Kelley, A., Maasch, K. A. and James, C. E. (*in press*). Getting into (and out of) hot water: climate hazards, resilience, and ENSO in the archaeological record. In C. Goudge (Ed.), *Archaeologies of Adaptation and Resilience to Climate Change and Environmental Hazards*. University Press of Florida.

Sulca, J., Takahashi, K., Espinoza, J-C., Vuille, M. and Lavado-Casimiro, W. (2018). “Impacts of Different ENSO Flavors and Tropical Pacific Convection Variability (ITCZ, SPCZ) on Austral Summer Rainfall in South America, with a Focus on Peru.” *International Journal of Climatology* 38 (1): 420–35. https://doi.org/10.1002/joc.5185.

Tanabe, K., Miyaji, T., Murakami-Sugihara, N., Shirai, K., and Moriya, K. (2020). Annual shell growth patterns of three venerid bivalve mollusk species in the subtropical northwestern Pacific as revealed by sclerochronological and stable oxygen isotope analyses. *Marine Biology*, *167*(2), 1-15.

Urban, H. J. (1994). Upper temperature tolerance of ten bi-valve species off Peru and Chile related to El Niño. *Marine Ecology Progress Series*, 107, 139–146.

Velarde, A. A., Flye-Sainte-Marie, J., Mendo, J., and Jean, F. (2015). Sclerochronological records and daily microgrowth of the Peruvian scallop (Argopecten purpuratus, Lamarck, 1819) related to environmental conditions in Paracas Bay, Pisco, Peru. *Journal of sea research*, *99*, 1-8.

Wanamaker Jr, A. D., Kreutz, K. J., Schöne, B. R. and Introne, D. S. (2011). Gulf of Maine shells reveal changes in seawater temperature seasonality during the Medieval Climate Anomaly and the Little Ice Age. *Palaeogeography, Palaeoclimatology, Palaeoecology*, *302*(1-2), 43-51.

Warner, J., DeLong, K. L., Chicoine, D., Wanamaker, A. D. and Thirumalai, K. (2016). Assessing El Niño Variability on the Coast of Peru Using Two Short-Lived Bivalve Species, Donax obesulus and Mesodesma donacium, From Archaeological and Modern Contexts. *American Geophysical Union*, *2016*, PC54A-2236.

Warner, J. P., DeLong, K. L., Chicoine, D., Thirumalai, K. and Andrus, C. F. T. (2022). Investigating the influence of temperature and seawater δ18O on *Donax obesulus* (Reeve, 1854) shell δ18O. *Chemical Geology*, *588*, 120638.

BIOGRAPHY OF THE AUTHOR

Frankie St. Amand is from Downeast Maine. Frankie is a candidate for the Doctor of Philosophy in Interdisciplinary Studies from the University of Maine in August 2022.